



Strål
säkerhets
myndigheten

Swedish Radiation Safety Authority

Authors:

Peter Dillström
Magnus Andersson
Iradj Sattari-Far
Weilin Zang

Research

2009:27

Analysis Strategy for Fracture
Assessment of Defects in
Ductile Materials

Title: Analysis Strategy for Fracture Assessment of Defects in Ductile Materials.
Report number: 2009:27.
Authors: : Peter Dillström, Magnus Andersson, Iradj Sattari-Far and Weilin Zang.
Inspecta Technology AB, Stockholm, Sweden .
Date: June 2009.

This report concerns a study which has been conducted for the Swedish Radiation Safety Authority, SSM. The conclusions and viewpoints presented in the report are those of the author/authors and do not necessarily coincide with those of the SSM.

Background

SSM has supported research for investigating the role of secondary stresses when fracture assessments are performed for cracked structures made of ductile materials. There are evidences that indicate that some secondary stresses, such as weld residual stresses, are not as important as primary stresses for estimating the safety margin against rupture (measured by the J-integral) for the type of ductile materials which can be found in nuclear power plants.

The project was initiated by SKI.

Objectives of the project

The objective of the project has been to perform numerical analyses of girth welds in pipes of different sizes for estimating the weld residual stresses and investigate how the weld residual stresses behave when cracks are introduced. Based on the results, an analysis strategy has been proposed on how the safety factor against these kinds of secondary stresses can be defined for evaluating pipe rupture in ductile materials.

Results

- For the studied cases with stainless steel welds or Alloy 182 welds in stainless steel piping, the relative contribution from the weld residual stresses to CTOD or J decreases rapidly for high values of the limit load parameter L_r . For very high values of L_r the analyses indicate that the contribution from the weld residual stresses to fracture becomes negligible.
- The precise limit of L_r at which the relative contribution from the weld residual stresses is small is likely to depend on the particular material properties, crack geometry and the weld residual stress distribution.
- Based on the analysis result, a new deterministic safety evaluation system is proposed. In the procedure, new safety factors against the fracture toughness are defined where it is distinguished between primary and secondary stresses. Based on the predicted value of L_r at fracture, the safety factor against the local through-thickness secondary stress is lowered. This is assumed also to be valid for thermally induced through-thickness stress gradients. However, no change in safety factor is proposed for global secondary stresses such as thermal expansion stresses.

Effects on SSM

The results of this project will be of use to SSM in safety assessments when cracks are detected in nuclear power plant components. However, SSM wants to further validate the analysis results in this project and the proposed revision of the deterministic safety evaluation system by performing experiments. Such experiments are planned in an ongoing research project.

Project information

Project Leader at SSM: Kostas Xanthopoulos

Project number: 14.42-011210/22094

Project Organisation: Inspecta Technology AB has been managed the project with Peter Dillström as project leader. Magnus Andersson, Iradj Sattari-Far and Weilin Zang have assisted in the development of the project.

SUMMARY

The main purpose of this work is to investigate the significance of the residual stresses for defects (cracks) in ductile materials with nuclear applications, when the applied primary (mechanical) loads are high. The treatment of weld-induced stresses as expressed in the SACC/ProSACC handbook and other fracture assessment procedures such as the ASME XI code and the R6-method is believed to be conservative for ductile materials. This is because of the general approach not to account for the improved fracture resistance caused by ductile tearing. Furthermore, there is experimental evidence that the contribution of residual stresses to fracture diminishes as the degree of yielding increases to a high level. However, neglecting weld-induced stresses in general, though, is doubtful for loads that are mostly secondary (e.g. thermal shocks) and for materials which are not ductile enough to be limit load controlled.

Both thin-walled and thick-walled pipes containing surface cracks are studied here. This is done by calculating the relative contribution from the weld residual stresses to CTOD and the J -integral. Both circumferential and axial cracks are analysed. Three different crack geometries are studied here by using the finite element method (FEM).

- (i) 2D axisymmetric modelling of a V-joint weld in a thin-walled pipe.
- (ii) 2D axisymmetric modelling of a V-joint weld in a thick-walled pipe.
- (iii) 3D modelling of a X-joint weld in a thick-walled pipe. t .

Each crack configuration is analysed for two load cases; (1) Only primary (mechanical) loading is applied to the model, (2) Both secondary stresses and primary loading are applied to the model.

Also presented in this report are some published experimental investigations conducted on cracked components of ductile materials subjected to both primary and secondary stresses.

Based on the outcome of this study, an analysis strategy for fracture assessment of defects in ductile materials of nuclear components is proposed. A new deterministic safety evaluation system is defined, that more realistically handles the contribution to J or CTOD from secondary stresses. In the new procedure we define new safety factors against fracture described by K_I and differentiate between $SF_K^{Primary}$ (relating to primary stresses) and $SF_K^{Secondary}$ (relating to secondary stresses). The procedure is consistent with the presented analyses and experimental data.

TABLE OF CONTENT

Page

1	INTRODUCTION	5
2	ANALYSIS OF INTERNAL CIRCUMFERENTIAL SURFACE CRACKS IN THIN-WALLED PIPES	7
2.1	Simulation of the welding process and crack growth	7
2.1.1	Finite element modelling	7
2.1.2	Thermal analysis	8
2.1.3	Structural analysis	10
2.1.4	Simulation of crack growth	11
2.2	A welded pipe subjected to a primary load	12
2.2.1	Contribution from residual stresses to J and CTOD using an axial loading	12
2.2.2	Relaxation of residual stresses due to unloading	17
2.2.3	Effect of tangent modulus	18
2.2.4	Effect of using linear isotropic hardening	23
2.3	A welded pipe subjected to a thermal load	24
2.4	Discussion on the results for thin-walled pipes	29
3	ANALYSIS OF INTERNAL CIRCUMFERENTIAL SURFACE CRACKS IN THICK-WALLED PIPES	31
3.1	Geometry	31
3.2	Material data	32
3.3	Element mesh	33
3.4	Loading and boundary conditions	35
3.4.1	Simulation of the weld process	35
3.4.2	Simulation of crack growth	35
3.4.3	Primary load	36
3.5	Results	36
4	ANALYSIS OF INTERNAL AXIAL SURFACE CRACKS IN THICK-WALLED PIPES	42
4.1	Geometry	42
4.2	Material data	42
4.3	Element mesh	42
4.4	Loading and boundary conditions	44
4.4.1	Simulation of the weld process	44
4.4.2	Simulation of crack growth	44
4.4.3	Primary load	44
4.5	Results	44
5	EXPERIMENTAL RESULTS	51
5.1	Wilkowski and Rudland, Battelle, USA	51
5.2	Dong et. al., Battelle, USA	52
5.3	Mohr et. al., Edison Welding Institute, USA	52
5.4	Sharples et. al., AEA Technology, UK	54
5.5	Sharples and Gardner, AEA Technology, UK	56
5.6	The IPIRG project, Battelle, USA	57
5.7	Lei et. al., Imperial College, UK	59
5.8	Discussion	60
6	A STRATEGY FOR FRACTURE ASSESSMENT OF DEFECTS IN DUCTILE MATERIALS	61
6.1	Motivation for a new strategy for fracture assessment of defects in ductile materials	61
6.2	Case study 1, a thin-walled pipe containing a circumferential surface crack	62
6.3	Case study 2, a thick-walled pipe containing a circumferential surface crack	65
6.4	Case study 3, a thick-walled pipe containing an axial surface crack	67
6.5	Case study 4, components with through-wall cracks	69
6.6	Recommendations for a new procedure for fracture assessment of defects in ductile materials	71
6.6.1	A new deterministic safety evaluation system	71

6.6.2	Application of the new deterministic safety evaluation system.....	76
7	IMPLEMENTATION OF THE NEW PROCEDURE IN THE FRACTURE	
	ASSESSMENT SOFTWARE PROSACC	80
7.1	Estimation of safety factors in the new deterministic safety evaluation system.....	80
7.1.1	Safety factors for a normal/upset load event, $SF_K = 3.162$	81
7.1.2	Safety factors for an emergency/faulted load event, $SF_K = 1.414$	81
7.2	Choice of options within the ProSACC software	82
8	CONCLUSIONS AND RECOMMENDATIONS	83
9	ACKNOWLEDGEMENT.....	85
10	REFERENCES	86
	APPENDIX A. THE J-INTEGRAL AND CTOD AS FRACTURE PARAMETERS.....	89
	APPENDIX B. CALCULATION OF CTOD	93
	APPENDIX C. LIMIT LOAD OF 2D MODEL	95
	APPENDIX D. LIMIT LOAD OF 3D MODEL	96

1 INTRODUCTION

Structures may fail because of crack growth both in welds and in the heat affected zone (HAZ). The welding process itself induces residual stresses in the weld and HAZ, which contribute to crack growth. The mechanism of growth can be sub critical i.e. IGSCC or fatigue, or critical growth initiation. Two examples of crack growth in welds are studied by Kanninen et al. [1981] and by Hou et al [1996]. So far, it is not self evident which characterising fracture parameter to use when the crack is subjected to weld-induced stresses. The results presented in the scientific literature indicate difficulties in using the J -integral as fracture parameter when residual stresses are present. Some researchers have proposed to use CTOD (Crack Tip Opening Displacement) as a suitable fracture parameters when secondary stresses are also present in the component, see for instance Kanninen et al. [1981] and Hou et al. [1996].

In this report both the J -integral and CTOD (obtained by the 90°-interception construction) are evaluated using finite element analysis, and their validity and usefulness as suitable fracture parameters are discussed.

The main purpose of this work is to investigate the significance of the secondary stresses for defects (cracks) in ductile materials within nuclear applications. The treatment of weld-induced stresses as expressed in the SACC handbook by Andersson et al [1996] is believed to be too conservative for ductile materials. This is because of the general approach does not account for the improved fracture resistance caused by ductile tearing and furthermore there is experimental evidence that the contribution of residual stresses to fracture diminishes as the degree of yielding increases to a high level. Green et al [1993, 1994] and Sharples et al [1993, 1995, 1996] showed in a series of experiments that at low load levels, i.e. small L_r , the influence of the residual stresses was large, but near plastic instability ($L_r = 1$) weld-induced stresses were of little importance. Available procedures for flaw assessments, such as the ASME XI code and the R6 procedure [Milne et al, 1988] treat this issue differently. For instance, the ASME XI code does not consider weld-induced residual stresses in some materials e.g. stainless steel welds. Neglecting weld-induced stresses in general, though, is doubtful for loads that are mostly secondary (e.g. thermal shocks) and for materials which are not ductile enough to be limit load controlled. Several references regarding simulation of the welding process can be found in the literature, see for instance Brickstad and Josefson [1996] and Hou et al. [1996].

The purpose of this study is to investigate the significance of the secondary stresses (mainly weld residual stresses has been studied) for cracks in pipes of ductile materials. Both thin-walled and thick-walled pipes are studied. This is done by calculating the relative contribution from the weld residual stresses to CTOD and the J -integral. Both circumferential and axial cracks are analysed. However, the conclusions from this study are also valid for others components made of ductile materials.

Three different crack geometries are studied here, by using the finite element method (FEM).

- The first analysis is a 2D axisymmetric modelling of a V-joint weld in a thin-walled pipe. The crack introduced in this analysis is a complete circumferential internal surface crack in the centre of the weld. The results of this analysis are given in Chapter 2 of this report.
- The second analysis is similar to the first analysis, but for a thick-walled pipe. The results of this analysis are given in Chapter 3 of this report.
- The third analysis is a 3D modelling of an X-joint weld in a thick-walled pipe. The crack geometry in this analysis is a semicircular axial internal surface crack in the centre of the weld. The results of this analysis are given in Chapter 4 of this report.

Each crack configuration is analysed for two load cases:

- Only primary (mechanical) loading is applied to the model.
- Both secondary stresses and primary loading are applied to the model.

The steps in the analyses of the cases subjected to both primary and secondary stresses are given below:

- The welding process is simulated to introduce weld residual stresses (secondary stresses) in the model of the pipe.
- The crack is introduced within the model.
- A primary load is applied. For this “combined” loading case, the fracture mechanics parameters J and CTOD are calculated.

The relative contribution from the secondary stresses (mainly weld residual stresses in this study) is calculated in this report according to the following definitions:

$$\begin{aligned}
 \text{CTOD}_{\text{contribution from residual stresses}} &= \frac{\text{CTOD}_{\text{combined}} - \text{CTOD}_{\text{primary}}}{\text{CTOD}_{\text{primary}}} \\
 J_{\text{contribution from residual stresses}} &= \frac{J_{\text{combined}} - J_{\text{primary}}}{J_{\text{primary}}}
 \end{aligned}
 \tag{1-1}$$

where

- $\text{CTOD}_{\text{combined}}, J_{\text{combined}}$ CTOD and J calculated from load cases with both weld residual stresses and primary loading.
- $\text{CTOD}_{\text{primary}}, J_{\text{primary}}$ CTOD and J calculated from load cases with primary loading only.

Details of these analyses are previously reported by Delfin et al. [1997] and Andersson and Dillström [2004].

This report covers the main parts of these two reports. Also presented in this report are some published experimental investigations conducted on cracked components of ductile materials subjected to both primary and secondary stresses. Based on the outcome of these results, an analysis strategy for fracture assessment of defects in ductile materials of nuclear components is proposed in Chapter 6 of this report. Implementation of this analysis strategy into the fracture assessment software ProSACC is given in Chapter 7 of this report.

2 ANALYSIS OF INTERNAL CIRCUMFERENTIAL SURFACE CRACKS IN THIN-WALLED PIPES

The finite element analysis of thin-walled pipes containing circumferential cracks subjected to welding residual stresses and mechanical loads is briefly presented in this section. More details of this analysis are given in Delfin et al. [1997].

2.1 Simulation of the welding process and crack growth

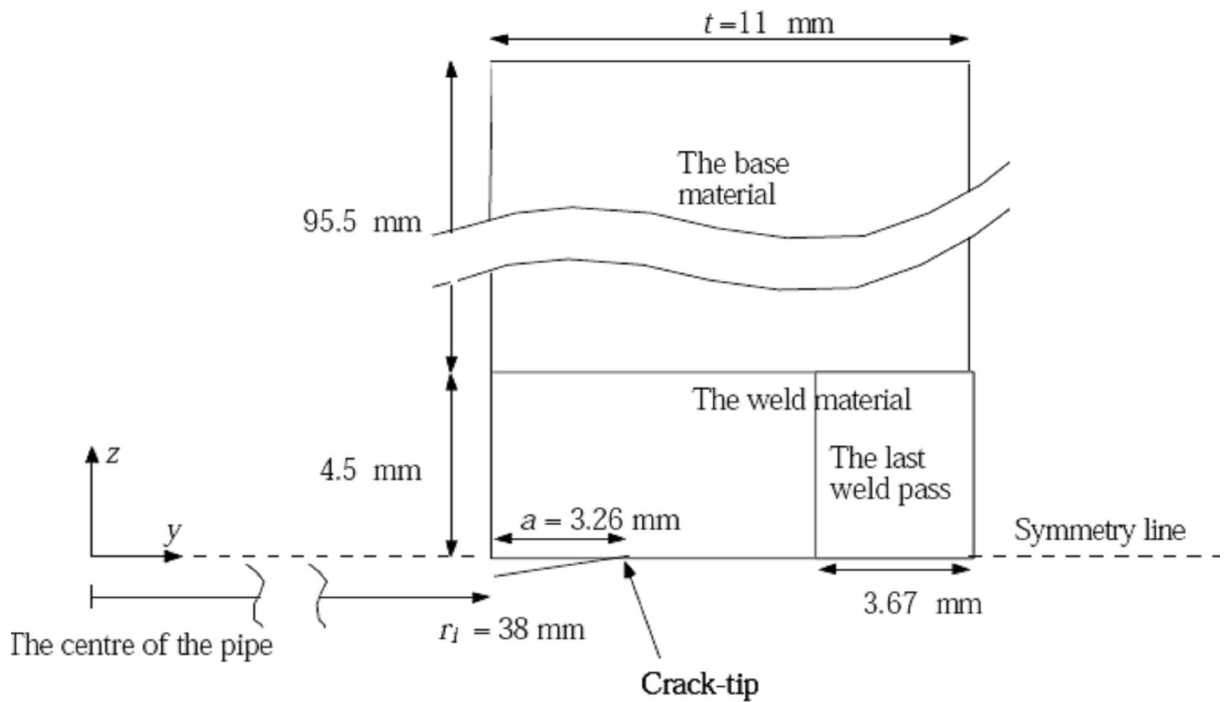
The modelled pipe has an inner radius, $r_i = 38$ mm and a wall-thickness, $t = 11$ mm. The geometry is depicted in Fig. 2.1. The weld is oriented circumferentially. The choice of geometry is guided by the type of stress field obtained for thin walled pipes. The axial stresses are essentially through-thickness bending, whereas in a thick-walled pipe they are more complex and also less severe. A non-linear uncoupled thermoplastic based model was used. The thermal analysis and the stress analysis are described in the two following subsections. The general procedure of simulation follows that of Brickstad and Josefson [1996].

The geometry of the weld modelling is simplified in the following ways:

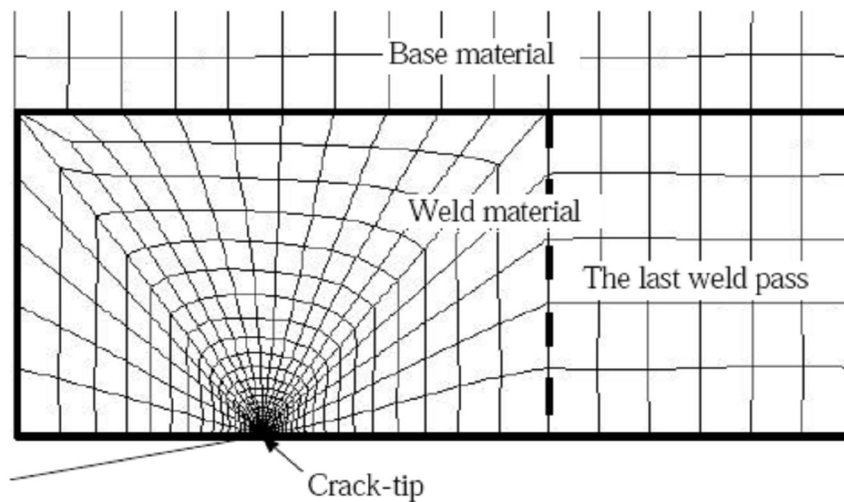
- Only the last weld pass is modelled. This is motivated by the fact that for a thin-walled pipe, as in this case, the last weld pass in a series of passes will cause a uniform heating of the entire thickness of the pipe.
- Only half of the pipe section is modelled since the crack plane coincides with the symmetry plane.
- It has been observed that the residual stresses in a circumferentially welded thin-walled pipe are approximately rotationally symmetric. This justifies the use of an axisymmetric model.
- The weld geometry is somewhat simplified, since a rectangular groove has been used.

2.1.1 Finite element modelling

The same mesh has been used in both the thermal and the stress analysis. The elements used are eight-noded biquadratic axisymmetric elements with full integration, which have proved to give the best convergent behaviour. The crack plane is also the symmetry plane which allows for the modelling of only half the pipe section, see Fig. 2.1. Anticipating that a crack is to be introduced, the mesh is focused on a point where the crack-tip will be located. The smallest elements used are of sizes 0.001 mm. This was necessary in order to evaluate the CTOD at low load levels. The FEM code ABAQUS [1995] uses a Newton iteration method improved by a line search algorithm, which is effective when the initial iterations are relatively far from the solution.



a)



b)

Fig. 2.1. a) The geometry of a cross section of the pipe wall in the z -direction. Only half the pipe is shown due to symmetry. b) Detail of the mesh used in the finite element analysis.

2.1.2 Thermal analysis

The thermal problem was treated as follows: A heat flux [W/m^3] was activated in the weld material that constitutes the last weld pass. The use of only the last weld pass simplifies the calculations substantially in the respect that birth of elements need not be considered. An unrealistic consequence of the assumption of axial symmetry is that the heat flux is applied instantaneously around the circumference of the pipe. This can to some extent be compensated for by assuming that the heat flux is applied during a finite period in time with an assumed triangular time variation corresponding to the approach and passing of the weld torch. The heat flux h can be expressed as

$$h = \frac{v}{V_p} Q_{line} \quad (2-1)$$

where Q_{line} is the net line energy [J/m] used during the welding and v is the travel speed of the weld electrode, V_p is the weld pass volume. However the weld pass volume V_p can not be defined in a 2-D model and must be chosen in such a way that some empirical observations are satisfied. The molten zone size and the distance from the weld-base material interface to HAZ must be realistic, see Brickstad and Josefson [1996]. Once its value has been set the duration Δt of the heat flux period can be determined from

$$\Delta t = \frac{V_p}{A_p v} \quad (2-2)$$

where A_p is the area of the cross section of the weld pass. However it should be pointed out that the objective here is to achieve a relatively high residual stress levels and properly infer the residual stresses through plastic strains, rather than simulating a particular stress field.

The boundary conditions allow for both convection and radiation. The axisymmetric conditions assumed imply that the heat losses in the axial direction are neglected. Radiation losses are dominant for higher temperatures near the weld. Convection losses are important for lower temperatures some distance away from the weld. A combined boundary condition, which takes both radiation and convection into account, is used in this work, Argyris et al [1983]. The resulting heat transfer coefficient α_h is

$$\begin{aligned} \alpha_h &= 0.0668T \text{ (W/m}^2\text{)}, & \text{for } 0 < T < 500 \text{ }^\circ\text{C} \\ \alpha_h &= 0.231T - 82.1 \text{ (W/m}^2\text{)}, & \text{for } T > 500 \text{ }^\circ\text{C} \end{aligned} \quad (2-3)$$

The other necessary thermal data for both the weld and base material are given in Table 2.1.

Table 2 1. Thermal properties used in the FEM analysis.

T [°C]	c_p [J/kg°C]	λ [W/m°C]	α [10 ⁻⁶ /°C]
20	442	15.0	19
200	515	17.5	19
400	563	20.0	19
600	581	22.5	19
800	609	25.5	19
1000	631	28.3	19
1200	654	31.1	19
1340	669	33.1	19
1390	675	66.2	19
2000	675	66.2	19

2.1.3 Structural analysis

In the structural analysis the temperatures taken from the thermal analysis are used to calculate the stresses. Only small strain theory is considered. In Brickstad and Josefson [1996], it was observed that the difference in the weld-induced stresses between small strain theory and large strain theory is small. The von Mises yield criterion and associated flow rule are used together with kinematic hardening and a bilinear representation of the stress strain curve. Kinematic hardening rather than isotropic hardening is chosen because it is believed to better model reverse plasticity and the Bauschinger effect that is expected to occur during welding. It is also believed that an insufficient number of stress cycles occur during the single-pass welding for symmetrization of the hysteresis loop to occur, a situation which would have been better represented by isotropic hardening. The use of only the last weld pass simplifies the calculations in the same way as in the thermal analysis in the respect that birth of elements need not be considered. The material in both the weld and the base has the same mechanical properties. This choice serves the purpose of limiting the number of parameters affecting the fracture problem. The mechanical properties used in the analysis are presented in Table 2.2.

Table 2.2. Mechanical properties used in the FEM analysis.

T [°C]	E [10 ¹¹ Pa]	ν	σ_y base [MPa]	E_T/E
20	2.0	0.278	230	0.014
200	1.85	0.288	184	0.014
400	1.70	0.298	132	0.014
600	1.53	0.313	105	0.014
800	1.35	0.327	77	0.014
1000	0.96	0.342	50	1 · 10 ⁻⁴
1200	0.50	0.350	10	1 · 10 ⁻⁴
1340	0.10	0.351	10	1 · 10 ⁻⁴
1390	0.10	0.353	10	1 · 10 ⁻⁴
2000	0.10	0.357	10	1 · 10 ⁻⁴

The resulting axial stress across the symmetry line at $T = 22.5$ °C is shown in Fig. 2.2. For this relatively thin-walled pipe the stress distribution is mainly that of bending. The small bump at the weld pass boundary is believed to be a consequence of the numerical modelling. The crack will be introduced with its crack-tip located at 3.26 mm from the inside surface, which is not close to the bump. Thus, the bump will not be of any significance for the fracture analysis.

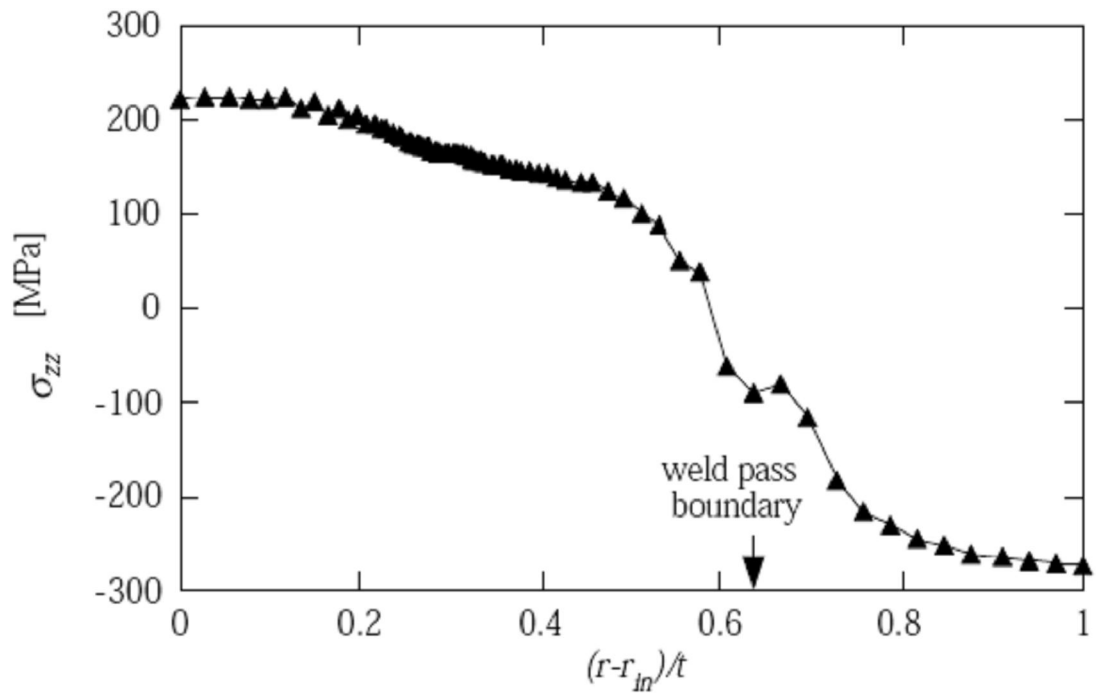


Fig. 2.2. The axial residual stress along the symmetry line i.e. in the weld centre line.

2.1.4 Simulation of crack growth

After the welding process is conducted and the pipe has cooled down to room temperature a crack is introduced at the weld centre line by means of gradual node relaxation starting from the inside of the pipe. The final crack depth is 3.26 mm. The axisymmetry of the problem allows only for a completely circumferential crack to be modelled. The crack is restricted to grow in the radial direction. A physical growth mechanism can be stress corrosion or fatigue. The chosen method of sequentially releasing the nodes along the chosen growth direction gives a path dependent J -integral. This is simply because growth does not represent proportional loading. When the crack reached its final length, loads will be applied and as the loads are increased the J -integral becomes, from a practical view, path independent.

2.2 A welded pipe subjected to a primary load

2.2.1 Contribution from residual stresses to J and CTOD using an axial loading

An axial tensile load was applied to the pipe both with and without residual stress present. As the axial load, which is a primary load, was increased in very small steps the J -integral and the CTOD were calculated. The limit load parameter L_r is defined as P/P_g where P is the applied load and P_g is the limit load. For $P = P_g$ the ligament is deformed plastically. In Fig. 2.3 the load-displacement curve $P - \delta$ is presented and P_g is determined by the intersection of the two straight lines shown. The displacement, δ , is evaluated at the loading point. The value of the limit load is found to be $P_g = 228$ MPa. In this way it is possible to define a limit load from the finite element solution which in a sense is more physically motivated than for example handbook solutions, where the material is assumed to behave elastic perfectly-plastic. This L_r -solution is used throughout this paper. The solution obtained from the handbook Andersson et al. [1996], which assumes that the material behave elastic perfectly-plastically, gives $P_g = 162$ MPa. The difference between these two definitions of P_g is quite significant. This can be explained by the effect of hardening and by the way the von Mises criterion is fulfilled. The introduction of a crack makes it possible for the stress components to redistribute in such a way that the axial stress becomes greater than the yield stress in the ligament, which is not allowed for in the handbook solution. To demonstrate the effect of this stress redistribution, the $P - \delta$ curve for the considered material with vanishing hardening, is also shown in Fig. 2.3. The elastic perfectly-plastic limit load is then found to be 192 MPa.

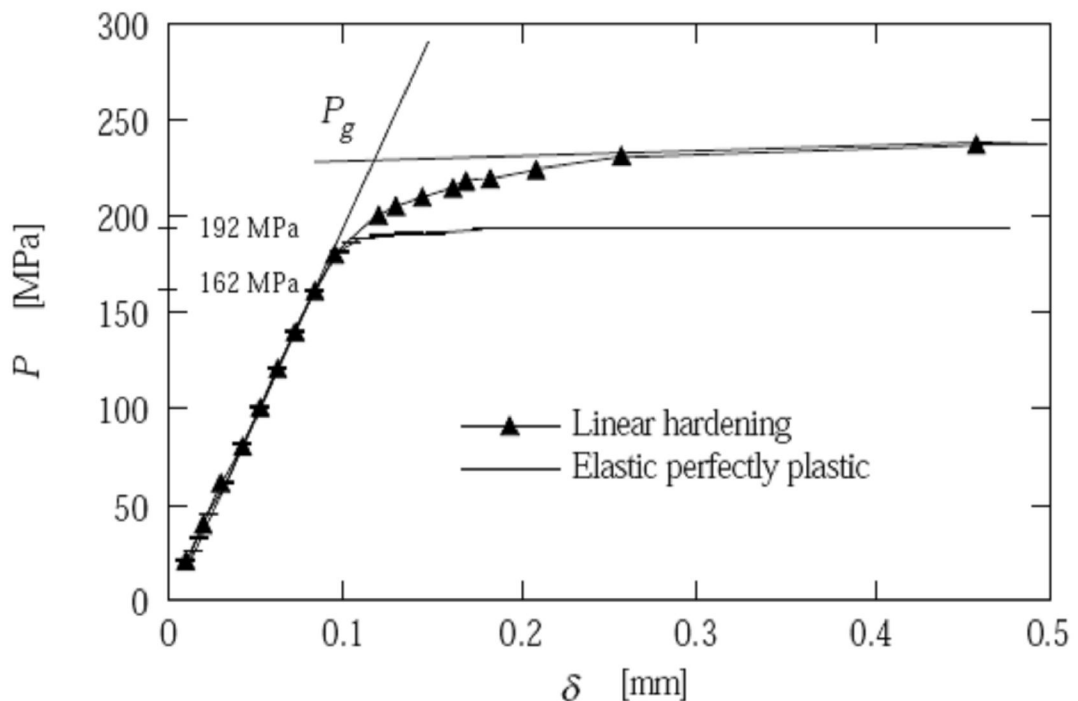


Fig. 2.3. Load versus the displacement at the end of the pipe.

The definition of P_g is somewhat arbitrary. Other limit load solutions may be used and the results may then be calibrated accordingly by multiplying the L_r scales in Fig. 2.4 to Fig. 2.9 by an appropriate factor.

The following three figures show the comparisons of J (Fig. 2.4), CTOD (Fig. 2.5), the relative contribution from residual stresses to J and $CTOD$ (Fig. 2.6), during axial loading. The relative contribution from the weld residual stresses is calculated according to Equation (1-1).

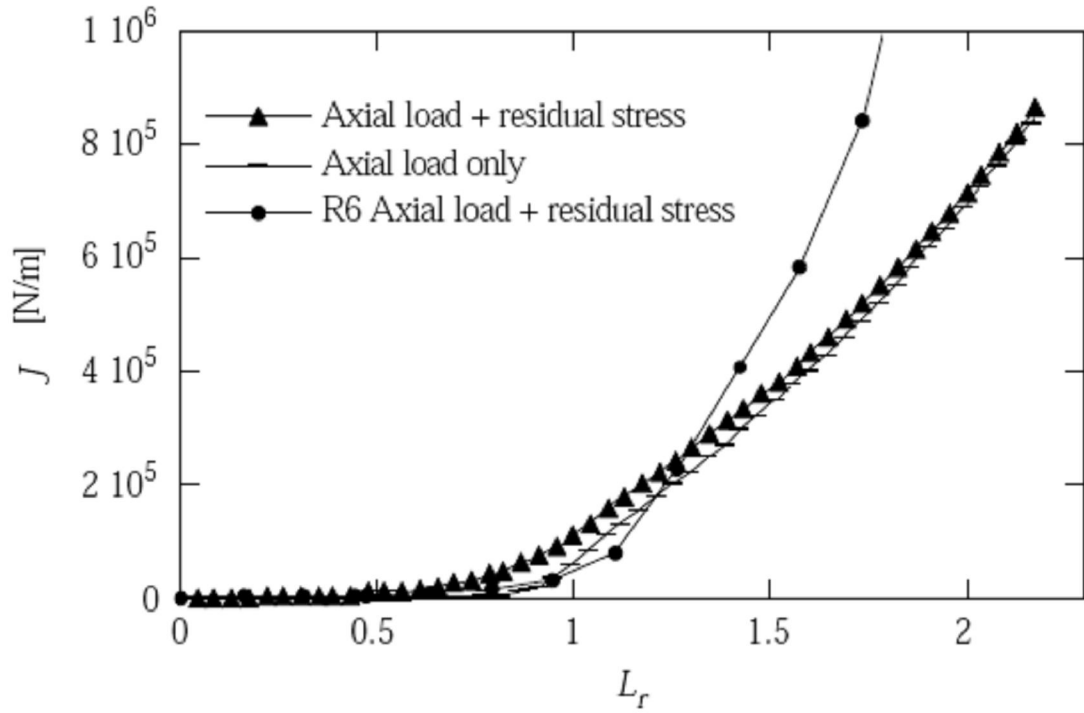


Fig. 2.4a. The J -integral as a function of L_r . The J -values are evaluated at the tenth contour i.e. a ring with a radius of nine elements from the crack tip.

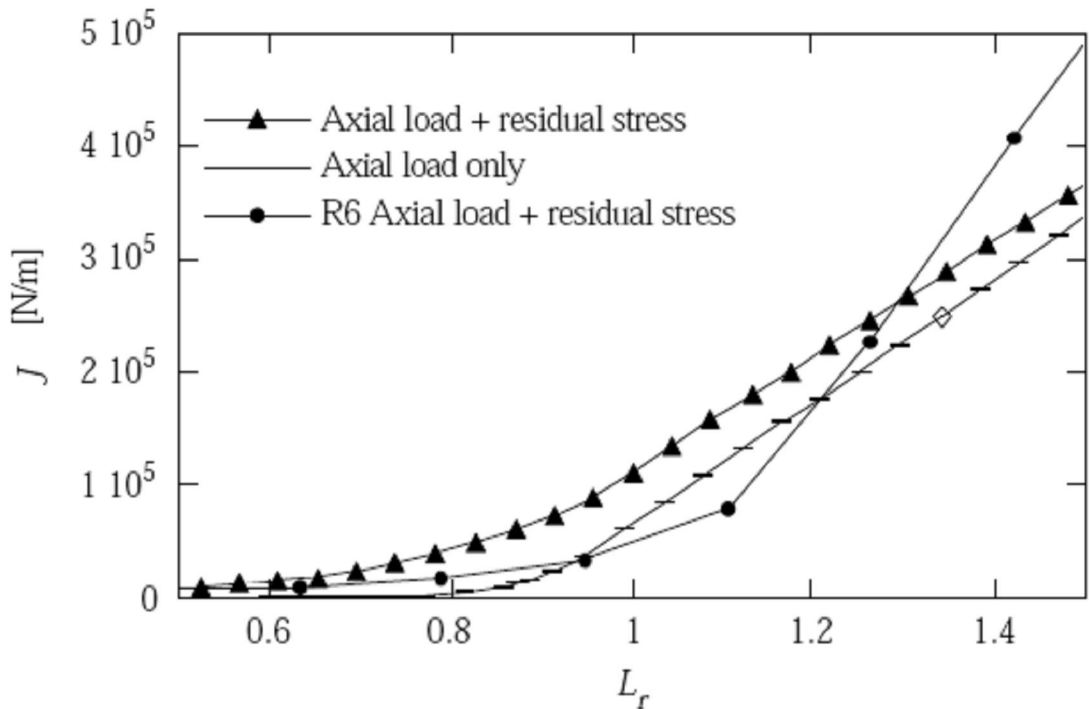


Fig. 2.4b. $J - L_r$ resolved for load values closer to $L_r = 1.0$.

A short description on J and CTOD as fracture parameters for welded structures is given in Appendix A. Also, a method to evaluate CTOD from finite element analyses is given in Appendix B.

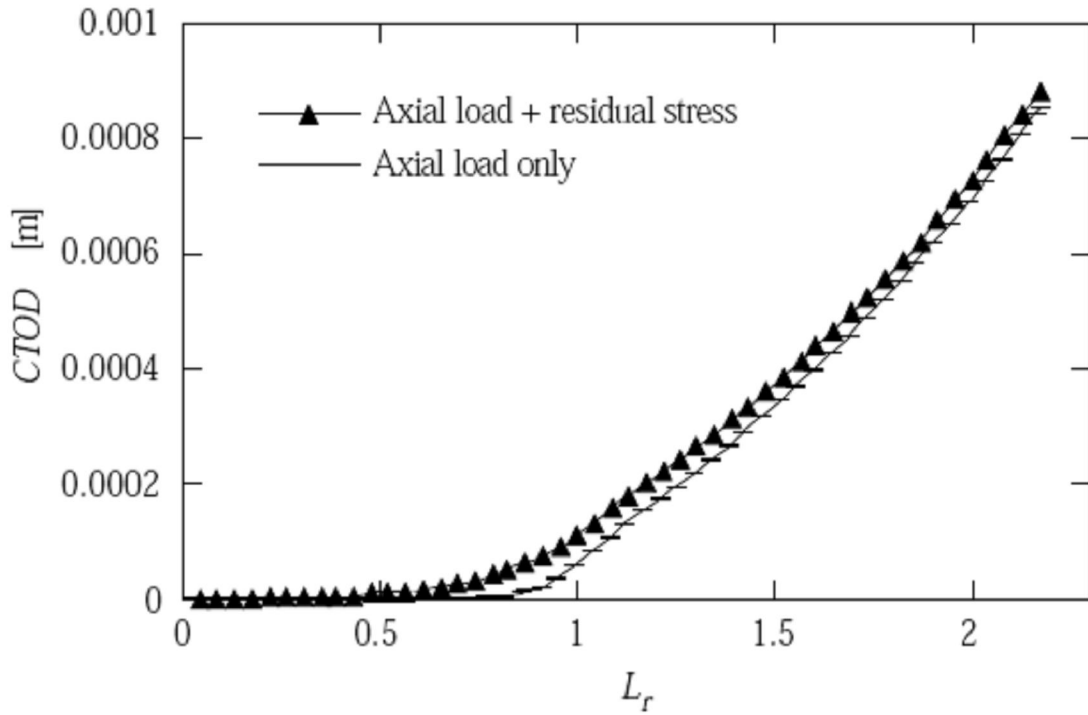


Fig. 2.5a. The CTOD as a function of L_r .

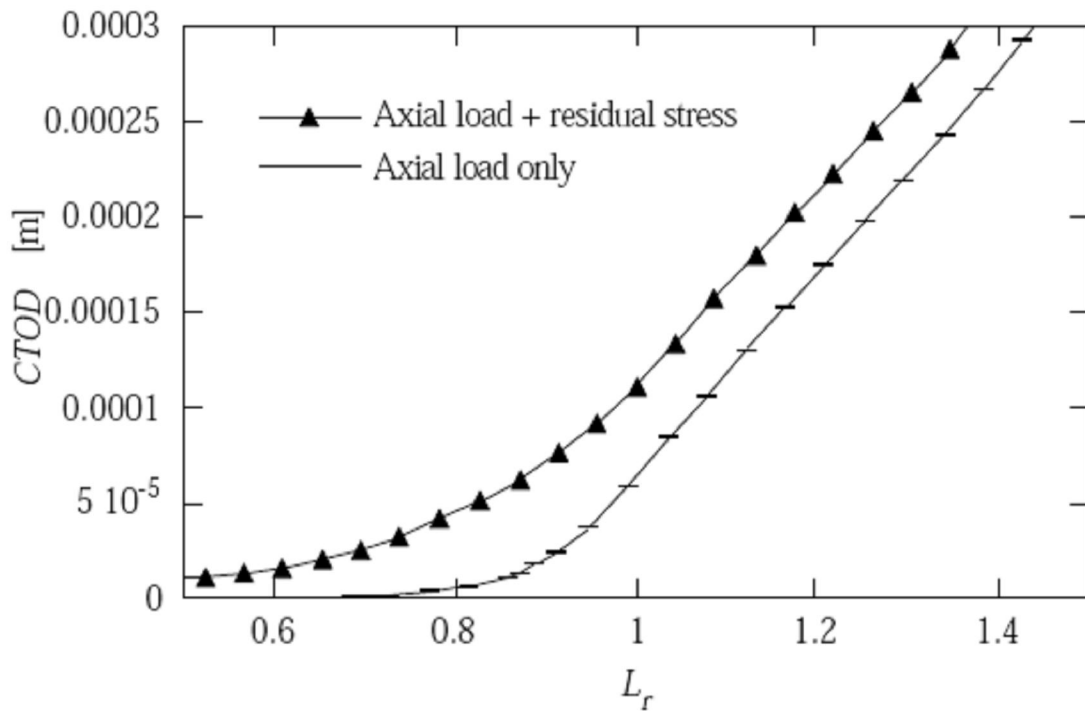


Fig. 2.5b. CTOD - L_r resolved for load values closer to $L_r = 1.0$.

The principal behaviour of the J -integral is as expected for primary loads. The curve in Fig. 2.4 is essentially composed of an elastic part and a plastic part with a steep slope; see Bergman [1991] for a review on differences between primary and secondary loads. The results of Kumar et. al. [1991] are quite similar, though they used a thermal load as secondary load.

An evaluation of the case using a combination of an axial load and residual stresses according to the R6-procedure is also included in Fig. 2.4. The R6-procedure gives a slightly non-conservative estimation between $L_r = 0.95$ and $L_r = 1.2$. However it should be remembered that L_r is not defined by a limit load equal to 162 MPa as would normally be the case in a standard handbook solution, such as Andersson et al. [1996], instead a definition of the limit load equal to 228 MPa based on fully plastic behaviour, as shown in Fig. 2.3, is used.

It is interesting to quantify the relative contribution from the residual stresses during axial loading for both the J -integral and the CTOD. In Fig. 2.6a below, the relative differences between J with both residual and axial stresses present, $J_{combined}$, and J with only axial stresses present, J_{axial} , are shown. The same type of quantity formed with J replaced by CTOD, is plotted in Fig. 2.6b below. The CTOD could not be evaluated for L_r less than about 0.7 for the case with only axial loading despite the fine mesh. The irregular behaviour for the case with both residual stresses and axial stresses present for L_r less than about 0.8 can be explained by path dependency of J at low axial load levels, which is a result of the stress history due to crack growth.

The close coincidence of the J -curves and the CTOD curves in Fig. 2.6 suggests that the relation in equation (2-4) holds. This suggests also that J can be a possible fracture parameter if the integration contours are not far from the crack-tip. However only an experimental investigation can give a definite answer to the question of whether J or CTOD can be useful fracture parameters during this type of loading situation with residual stress- and strain-fields present. The contribution to the fracture parameters from the residual stresses is negligible for large L_r as shown in Fig. 2.6b. The contribution from the residual stresses decreases rapidly between $L_r = 0.8$ and $L_r = 1.3$. For $L_r = 1.3$ the contribution of the residual stresses is 20% of the axial load contribution. For $L_r = 1.6$ the contribution of the residual stresses is about 7%. An important observation is that this makes it essential to have a reliable value for L_r when plastic failure occurs i.e. when $L_r = L_r^{max}$. In the present investigation the value of L_r at plastic collapse can not be defined. This is due to the linear hardening material model adopted (with its bilinear representation). Reasonably close to $L_r = 1.0$ the results should be valid also for other type of hardening behaviour. However, the results should be viewed with caution if a quantitative conclusion is desired. This is because the results are qualitative in the sense that a particular geometry and material model are chosen in this work.

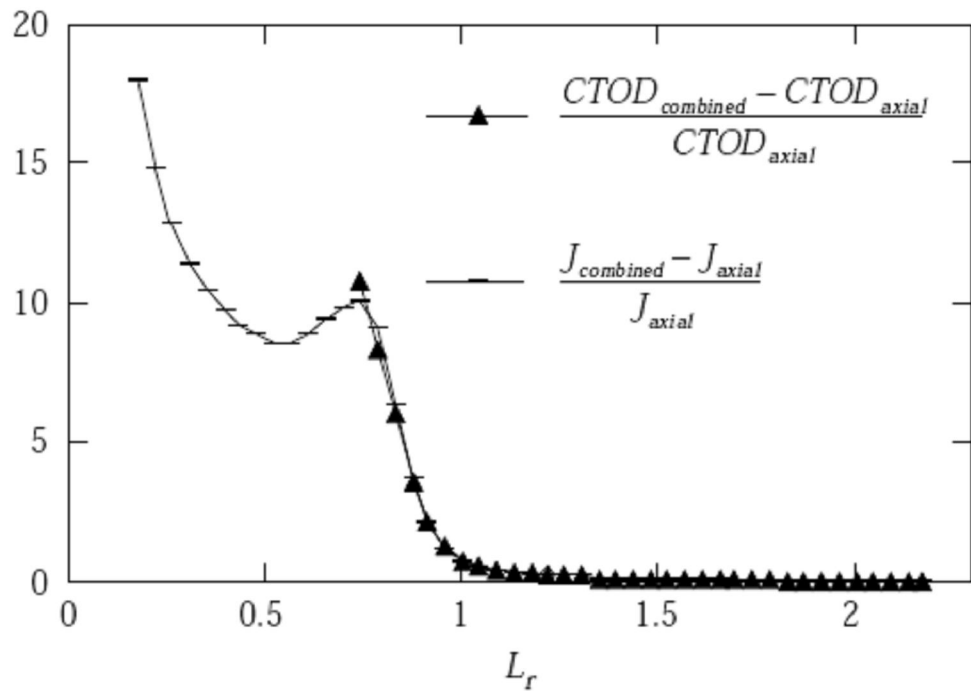


Fig. 2.6a. The relative difference of J and CTOD with and without residual stresses.

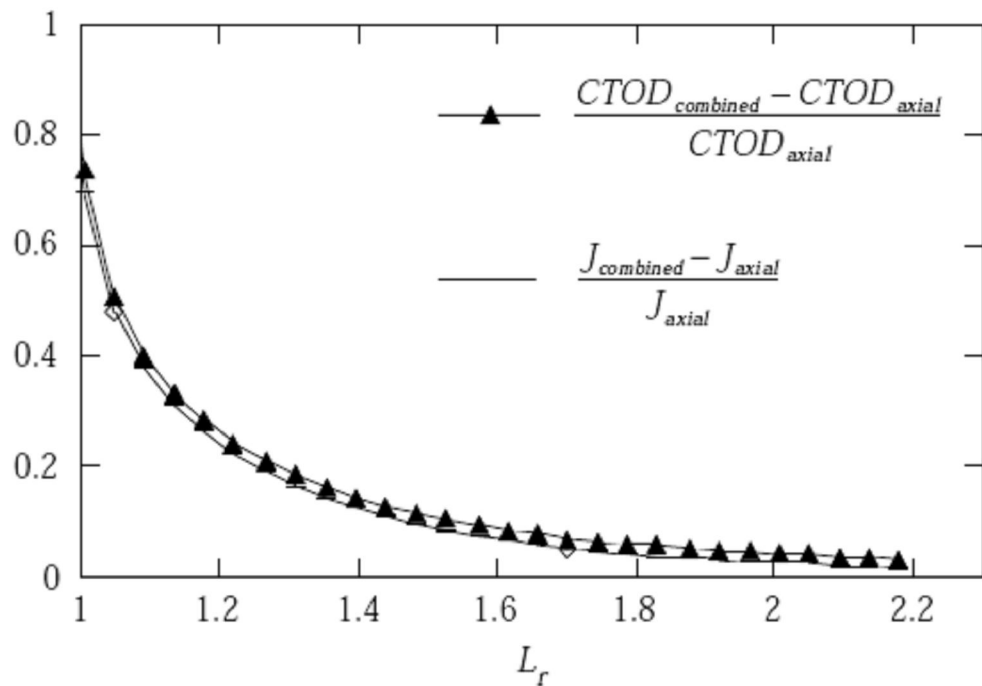


Fig. 2.6b. Close up for a better resolution at high L_r -values.

The parameter d is shown in Fig. 2.7 below, for the load cases with and without residual stresses. The non-dimensional parameter d is defined through the relation, c.f. Shih et al [1981],

$$CTOD = d \cdot J_{SSY} \tag{2-4}$$

It should be mentioned that in Shih et al. [1981], a Ramberg-Osgood material is considered.

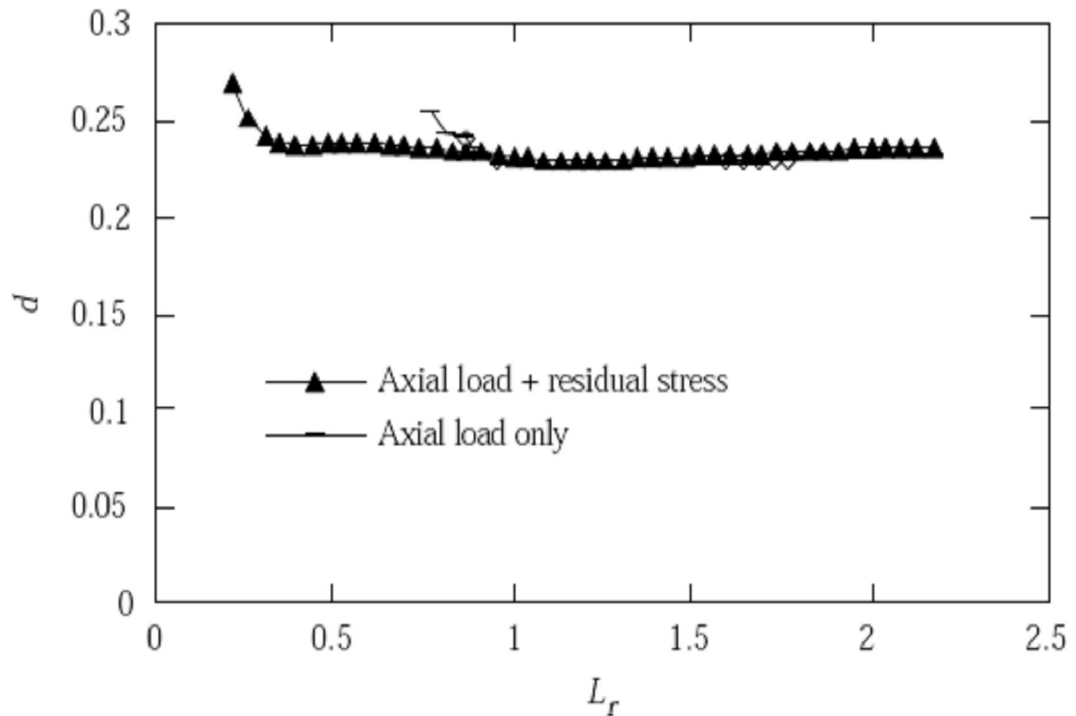


Fig. 2.7. The values of the non-dimensional parameter d as a function of L_r . The parameter d is defined according to Eq. (2-4).

The values of d in Fig. 2.7 for both the case with the residual stresses present and the case with only axial stresses, are scattered very little from the value 0.23. This means that at least in this investigation the J -integral is well defined through Equation (2-4) with $d = 0.23$. However remember that for J evaluated with remote contours the J -integral seems definitely path dependent. Appendix A provides a discussion of this problem. The reason for the cut-off at $L_r = 0.8$, for the case of axial loading only, is that CTOD could not be evaluated even with the fine mesh used. The corresponding cut-off for the case of both axial loading and residual stresses is $L_r = 0.25$. In this case CTOD may be undefined because of the crack growth prior to the application of axial loading, see Appendix B.

2.2.2 Relaxation of residual stresses due to unloading

To investigate the effect of relaxation, unloading were performed for the uncracked geometry from different axial load levels, see Fig. 2.8. The stress distribution along the symmetry line may serve as an input in an engineering estimation e.g. a fracture assessment according to the R6-procedure. It is not relevant to unload the cracked pipe since the J -integral and the CTOD become meaningless in this type of unloading situations.

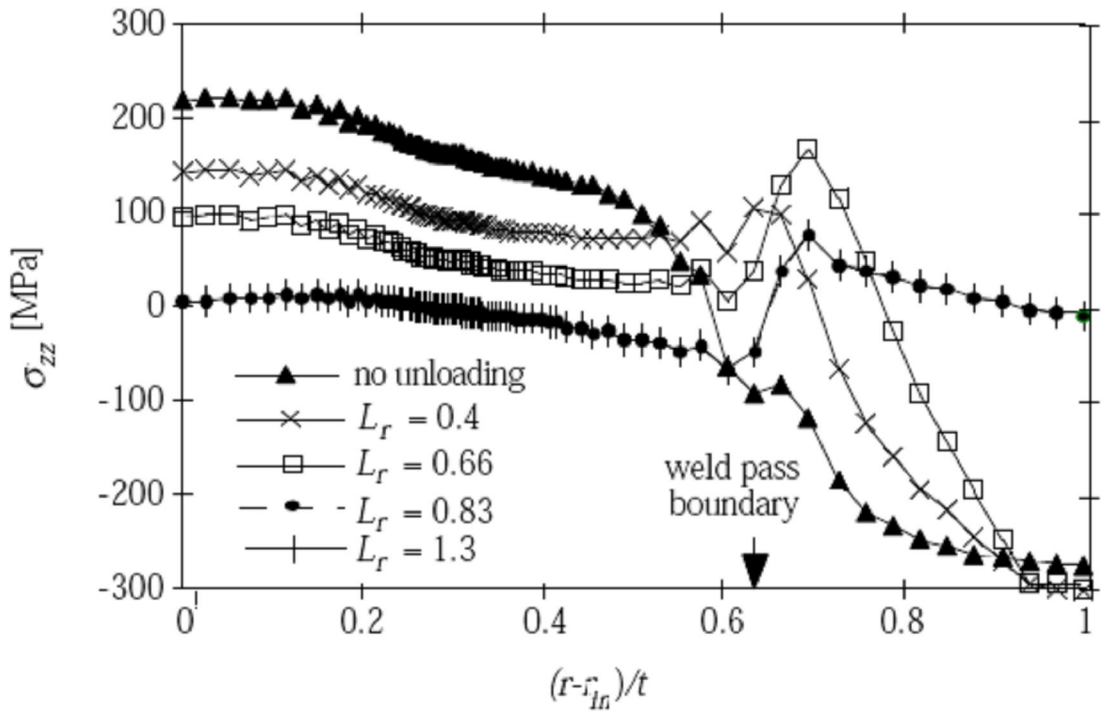


Fig. 2.8. The axial stresses at the symmetry line after unloading. The L_r -values represent the different load levels from which the unloading was performed.

The resulting levels of the residual stress distributions, after unloading, decreases with increasing L_r , and does not change for load levels larger than $L_r = 0.8$. For a circumferential surface crack, on the inside of the pipe, not deeper than 40% of the wall-thickness, there will clearly be only very small residual stresses after unloading from a high level of axial load. The stress peak of 80 MPa for the case $L_r = 0.8$ is located about 70% of the wall thickness from the inside of the pipe, through the wall.

2.2.3 Effect of tangent modulus

The chosen bi-linear kinematical hardening material model limits the analyses in two ways. It can only approximately account for the more realistic non-linear hardening behaviour of materials. Secondly, a point of plastic collapse can not be defined, in our notation, this means that no L_r^{max} exists. This section addresses those limitations.

To get some understanding on how these limitations affect conclusions, a series of runs was performed on the same pipe geometry. The material models were the same except for a different tangent modulus, E_T . The residual stresses, CTOD and J , the relative differences, $(J_{combined} - J_{axial})/J_{axial}$ and $(CTOD_{combined} - CTOD_{axial})/CTOD_{axial}$ were calculated and the results are shown in Fig. 2.9 to Fig. 2.12.

In Fig. 2.9 it can be seen that for $E_T/E = 0.0001$, which is nearly perfectly plastic material behaviour, the residual stresses attain the highest tensile stress level. The stress distribution changes shape somewhat but the stress level does not change very much with different amount of hardening. Note however that close to the inside of the pipe the stresses are fairly independent of the tangent modulus.

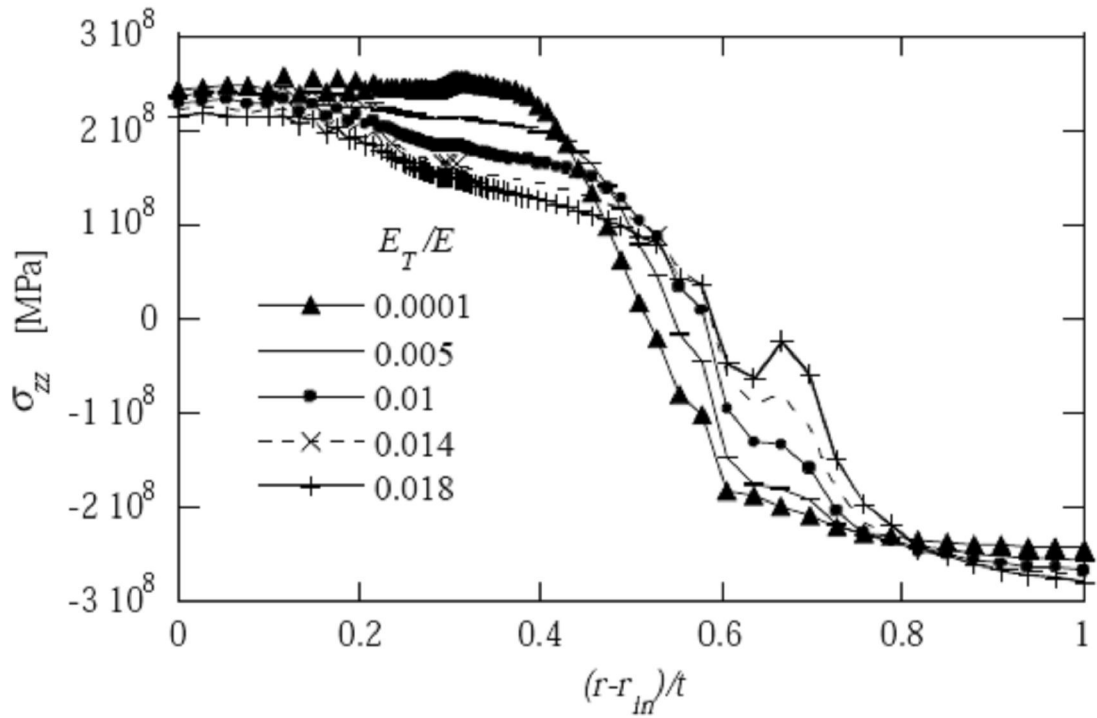


Fig. 2.9. Axial residual stresses at the weld centreline for $E_T/E = 0.0001, 0.005, 0.01, 0.014, 0.018$.

The limit load P_g definition, with graphical determination, used in section 2.1.1 is not appropriate here. In order to compare J and CTOD using the same scale, L_r is defined as $L_r^{R6} = P/P_g^{R6}$ where P_g^{R6} is the limit load used in the R6-method and in the handbook of Andersson et al. [1996].

For the same L_r -value, more plasticity is introduced with decreasing hardening. This is consistent with the behaviour of the $J - L_r$ and the CTOD - L_r curves, Fig. 2.10 and Fig. 2.11, which rise steeper with decreasing hardening.

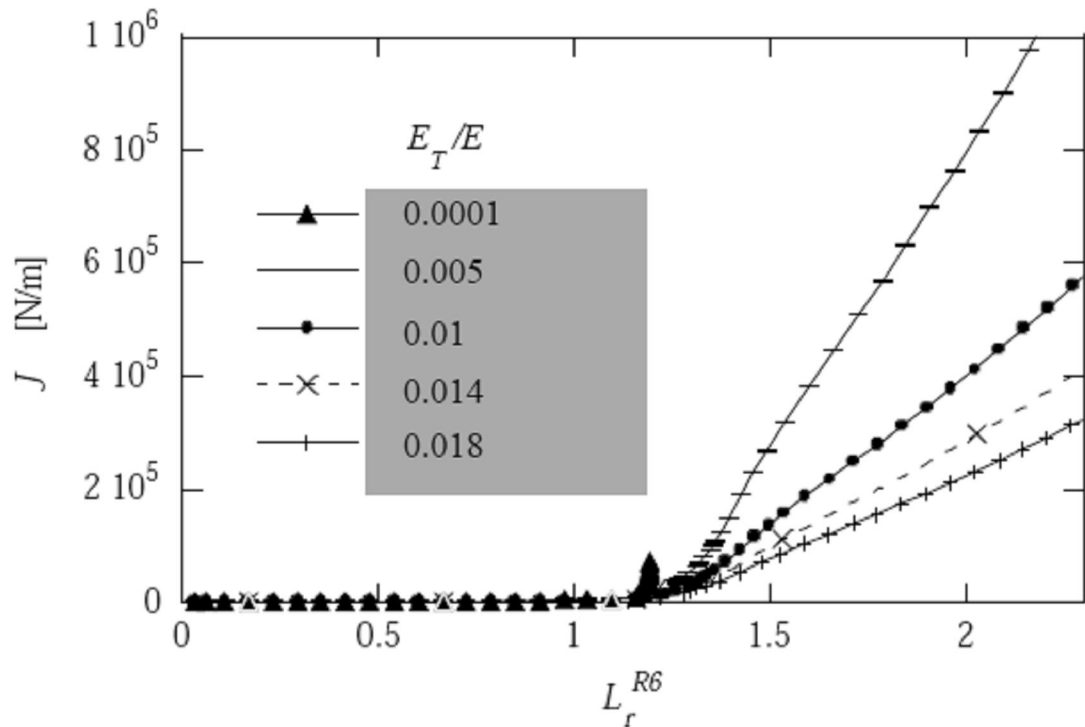


Fig. 2.10a. J_{axial} (axial load only) as a function of L_r for different E_T/E .

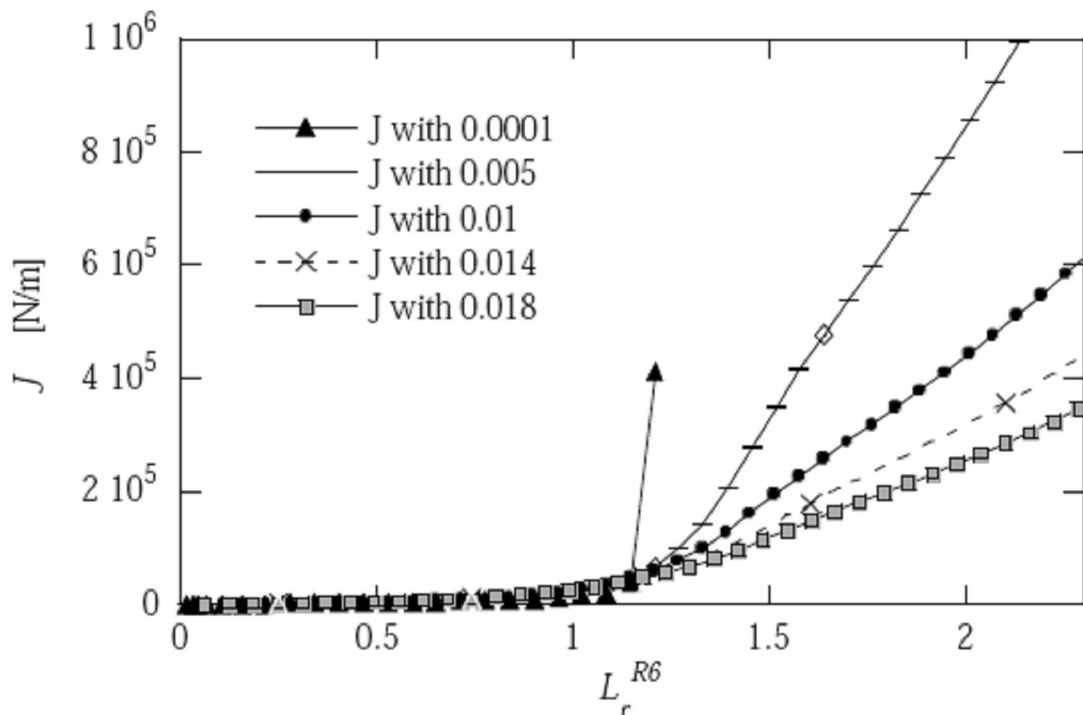


Fig. 2.10b. $J_{combined}$ (axial load and residual stresses) as a function of L_r for different E_T/E .

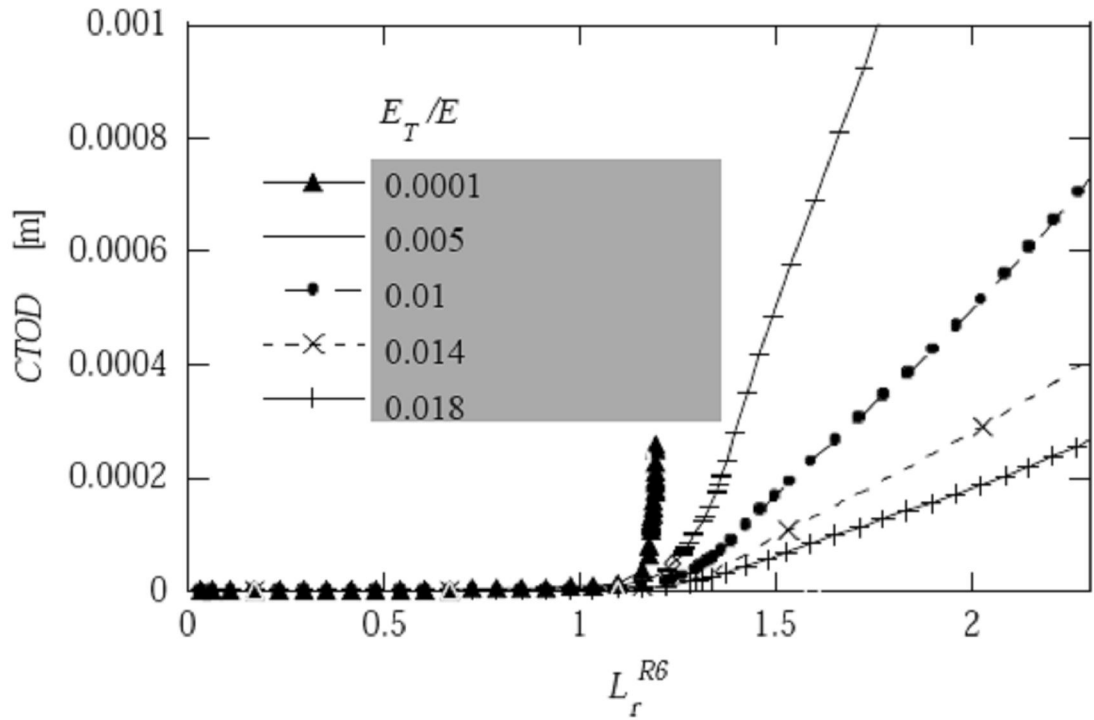


Fig. 2.11a. $CTOD_{axial}$ (axial load only) as a function of L_r for different E_T/E .

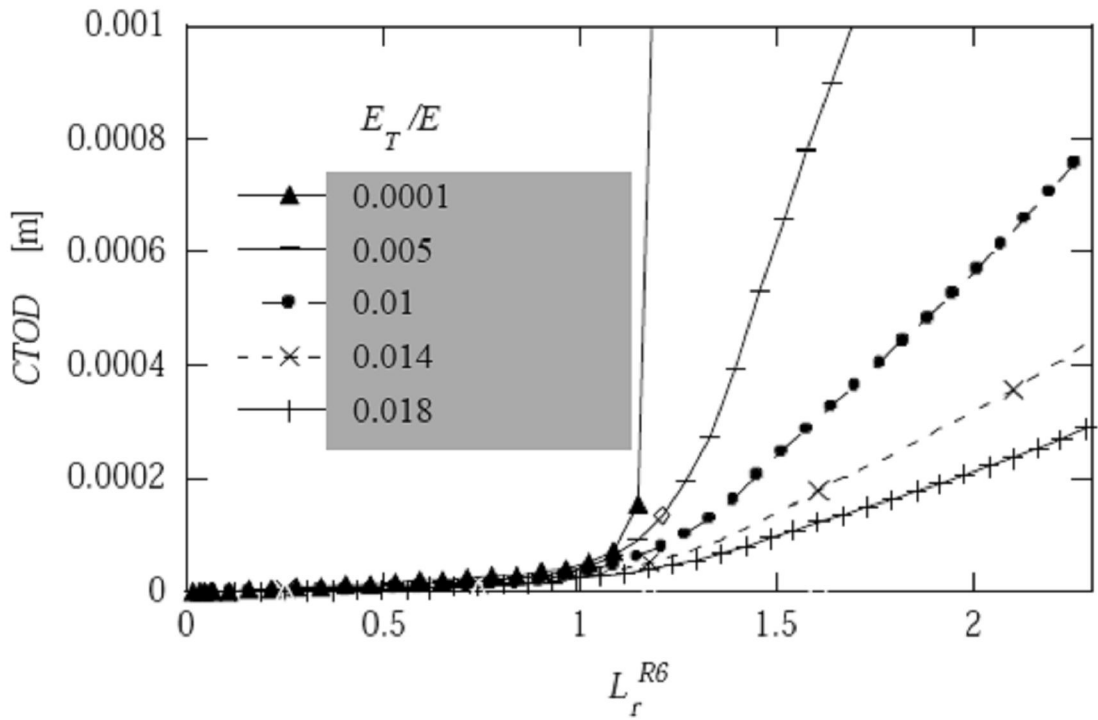


Fig. 2.11b. $CTOD_{combined}$ (axial load and residual stresses) as a function of L_r for different E_T/E .

The relative differences of J and CTOD, Fig. 2.12, vanish at a higher rate the lower the hardening is. For $E_T/E = 0.0001$ there is no curve because L_r does not get higher than $L_r = 1.25$ because of widespread plasticity.

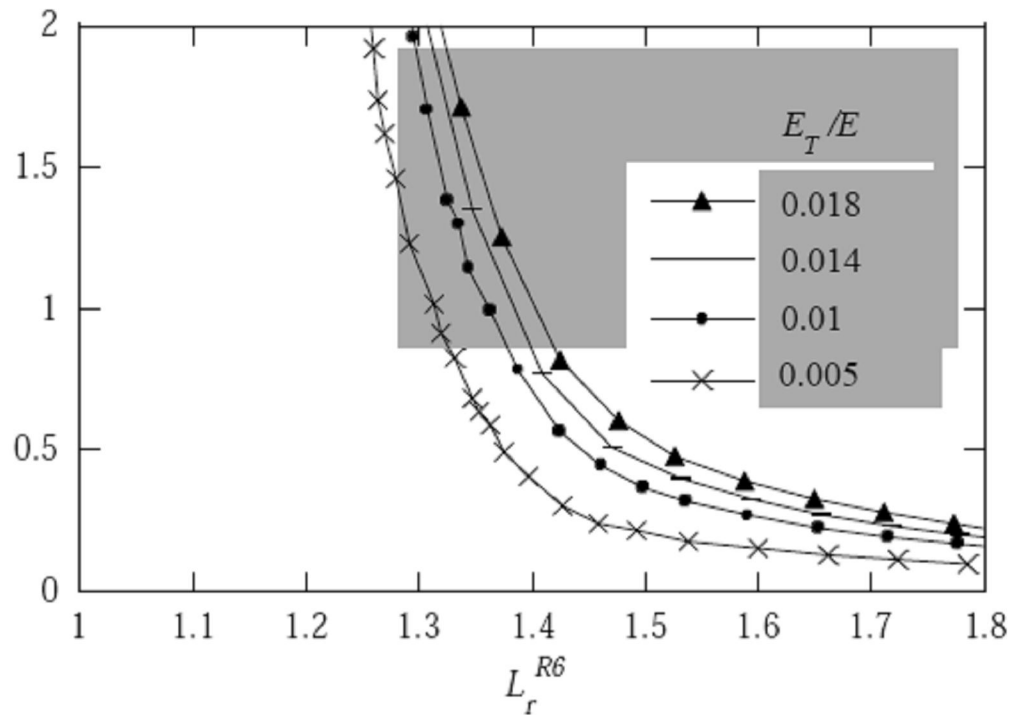


Fig. 2.12a. The quantity $(J_{combined} - J_{axial})/J_{axial}$ as a function of L_r for different E_T/E .

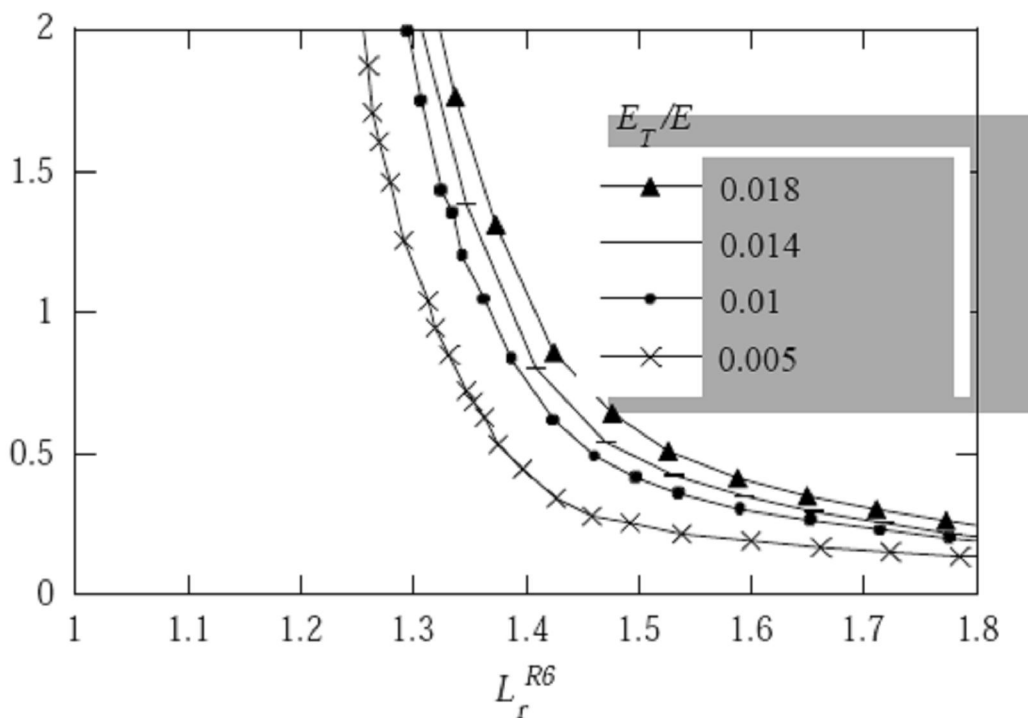


Fig. 2.12b. $(CTOD_{combined} - CTOD_{axial})/CTOD_{axial}$ as a function of L_r for different E_T/E .

The lowering of hardening has thus the effect of reducing the contribution from the residual stress to J or CTOD. In a real material the same should occur as L_r approaches L_r^{max} . This implies that not only does the contribution from residual stresses decrease with increasing L_r but also that an additionally decreasing effect due to decreasing hardening, should be taken into account for high L_r -values.

2.2.4 Effect of using linear isotropic hardening

Although a very exact model of the hardening behaviour during welding certainly would be very complex, including both expansion and translation of the yield surface in stress space, it is believed that kinematic hardening models the plastic behaviour better than isotropic hardening. To study the effect of the chosen hardening model, the J -integral and CTOD were also calculated assuming linear isotropic hardening with and without weld residual stresses during axial loading of the pipe. It is seen in Fig. 2.13 that the choice of hardening behaviour is important. When using isotropic hardening, the stresses are unloaded, close to the crack-tip, during part of the loading history. This is reflected in the negative J -values at $L_r = 1.25$. In fact for $L_r = 1$ it would be more favourable to include the residual stresses than not to include the residual stresses. The trend for CTOD is the same. The results are similar to those of Hou et. al. [1996], who also used a linear isotropic hardening model.

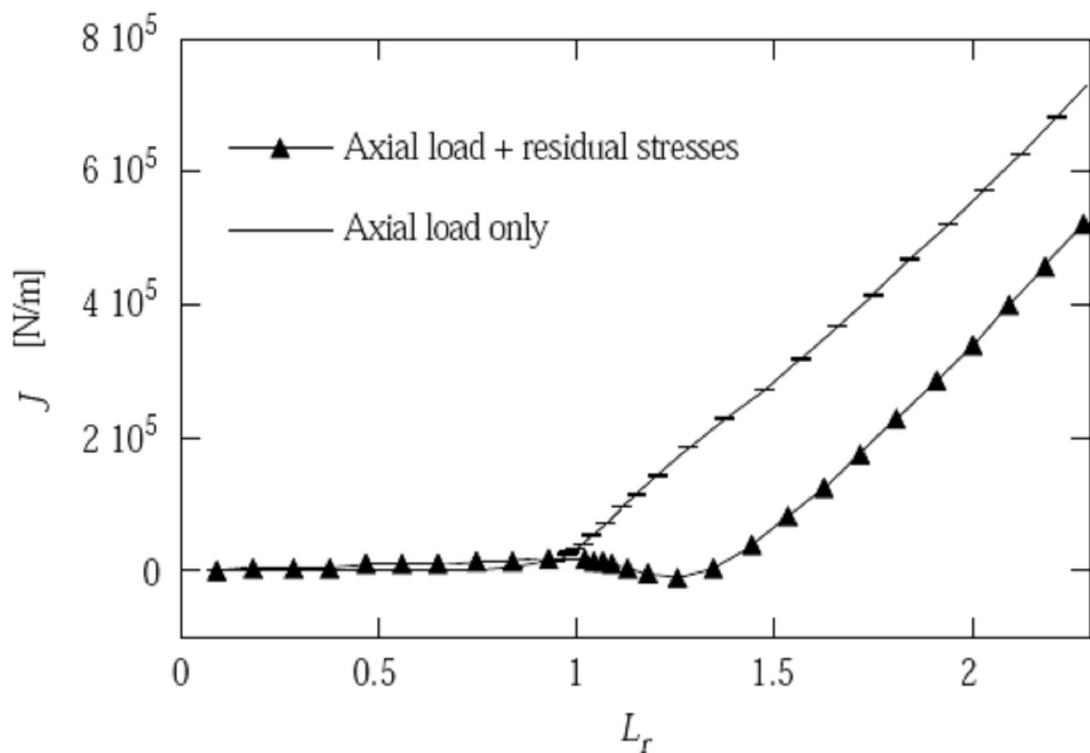


Fig. 2.13a. The J -integral as a function of L_r , with isotropic hardening.

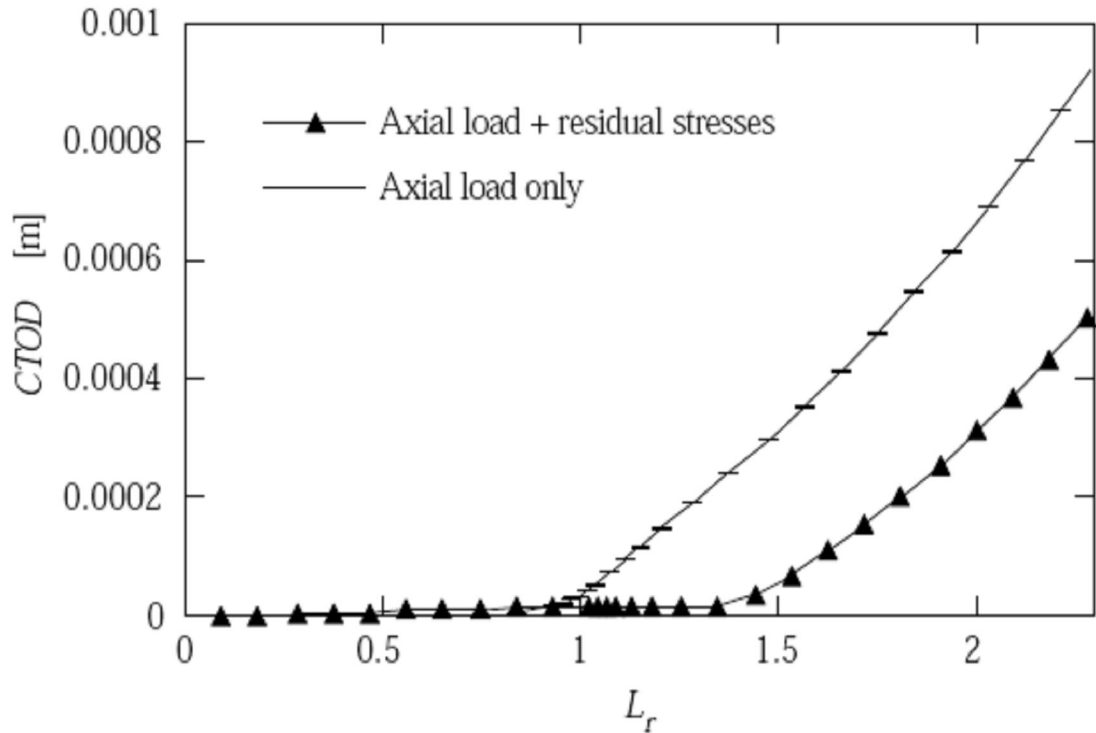


Fig. 2.13b. The CTOD as a function of L_r , with isotropic hardening.

2.3 A welded pipe subjected to a thermal load

A thermal load was applied to the pipe with a circumferential surface crack both with and without the residual stresses present. The thermal load was imposed by specifying a radial temperature distribution in the pipe according to

$$T(r) = 22.5 - n \cdot \exp(r - r_i) \frac{(r - (r_i + t))}{t} \quad (2-5)$$

which is presented together with the resulting axial stresses for the linear elastic case in Fig. 2.14. As the thermal load was increased in very small steps by increasing the value of the scaling parameter n in Equation (2-5), the J -integral and the CTOD were calculated. A limit load parameter can not be defined for the type of secondary thermal load used here since the pipe can not yield completely.

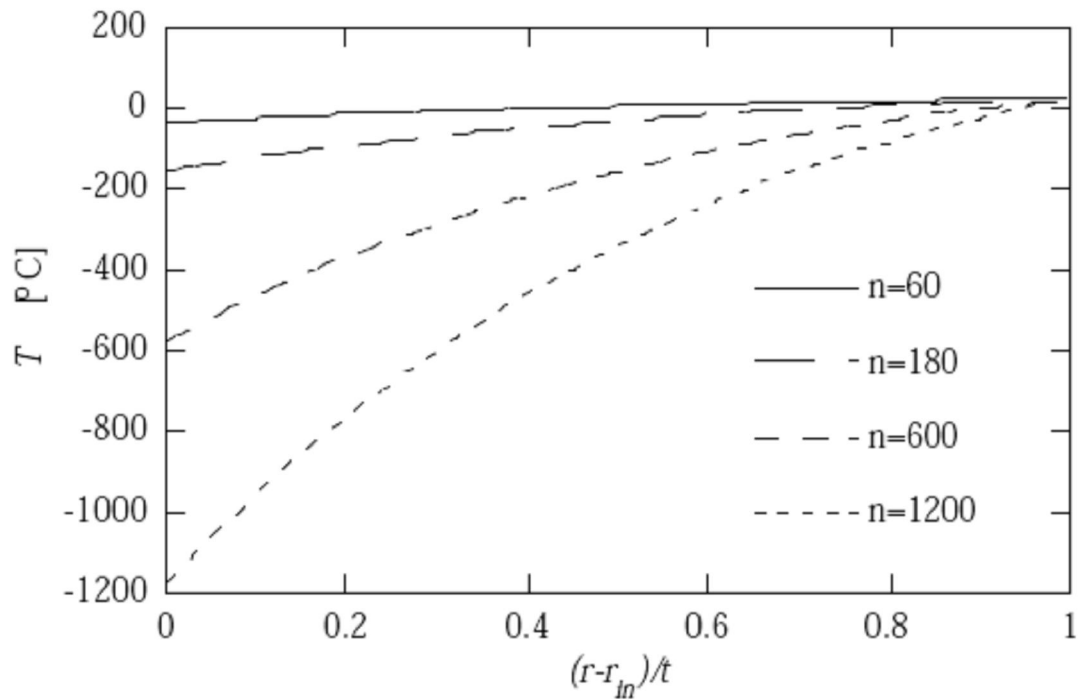


Fig. 2.14a. The temperature distribution through the thickness of the pipe (according to Equation (2-5)).

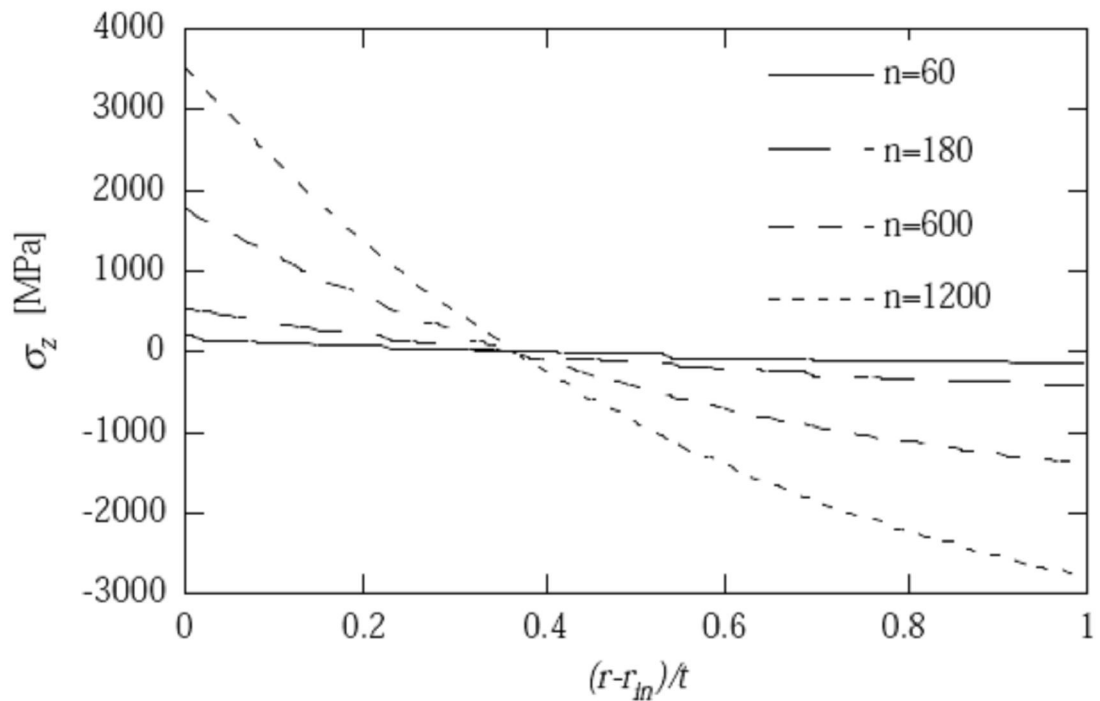


Fig. 2.14b. The corresponding axial stress distribution through the thickness of the pipe (for the linear elastic case).

The thermal load at which the innermost fibre begins to yield may serve as a point of reference. This occurs when

$$\frac{E\alpha\Delta T}{(1-\nu)\sigma_Y} = 1.27 \quad (2-6)$$

where $\Delta T = 20^\circ\text{C} - T$, i.e. the difference in temperature between room temperature and the temperature T at $r = r_i$ in Equation (2-5).

Fig. 2.15, Fig. 2.16 and Fig. 2.17 show the comparisons of J , $CTOD$ and d respectively, for the different temperature distributions, as given in Fig. 2.14a, with and without the residual stress present. The behaviour of J and $CTOD$ is similar. It is related through the non-dimensional parameter d according Equation (2-4). In Fig. 2.17, it is shown that the value of d is 0.23, which is the same as determined for the case of an axial loading.

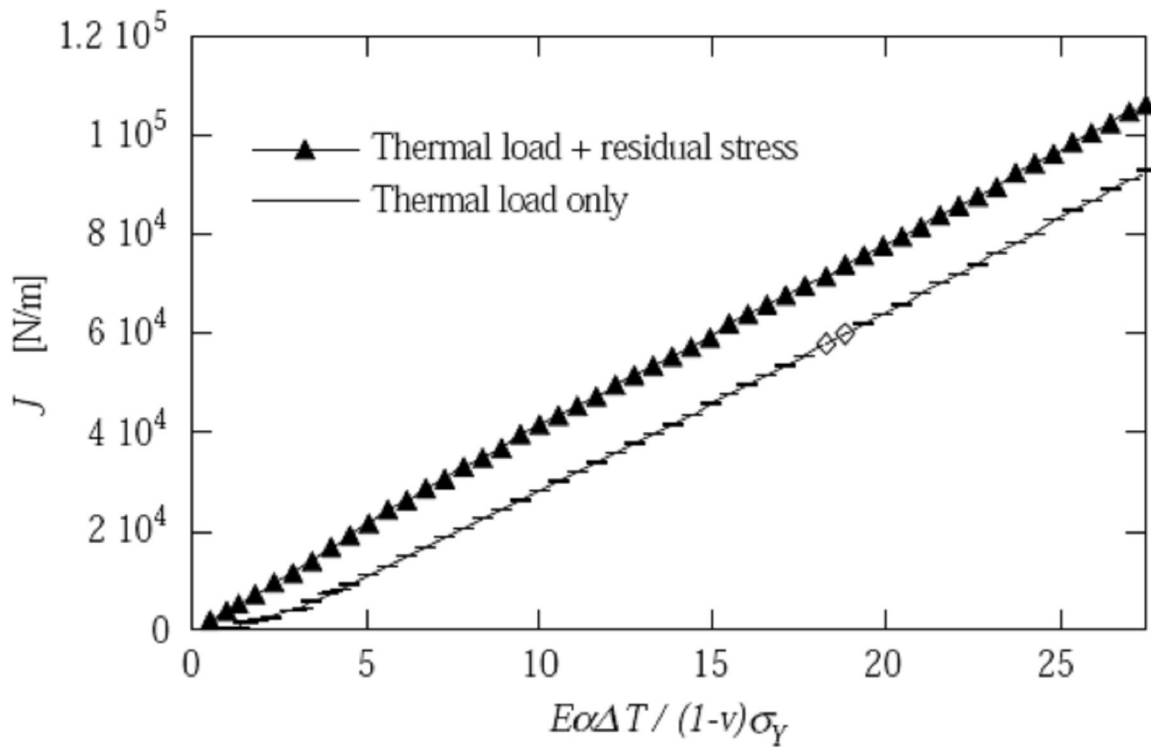


Fig. 2.15a. The J -integral as a function of a non-dimensional load parameter.

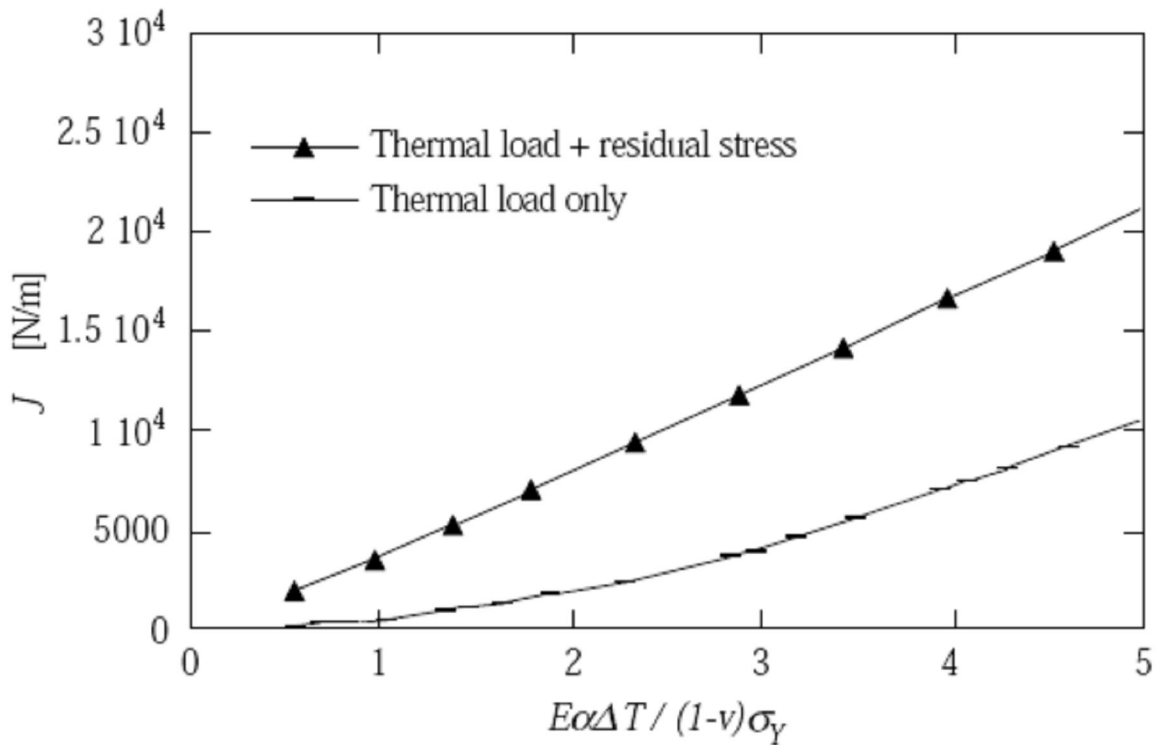


Fig. 2.15b. The J -integral as a function of a non-dimensional load parameter (close up for low values of the load parameter).

The loading curves for J (see Fig. 2.15) and CTOD (see Fig. 2.16 below) are very different from the corresponding curves for the pipe subjected to an axial load. This is because the thermal load is secondary and cannot cause plastic collapse. There is always a portion of the pipe cross section that does not yield. An important consequence of this is that the contribution of the residual stresses is approximately constant in absolute terms during the increase of the thermal load. The smallest contribution of residual stresses is found for low load levels. It must be remembered, however, that for low load levels the values of J are less reliable because of the effect of crack growth prior to loading.

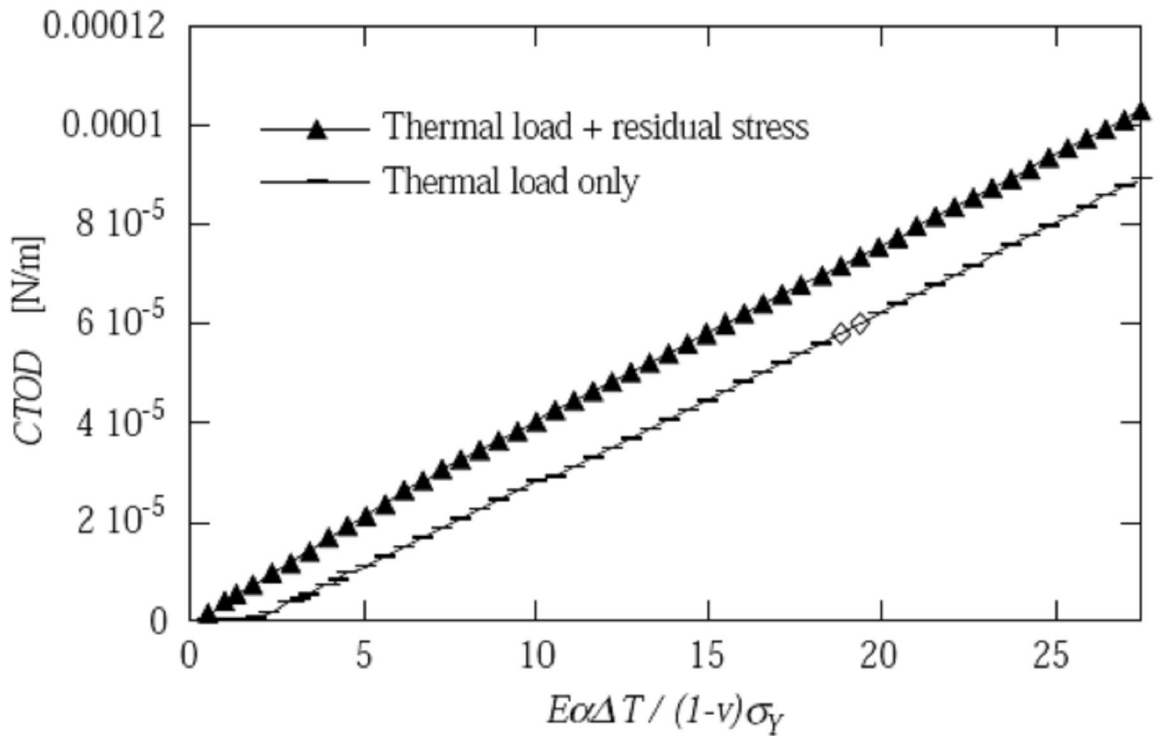


Fig. 2.1a. The *CTOD* as a function of a non-dimensional load parameter.

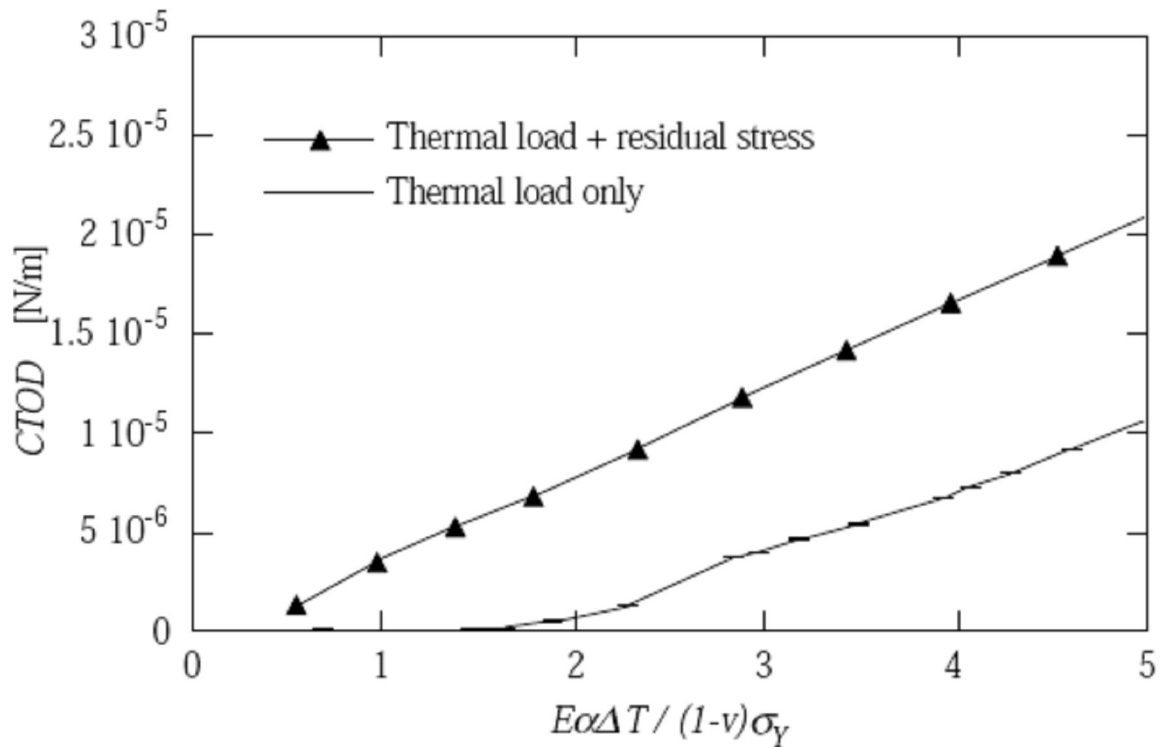


Fig. 2.2b. The *CTOD* as a function of a non-dimensional load parameter (close up for low values of the load parameter).

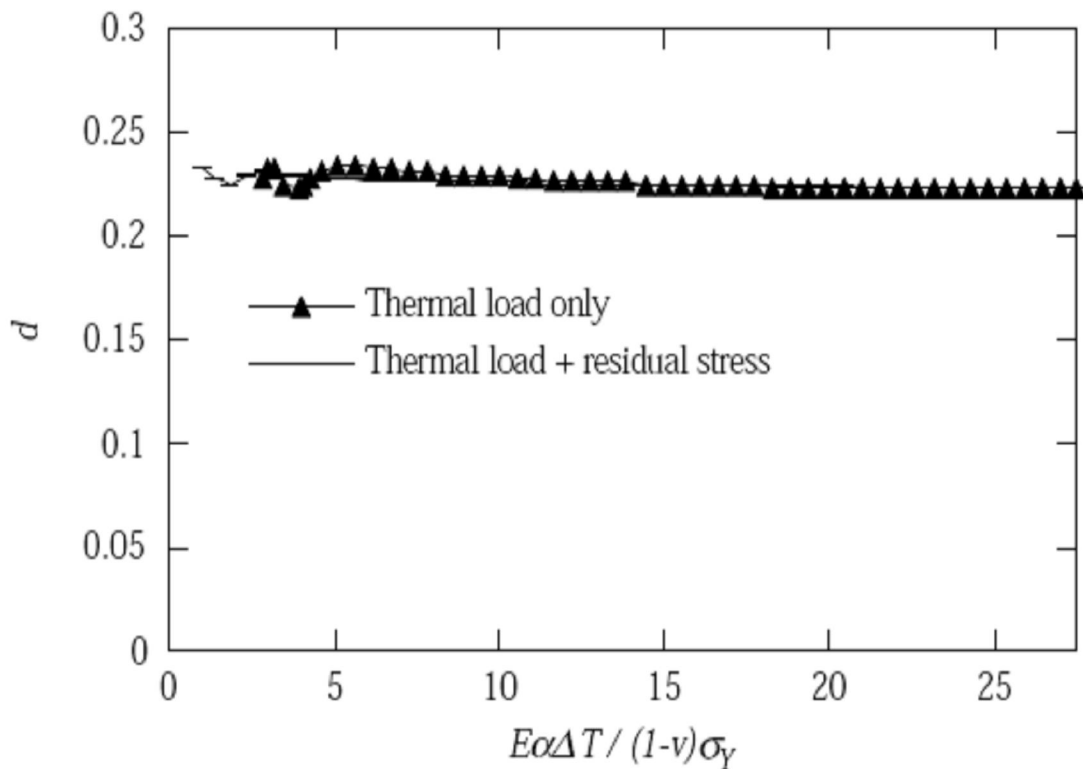


Fig. 2.17. The values of the non-dimensional parameter d as a function of L_r . The parameter d is defined according to Equation (2-4).

2.4 Discussion on the results for thin-walled pipes

The main result of the study by Delfin et. al. [1997] is shown in Fig. 2.6. The relative contribution as defined in Fig. 2.6 from the residual stresses to CTOD or J decreases rapidly between $L_r = 0.8$ and $L_r = 1.3$. For $L_r = 1.25$ the relative contribution from the residual stresses is 20% compared to the axial load. For very high L_r -values the contribution becomes negligible. Thus, for the particular pipe studied the contribution of the residual stresses is negligible only for very high values of L_r . However, because of the linear hardening material model adopted (with its bilinear representation), plastic collapse can not be defined. This means that one do not know for a particular value of L_r , exactly how far the load is from a fully plastic situation corresponding to true plastic collapse.

In the work by Kumar et al [1991] the contribution of a thermal load to the J -integral during a mechanical loading has been studied. They concluded that thermal loads can be neglected for high mechanical loads. A corresponding analysis made with a much more severe thermal loading than in the work by Kumar et al [1991], showed that the contribution to J from the thermal stresses can be significant also for L_r larger than 1. In this case, the value of L_r must be raised to more than 1.4 for the relative contribution from the thermal stresses to be small.

Green et al [1993, 1994] proposed that residual stresses need not to be included in fracture assessments of austenitic steels if L_r is larger than the ratio of the 1% proof stress to the 0.2% proof stress. In the present study this would correspond to an L_r -value of about 1.1. The investigation in Delfin et. al. [1997] indicates that this limit should be larger, approximately $L_r = 1.3$. If it can be shown that instability in a ductile material occurs beyond this limit, the weld residual stresses may be ignored, at least for estimation of the crack size or load at instability.

The opinion in Delfin et. al. [1997] is that great care must be taken in the treatment of the contribution of welding residual stresses or thermal stresses in fracture assessments. The results with proper simulation of the weld-induced stresses do support the idea of giving weld residual stresses a lower weight in a fracture evaluation if high primary loads are present. However, the limit of L_r at which the relative contribution from weld residual stresses (or thermal loads) to CTOD or J is small enough, is likely to depend on the particular material model, crack geometry and the shape and level of the residual (or thermal) stress distribution. More analyses needs to be done (and also a comparison with experimental data), which is presented in the following sections of this report.

3 ANALYSIS OF INTERNAL CIRCUMFERENTIAL SURFACE CRACKS IN THICK-WALLED PIPES

The finite element analysis of thick-walled pipes containing circumferential surface cracks subjected to welding residual stresses and mechanical loads is briefly presented in this section. More details of this analysis are given in Anderson and Dillström [2004].

3.1 Geometry

The analysed pipe is thick walled with an inner radius of 300 mm and a thickness of 40 mm. The geometry is taken from Brickstad and Josefson [1996]. The weld is oriented circumferentially and consists of 36 passes in 15 layers through the thickness. However since only half of the pipe is modelled due to symmetry only 23 passes are included in the model, see Fig. 3.1 and Fig. 3.2. Number 1, 2, 9, 11, 13, 15, 17, 19, 21 and 23 of these passes are half passes due to symmetry.

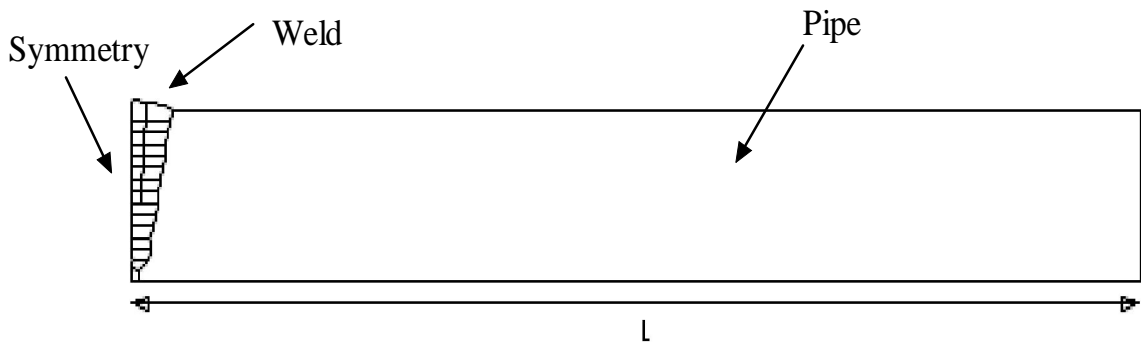


Fig. 3.1. Geometry of the welded pipe.

In the analysis, a crack is later introduced in the centre of the weld at the inside of the pipe. As the model is in 2D, the crack is fully circumferential. The crack depth is $a = 5$ mm.

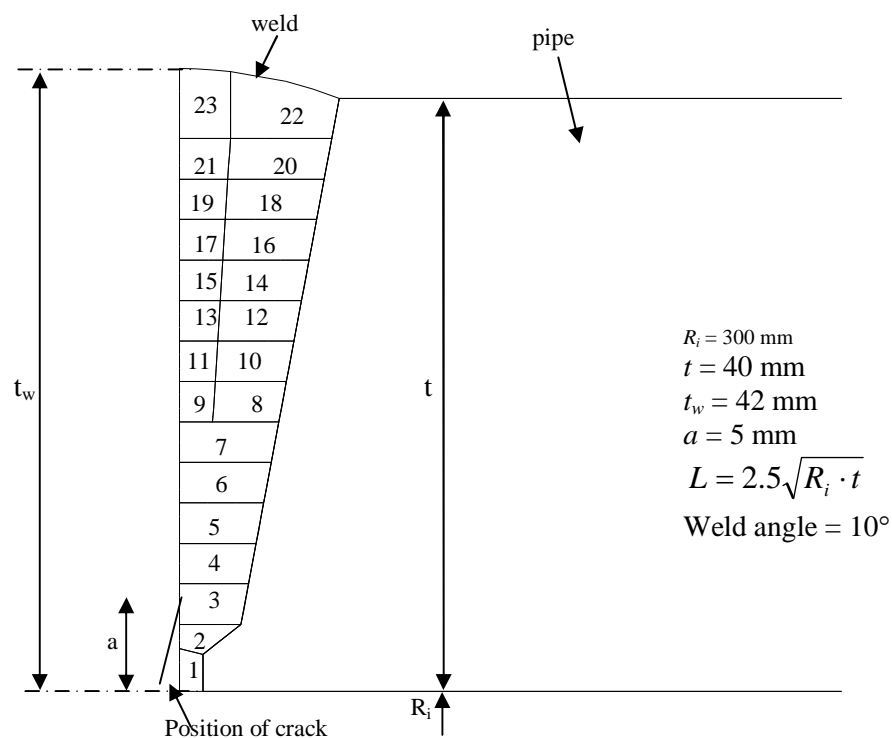


Fig. 3.2. Geometry of the weld, with the 23 weld passes that were included in the model.

3.2 Material data

The material in both the pipe and the weld are stainless steel. The data are taken from Brickstad and Josefson [1996] and summarised in Table 3.1 and Table 3.2.

Table 3.1. Material data for pipe and weld, thermal analysis.

Temperature T [°C]	Specific heat C_p [J/kg °C]	Conductivity λ [W/m °C]	Density ρ [kg/m ³]
20	442	15.0	7840
200	515	17.5	7840
400	563	20.0	7840
600	581	22.5	7840
800	609	25.5	7840
1390	675	66.2	7840

Table 3 2. Material data for pipe and weld, structural analysis.

Temperature T [°C]	Young's modulus E [MPa]	Poisson's ratio ν [-]	Thermal expansion coefficient α [$10^{-6}/^{\circ}\text{C}$]	Yield stress σ_y [MPa]	Plastic tangent modulus E_T [MPa]	E_T / E [-]
20	200000	0.278	17.0	230	28000	0.14
200			17.5			
400	170000	0.298	18.5	132	23800	0.14
600			19.0			
800	135000	0.327	19.5	77	1890	0.14
1000	95000	0.342	20.0	50	9.5	$1 \cdot 10^{-4}$
1100	50000	0.350	20.0			

3.3 Element mesh

The ABAQUS [2003] elements used for all 2D analyses were the eight nodes bi-quadratic axisymmetric elements DCAX8 (thermal analysis) and CAX8 (structural analysis), both with full integration.

Anticipating that a crack is introduced and that CTOD is calculated for a primary loading in the interval $0.8 \leq L_r \leq 2$, the element size near the crack tip must be very small. The smallest element length is $2.5 \cdot 10^{-3}$ mm, see Fig. 3.3. An analysis with a coarser mesh has also been done where the smallest element length was $20 \cdot 10^{-3}$ mm. With this coarser mesh similar results were obtained for CTOD when $L_r > 1.0$.

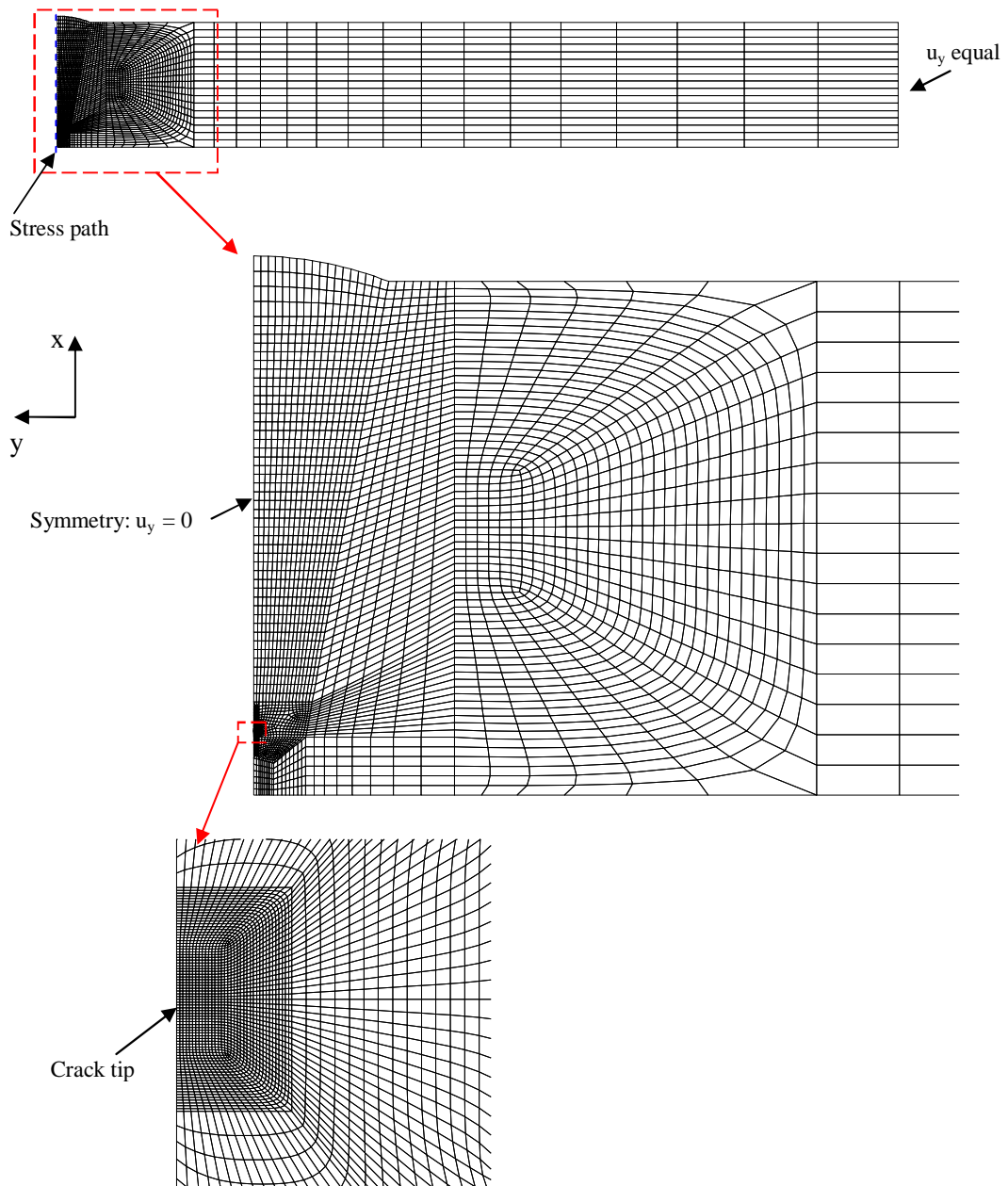


Fig. 3.3. Element mesh of the pipe, weld and crack tip (smallest element length $2.5 \cdot 10^{-3}$ mm).

3.4 Loading and boundary conditions

Below, the different loadings are presented. The analysis consists of three phases, the welding process, crack growth and finally applying the primary loading. The boundary condition at the start of the analysis is an applied symmetry condition at the centre of the weld ($u_y = 0$). Also the axial degrees of freedom (dof), u_y , are constrained to be equal at the free end of the pipe, see Fig. 3.3.

3.4.1 Simulation of the weld process

The technique to compute the weld induced residual stresses is described in detail in Delfin et. al. [1998]. The welding process simulation was done with an uncoupled thermo-plastic analysis. First a transient thermal analysis is performed during which the time dependent temperature distribution is determined for the successive build up of the welding passes. The stress field due to the temperature field is then evaluated at each time step in a structural analysis.

The weld is modelled by introducing the 23 passes successively. During the thermal analysis radiation and convection boundary condition are applied. These vary with each weld pass. The resulting heat transfer coefficient (including both radiation and convection), α_h , is taken from Delfin et. al. [1998] and given by Equation (3-1).

$$\begin{aligned}\alpha_h &= 0.0668 \cdot T & \left[\text{W}/(\text{m}^2 \text{ } ^\circ\text{C}) \right] & \quad 20^\circ\text{C} \leq T \leq 500^\circ\text{C} \\ \alpha_h &= 0.231 \cdot T - 82.1 & \left[\text{W}/(\text{m}^2 \text{ } ^\circ\text{C}) \right] & \quad T > 500^\circ\text{C}\end{aligned}\tag{3-1}$$

In the subsequent structural analysis the stresses are calculated with an elastic-plastic material model. The von Mises yield criterion with associated flow rule and bi-linear kinematic hardening is used. In Delfin et. al. [1997], it was observed that differences between analyses with small strain theory and large strain theory are small. Therefore only small strain theory is used. The multi pass weld is modelled by activating the elements belong to the current pass at a proper time during the transient phase. The elements are introduced strain-free.

3.4.2 Simulation of crack growth

After the welding process and after the pipe and weld have cooled, a crack is introduced in the centre of the weld starting from the inside of the pipe. The final crack length is $a = 5$ mm. The crack is introduced by releasing the constrained degrees of freedoms in the centre of the weld. The 2D axis-symmetric model allows only a complete circumferential crack to be introduced. The crack growth is restricted to the radial (x) direction. The method of releasing nodes along the chosen growth direction gives a path dependent J -integral. This has to do with the fact that the growth does not represent a proportional loading. However, when the primary loading is introduced and then increased to higher L_r -values, the J -integral becomes path independent from a practical standpoint.

3.4.3 Primary load

After the crack is introduced a primary load is applied. The load consists of an axial tension force applied at the free end of the pipe. The primary load is increased gradually to the final value $L_r = 2.0$. For different L_r -values the J -integral and CTOD is computed. The limit load for this 2D crack geometry is calculated in Appendix C.

3.5 Results

In Fig. 3.4 the axial stress (σ_{22}) in the centre of the weld (the stress path in Fig. 3.3) is shown as a function of a normalised coordinate, u , through the thickness. The axial stress is shown for different phases of the analysis, after welding and after crack growth ($a = 0.125 \cdot t$). As can be seen, a singularity occurs at the crack tip and for $u > 0.45$ the axial stress is not affected by the crack growth. The limit load parameter, L_r , is defined as $\sigma_{axial} / \sigma_{axial,limit}$ where σ_{axial} is the applied axial load and $\sigma_{axial,limit}$ is defined in appendix C.

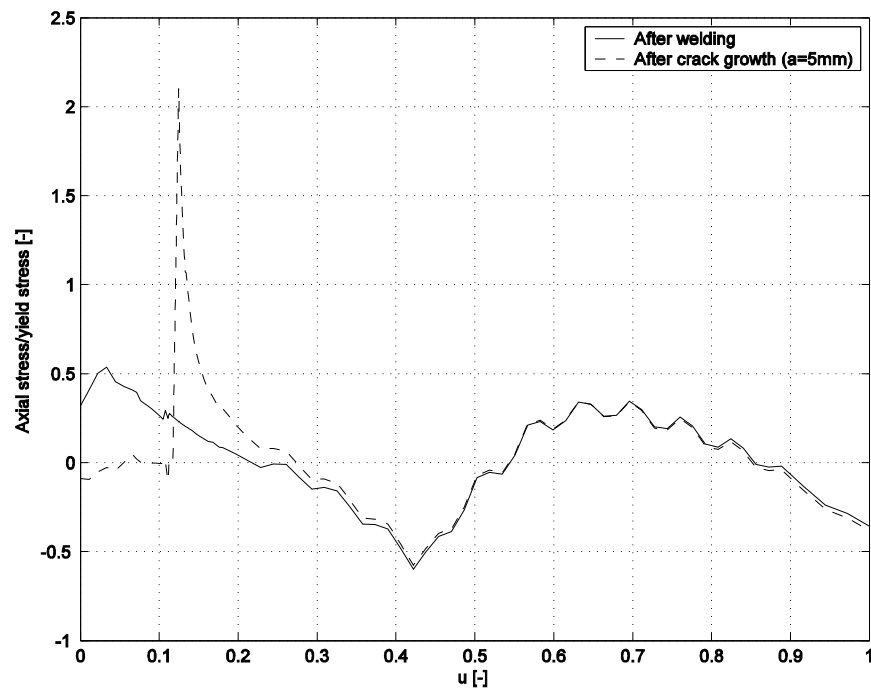


Fig. 3.4. Axial stress, in the centre of the weld, through the thickness of the pipe. $u = 0$ is located at the inside and $u = 1.0$ at the outside of the pipe. The crack depth $a = 5$ mm.

Fig. 3.5 and Fig. 3.6 show the difference in axial stress for $L_r = 0.99$ and $L_r = 1.98$ for the cases if the weld residual stresses are present or not. As can be seen the stress distribution for the case with residual weld stresses approaches the stress distribution for the case without weld residual stresses for L_r -values greater than 1.0. Fig. 3.7 and Fig. 3.8 show the stress distribution in the weld and pipe after the weld simulation and after crack growth.

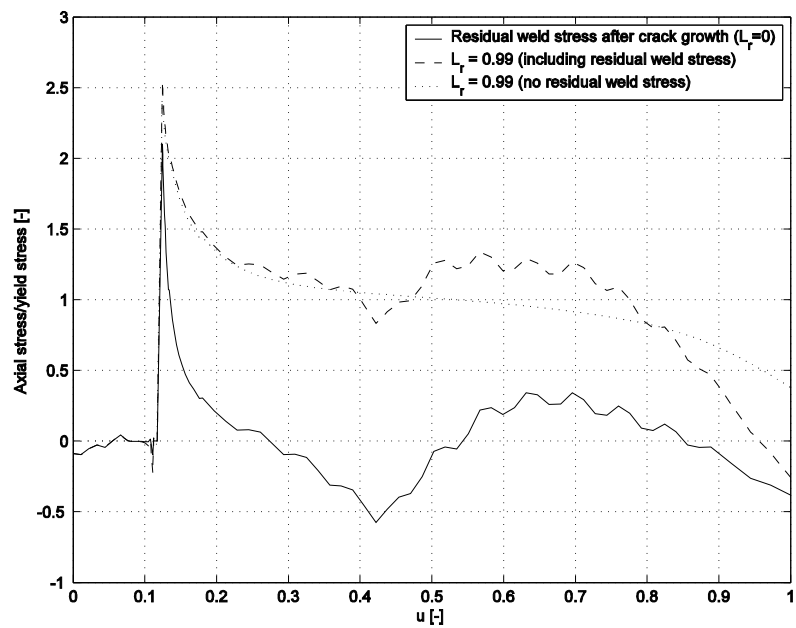


Fig. 3.5. Normalised axial stress distribution through the thickness (from the inside to the outside of the pipe) at the centre of the weld with and without weld residual stresses. The primary load level is $L_r = 0.99$.

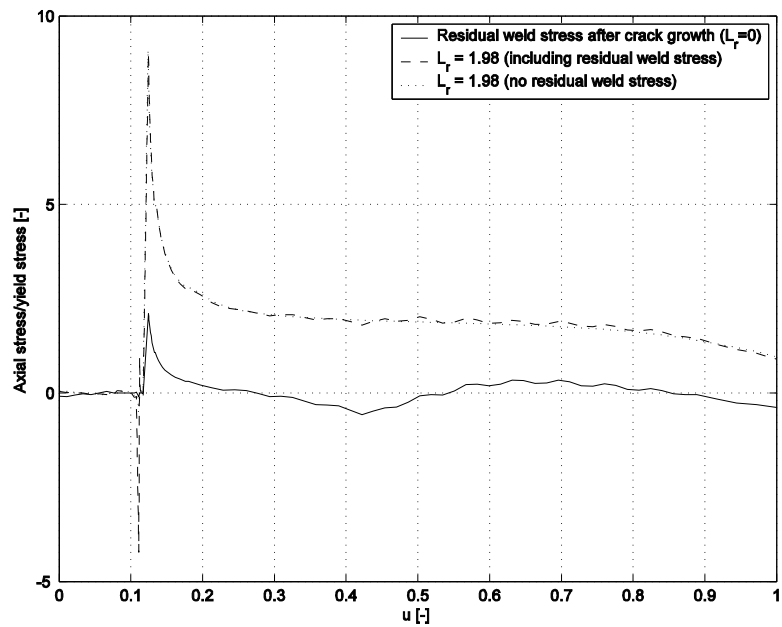


Fig. 3.6. Normalised axial stress distribution through the thickness (from the inside to the outside of the pipe) at the centre of the weld with and without weld residual stresses. The primary load level is $L_r = 1.98$.

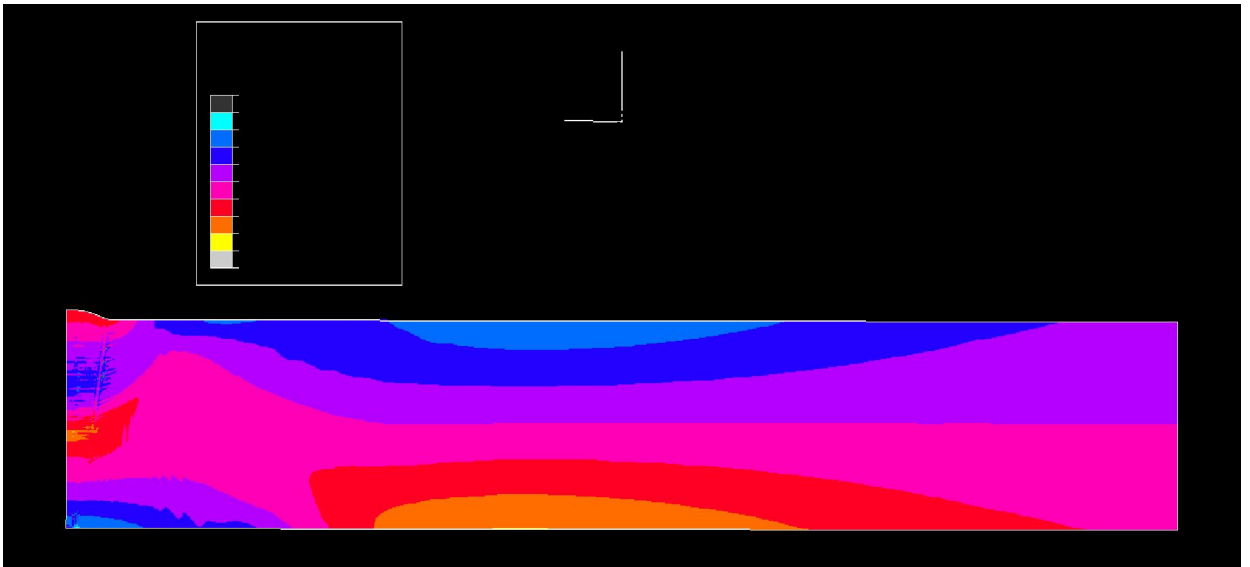


Fig. 3.7. Axial stress distribution [Pa] after welding.

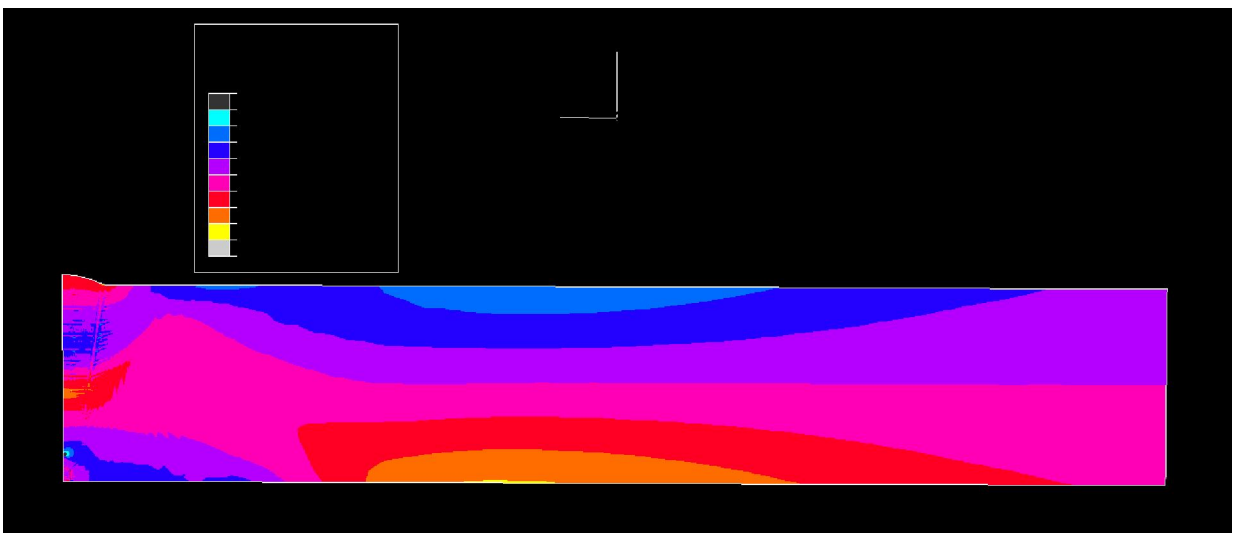


Fig. 3.8. Axial stress distribution [Pa] after crack growth.

Fig. 3.9 and Fig. 3.10 show the path independence of the J -integral for higher L_r -values for the primary loading and the combined primary and secondary loading respectively.

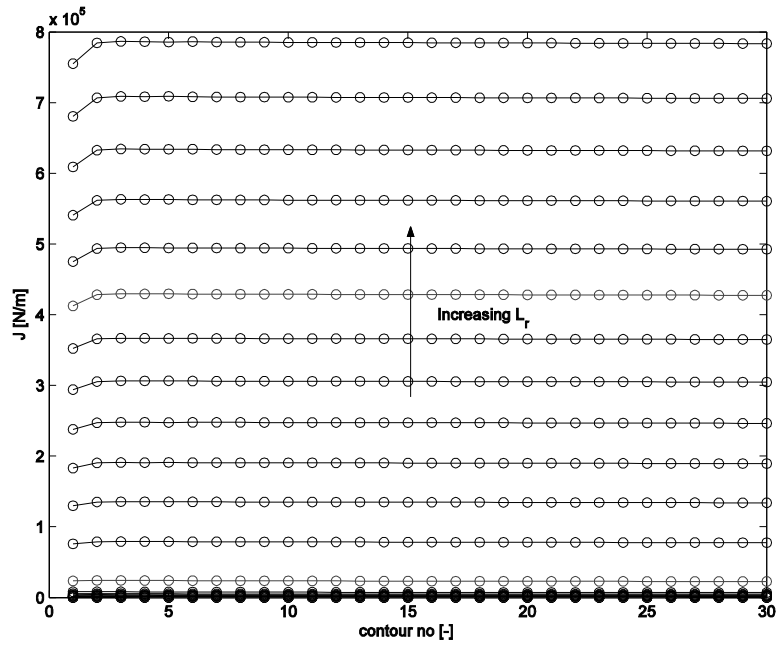


Fig. 3.9. The J -integral as a function of contour number for the load case with a primary loading only. The distance between the contours is approximately 0.0025 mm.

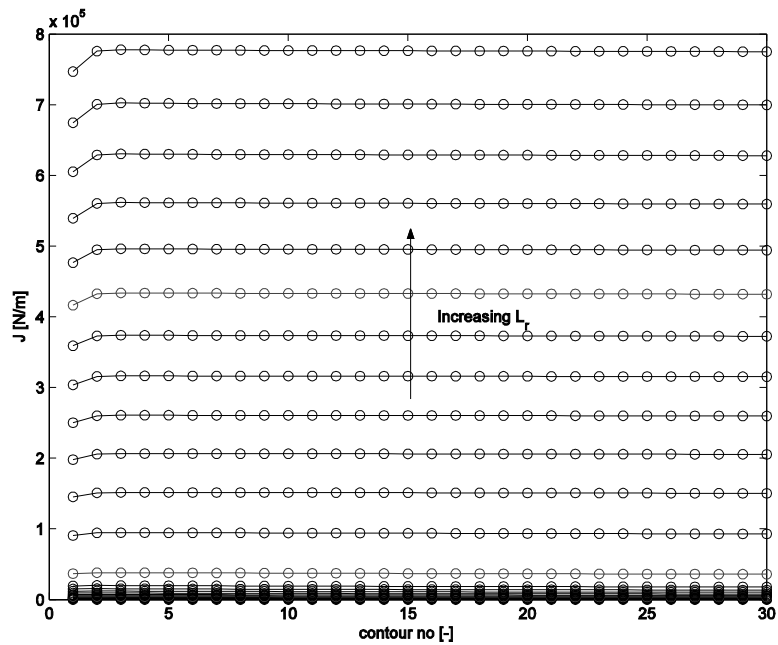


Fig. 3.10. The J -integral as a function of contour number for the load case with both primary and secondary loading. The distance between the contours is approximately 0.0025 mm.

In Fig. 3.11 and Fig. 3.12 the J -integral (for contour 8) and the CTOD-value are shown as a function of L_r . As can be seen, the difference decreases for higher L_r values.

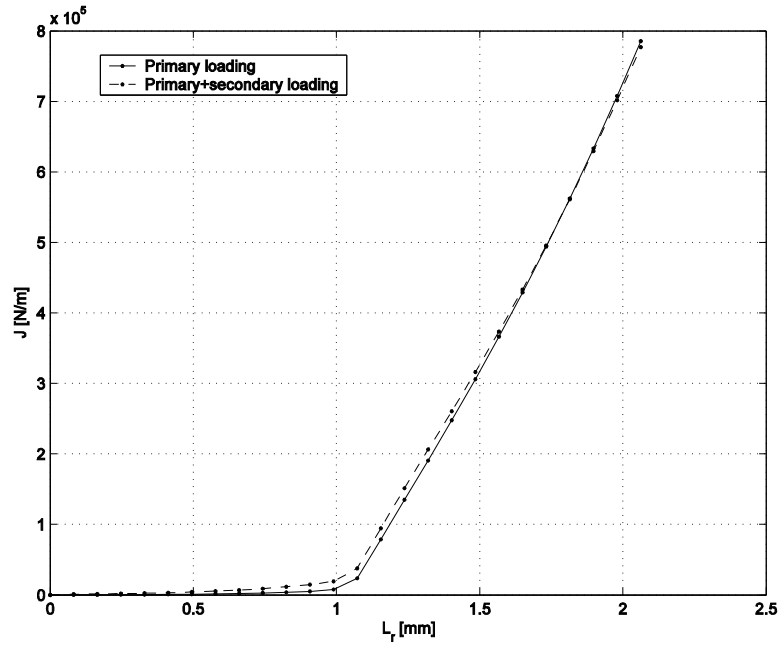


Fig. 3.11. The J -integral as a function of L_r for both load cases (with and without secondary loading).

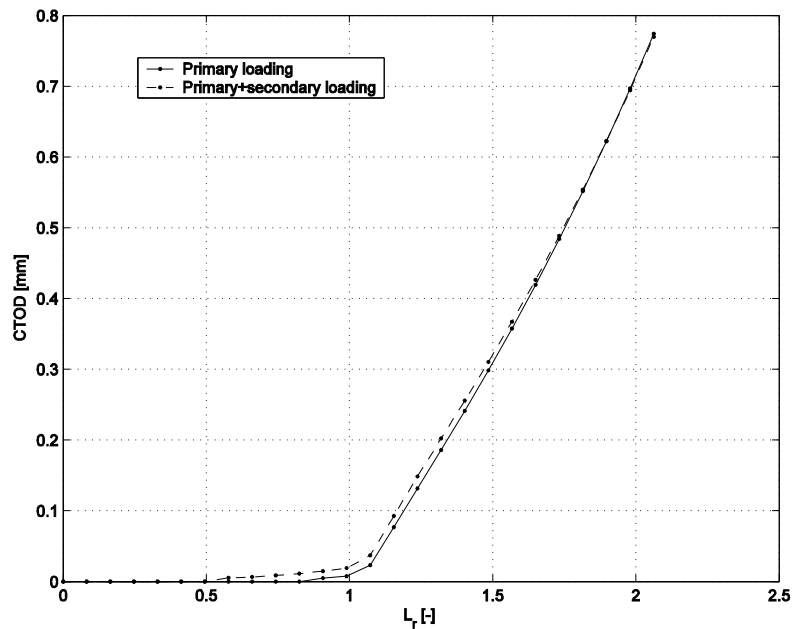


Fig. 3.12. CTOD as a function of L_r for both load cases (with and without secondary loading).

In Fig. 3.13 and Fig. 3.14 (a comparison using two different contours when calculating J), this decreasing difference for higher L_r -values is shown as expressed in Equation (1-1).

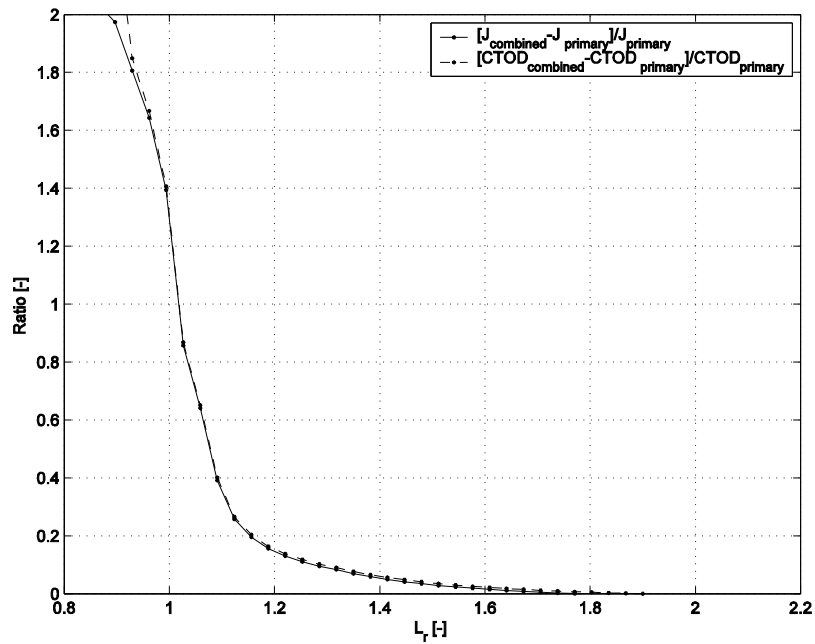


Fig. 3.13. The relative contribution of the weld residual stresses to J and CTOD according to Equation (1-1) for increasing L_r . Contour No. 8 is used.

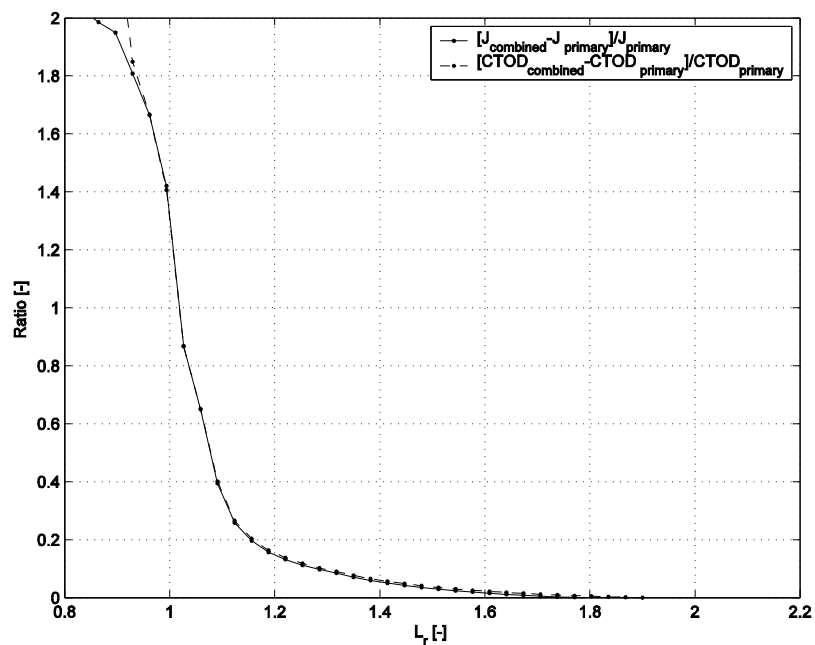


Fig. 3.14. The relative contribution of the weld residual stresses to J and CTOD according to Equation (1.1) for increasing L_r . Contour No. 20 is used.

The contribution to the fracture parameters from the residual stresses is negligible for large L_r as shown in Fig. 3.13-3.14. The contribution from the residual stresses decreases rapidly with increasing L_r . For $L_r = 1.3$ the contribution of the residual stresses is 10% of the axial load contribution. For $L_r = 1.6$ the contribution of the residual stresses is about 2%.

4 ANALYSIS OF INTERNAL AXIAL SURFACE CRACKS IN THICK-WALLED PIPES

The finite element analysis of thick-walled pipes containing axial surface cracks subjected to welding residual stresses and mechanical loads is briefly presented in this section. More details of this analysis are given in Anderson and Dillström [2004].

4.1 Geometry

The analysed pipe is thick walled with an inner radius of 348.5 mm and a thickness of 84 mm, see Fig. 4.1. The geometry is taken from Delfin et. al. [1998] (type VI pipe). The weld is an X-joint, which is oriented circumferentially and consists of 21 passes. In the analysis an axial circular crack is also introduced in the centre of the weld at the inside of the pipe. Different crack depths was used (between $0.06 \cdot t \leq a \leq 0.14 \cdot t$).

4.2 Material data

To simplify the analysis, the same material was used for both the pipe and the weld (Inconel 182). The data are taken from Delfin et. al. [1998] and summarised in Table 4.1.

Table 4.1. Material data for pipe and weld, Inconel 182.

Temperature T [°C]	Young's modulus E [MPa]	Poisson's ratio ν [-]	Thermal expansion coeff. α [$10^{-6} / ^\circ\text{C}$]	Yield stress σ_y [MPa]	Plastic tangent modulus E_T [MPa]	E_T / E [-]
20	207000	0.324	13.0	380	2898	0.14
200			14.0			
400	185000	0.301	15.3	302	25900	0.14
600			16.2			
800	150000	0.320	17.0	185	2100	0.14
1000	125000	0.339	17.3	50	12.5	$1 \cdot 10^{-4}$
1200	50000	0.350	17.3			

4.3 Element mesh

The ABAQUS elements [2003] used for all 3D analyses were the 20 nodes quadratic brick elements C3D20. For the 3D analysis it is not practical to use as small elements that were required for calculating CTOD for primary loading in the interval $0.8 \leq L_r \leq 2.0$. The smallest element length in these analyses is approximately 0.5-0.8 mm. Fig. 4.1 shows the element mesh.

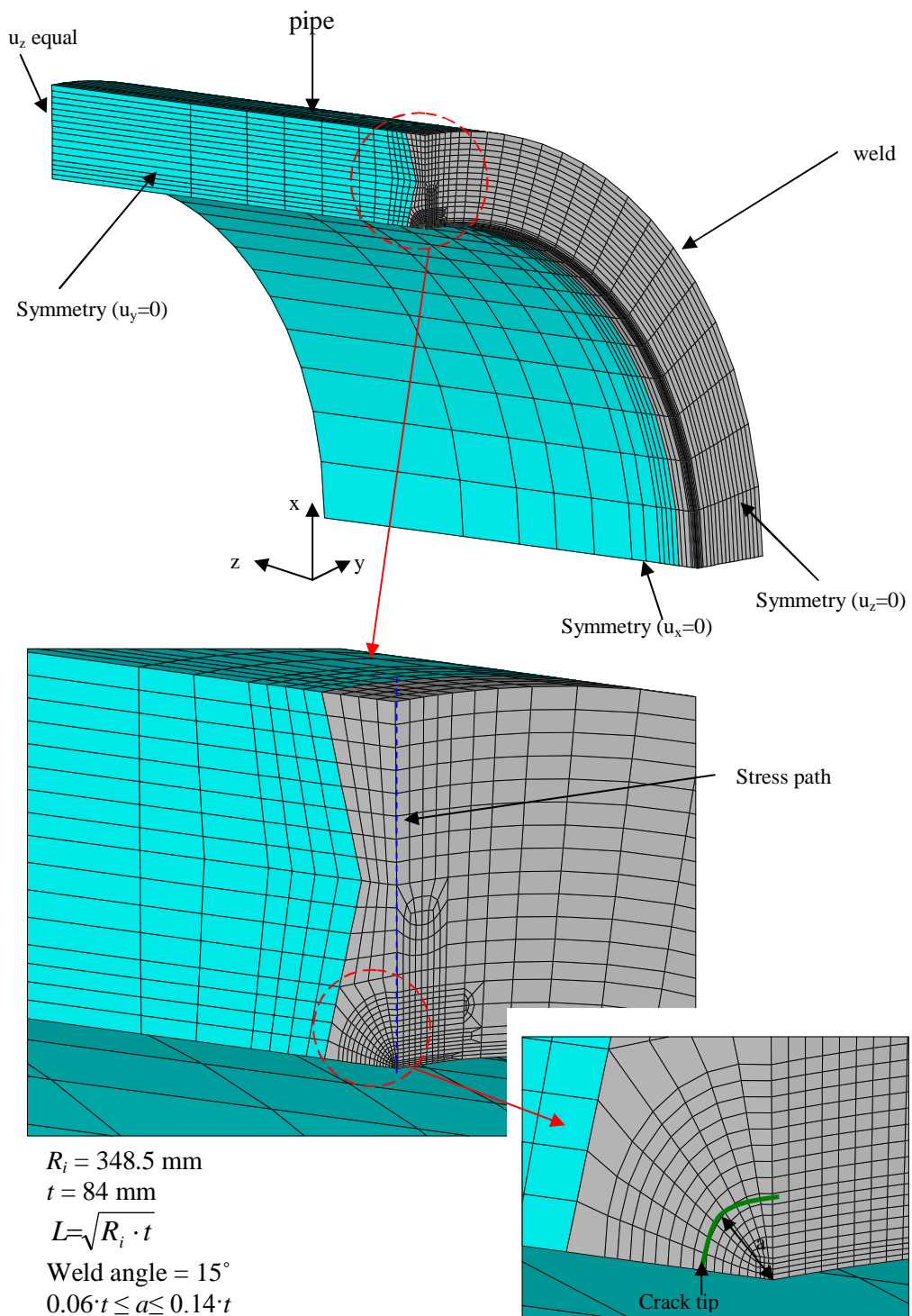


Fig. 4.1. Element mesh of the 3D model, with an axial crack.

4.4 Loading and boundary conditions

Below the different loadings are presented. As for the 2D case this analysis also consists of three phases, the welding process, crack growth and finally an applied primary loading. The boundary condition at the start of the analysis is an applied symmetry condition at the centre of the weld ($u_z = 0$) and at the parts where the pipe is cut, $u_y = 0$ and $u_x = 0$ respectively. Also the axial degrees of freedom, u_z , are constrained to be equal at the free end of the pipe, see Fig. 4.1.

4.4.1 Simulation of the weld process

The technique to compute the weld induced residual stresses differs from the method used in the 2D analysis. This is due to the fact that the elastic-plastic analysis with element birth and death technique used in the 2D case is too time-consuming in the 3D case. Instead a simplified two step simulation to obtain the correct weld residual stresses is done. First the weld is given a temperature gradient through the thickness. This temperature gradient does not vary circumferentially. This applied temperature gradient leads to plastic deformation. In the next step the pipe is cooled down by setting the temperature uniformly to room temperature. The weld residual hoop stresses are then compared to the corresponding residual stresses obtained in a 2D analysis in Delfin et. al. [1998]. The same technique is used for weld simulation as the one for the 2D case in section 3 of this report. The von Mises yield criterion with associated flow rule and bi-linear kinematic hardening is used for the analysis.

4.4.2 Simulation of crack growth

After the welding process and after the pipe and weld have cooled, a circular axial crack is introduced in the centre of the weld starting from the inside of the pipe. The final crack depth is varied for different analyses in the interval of $0.06 \cdot t \leq a \leq 0.14 \cdot t$, see Fig. 4.1. The crack growth is restricted to grow in the radial (x) direction only. As in the 2D case, the method of releasing nodes along the chosen growth direction gives a path dependent J -integral. This has to do with the fact that the growth does not represent a proportional loading. However, when the primary loading is introduced and increased to higher L_r -values, the J -integral becomes path independent from a practical standpoint.

4.4.3 Primary load

After the crack is introduced a primary load is applied. The load consists of internal pressure. However, the pressure is only applied in the radial direction (no axial component). The primary load is increased gradually to the final value $L_r = 2.0$. For different L_r -values the J -integral is computed. The limit load for this 3D crack geometry is calculated in Appendix D.

4.5 Results

In Fig. 4.2 the hoop stress (σ_{22}) in the centre of the weld (the stress path in Fig. 4.2) is shown as a function of a coordinate through the thickness. The hoop stress is shown for different phases of the analysis, after welding and after crack growth ($a = 0.08 \cdot t$). All results are taken from a crack growth of $a = 0.08 \cdot t$ (unless otherwise stated). Similar results are obtained with different crack lengths (up to $a = 0.14 \cdot t$). The limit load parameter, L_r , is defined as p / p_{limit} where p is the applied load and p_{limit} is defined in Appendix D.

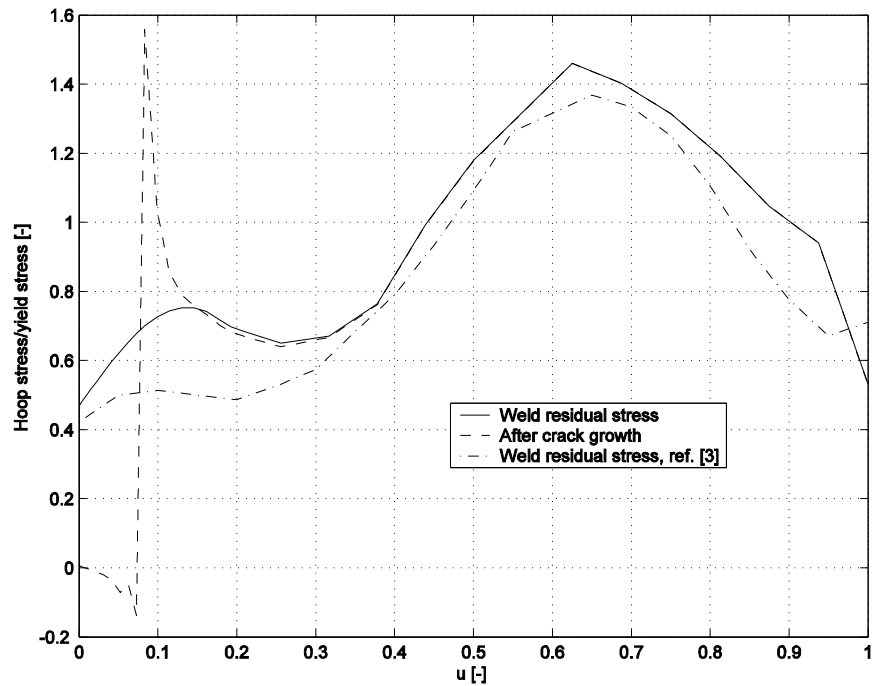


Fig. 4.2. Hoop stress in the centre of the weld through the thickness. $u = 0$ is located at the inside of the pipe. The crack length $a = 0.08t$.

Fig. 4.2 also shows the corresponding residual weld hoop stress from Delfin et. al. [1998]. When comparing the residual stress profiles, it is evident that the approximation (using a temperature gradient) in this 3D analysis gives similar results as in the complete 2D analysis given in Delfin et. al. [1998]. The present 3D analysis is more conservative, i.e. gives larger residual stresses, for small cracks.

Fig. 4.3 and Fig. 4.4 show the difference in hoop stress for $L_r = 0.93$ and $L_r = 1.98$. In both figures a comparison is made for the cases when the weld residual stresses are present or not. As can be seen the stress distribution for the case with residual weld stresses approaches the stress distribution for the case without weld residual stresses for L_r -values greater than 1.0.

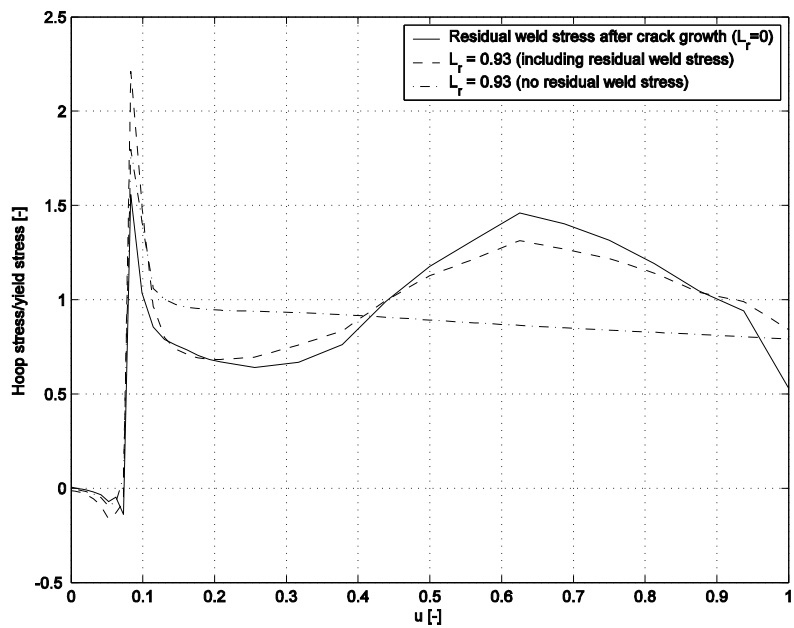


Fig. 4.3. Normalised hoop stress distribution through the thickness (from the inside to the outside of the pipe) at the centre of the weld with and without weld residual stresses. The primary load level is $L_r = 0.93$.

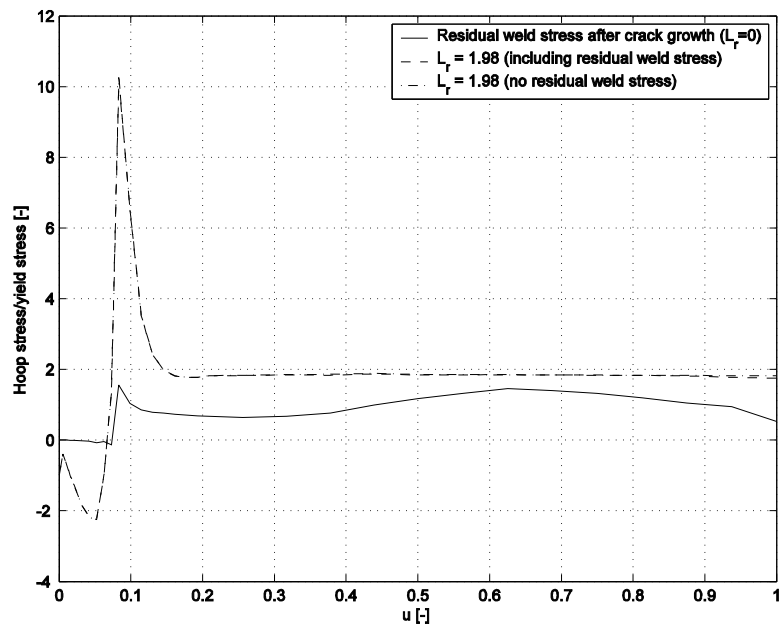


Fig. 4.4. Normalised hoop stress distribution through the thickness (from the inside to the outside of the pipe) at the centre of the weld with and without weld residual stresses. The primary load level is $L_r = 1.98$.

Fig. 4.5 and Fig. 4.6 show the stress distribution in the weld and pipe after the weld simulation and after crack growth.

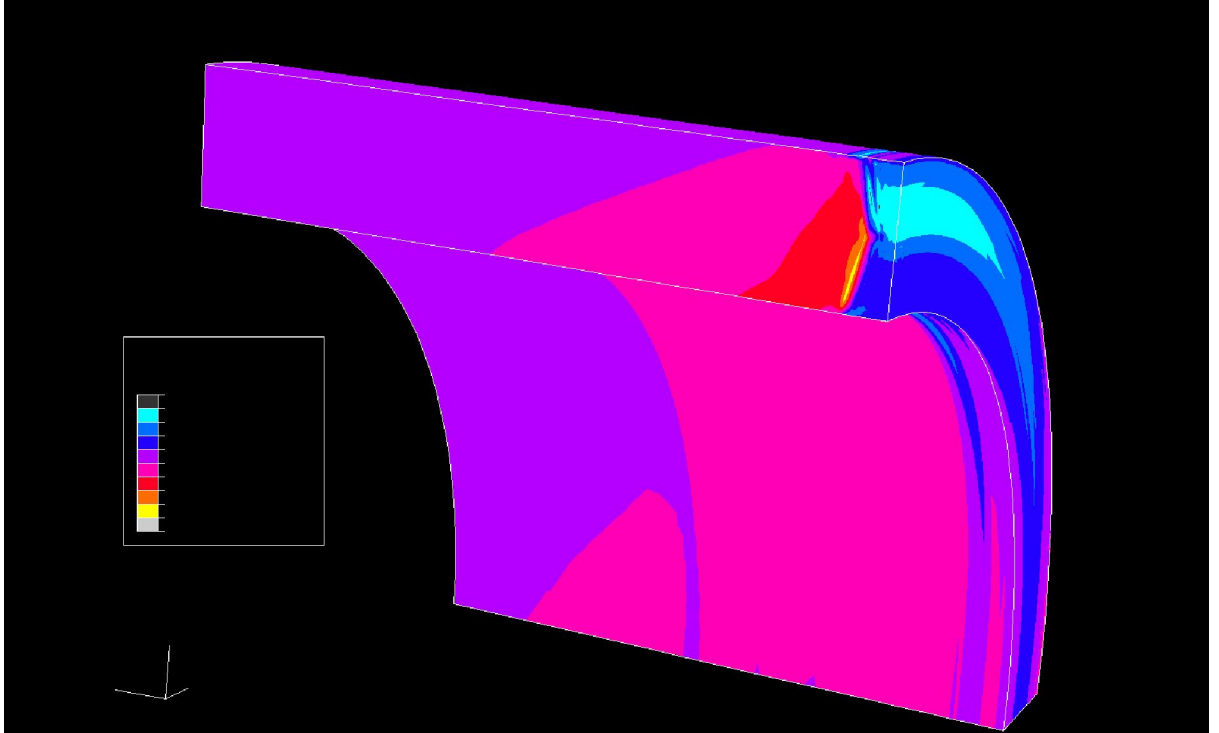


Fig. 4.5. Stresses in the circumferential direction [Pa] after welding.

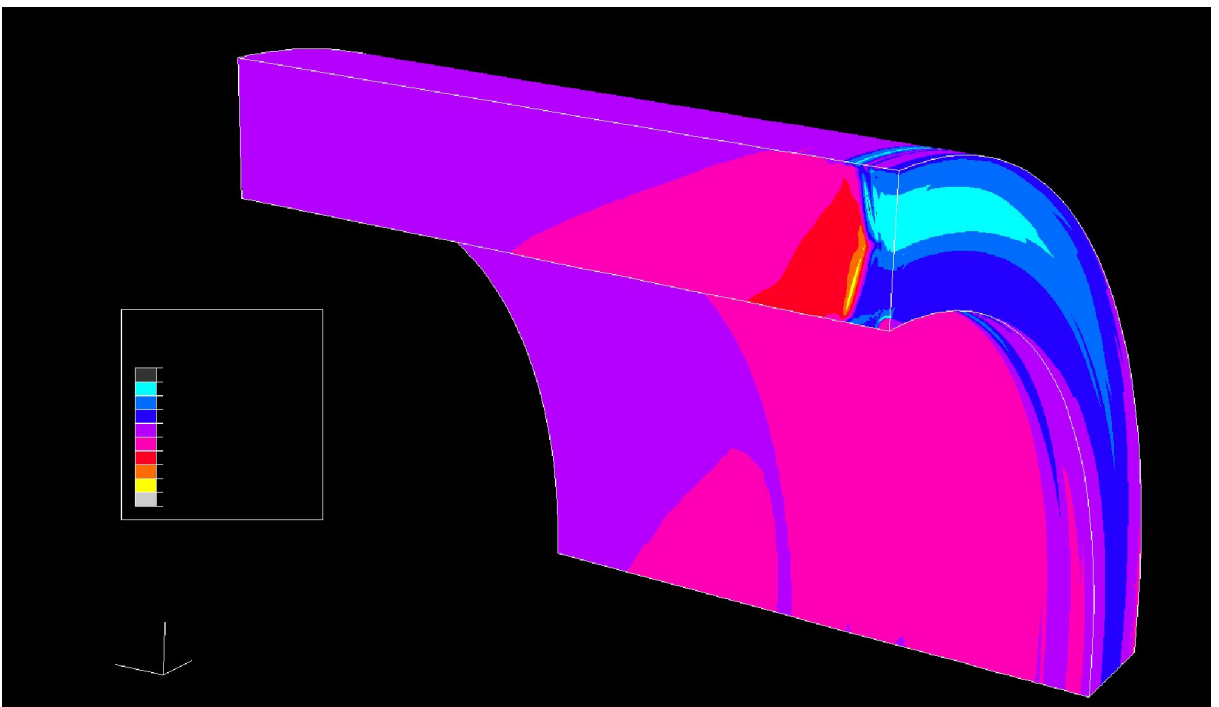


Fig. 4.6. Stresses in the circumferential direction [Pa] after crack growth.

Fig. 4.7 and Fig. 4.8 show the path independence of the J -integral for different contour paths. The distance between each contour number is 1.93 mm.

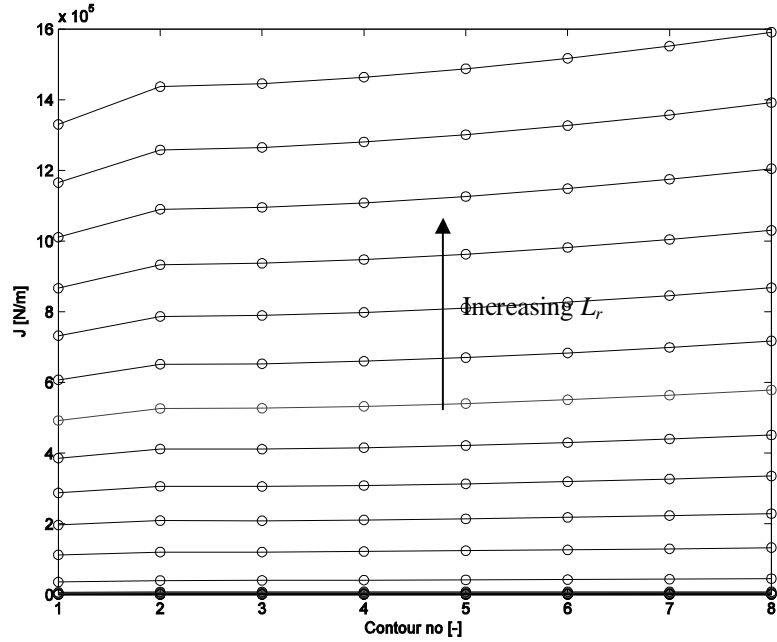


Fig. 4.7. J -integrals in different contour paths for the case without weld residual stress. Each curve corresponds to a specific L_r .

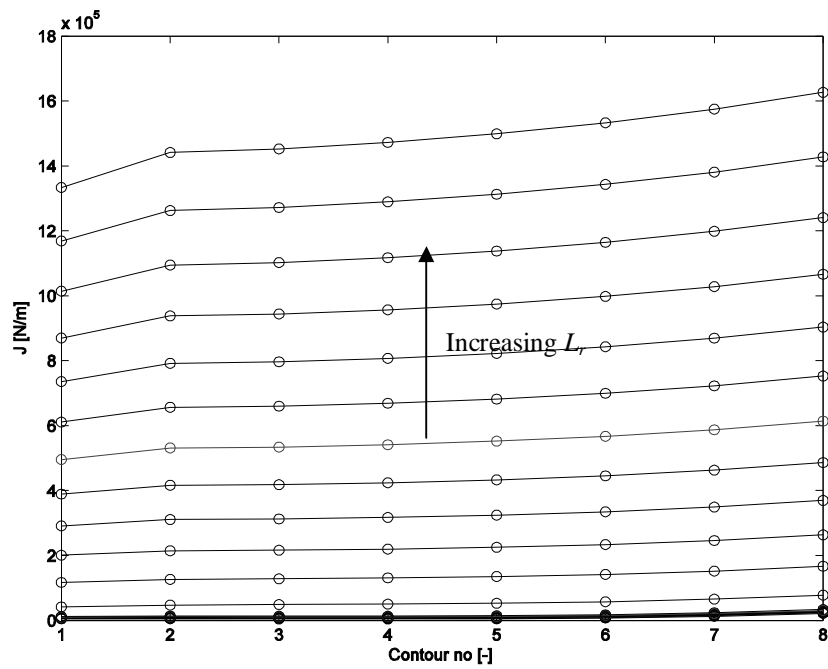


Fig. 4.8. J -integrals in different contour paths for the case with weld residual stress. Each curve corresponds to a specific L_r .

The J -integral as a function of the primary loading is shown in Fig. 4.9 for the case with and without weld residual stresses. Contour No. 4 is used in this plot.

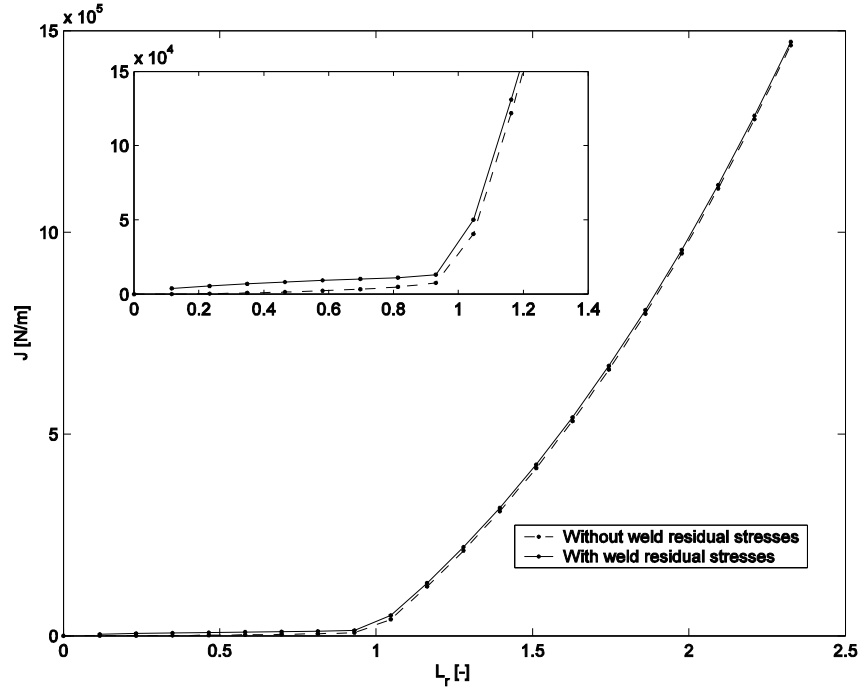


Fig. 4.9. J -integral as a function of L_r for the cases with and without weld residual stress.

In Fig. 4.10 and Fig. 4.11 the ratio defined in Equation (1-1) showing the decreasing contribution from the residual stresses to the J -integral for higher values of L_r . The results using different crack depths are also compared.

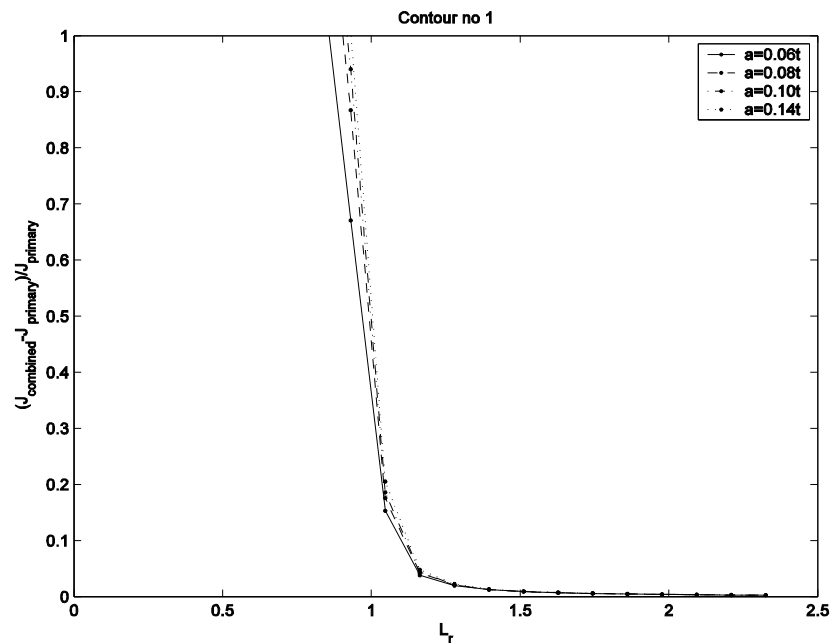


Fig. 4.10. The contribution of the weld residual stresses to the J -integral as a function of L_r for different crack depths, a . The ratio is calculated for contour No. 1.

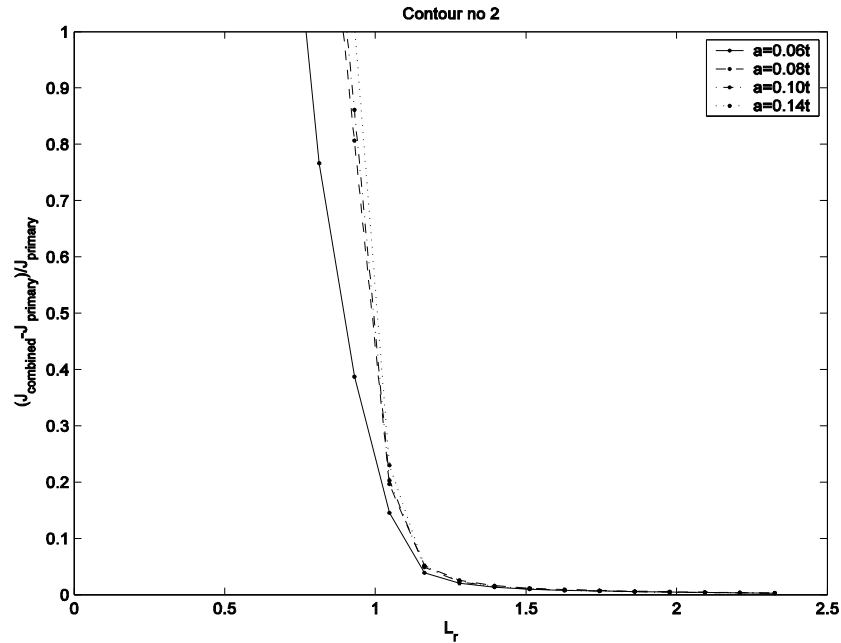


Fig. 4.11. The contribution of the weld residual stresses to the J -integral as a function of L_r for different crack depths, a . The ratio is calculated for contour No. 2.

The contribution to the fracture parameters from the residual stresses is negligible for large L_r , as shown in Fig. 4.10-4.11. The contribution from the residual stresses decreases rapidly with increasing L_r . For $L_r \geq 1.1$ the contribution of the residual stresses is less than 10% of the axial load contribution. For $L_r \geq 1.5$ the contribution of the residual stresses is almost 0%.

5 EXPERIMENTAL RESULTS

To validate the outcomes of the finite element calculations in the previous sections of this report, experimental results considering the effects of secondary stresses are needed. Although this has been addressed as an important issue in the context of fracture mechanics analysis of cracked components, there are very limited experimental results published in the open literature. Some relevant results are presented below.

5.1 Wilkowski and Rudland, Battelle, USA

Battelle is a well-known research laboratory regarding large scale tests used in fracture mechanics research. At a LBB Workshop within the SMiRT-16 conference, Wilkowski and Rudland presented a Battelle study regarding the effects of secondary stresses on pipe fracture [2001]. The study aimed to validate the treatment of the secondary stresses in pipe flaw evaluations as outlined in the ASME Section XI and the NRC LBB Regularity Guide, where the following are given:

- Uses a safety factor of 1.0 for stainless steel welds, ferritic base metals and welds.
- Does not include secondary stresses for wrought stainless steel base metals and austenitic TIG welds.
- Originally included only thermal expansion as a secondary stress, but seismic anchor motion (SAM) was recently included.
- NRC's draft SRP 3.6.3 for LBB evaluation includes primary and secondary stresses together with the same safety factor on stress or flaw size for all cases except for (wrought) austenitic base metal or austenitic TIG welds, where the thermal expansion stresses are not included.
- New suggested technical basis approach for an NRC LBB Regulatory Guide has three options:
 - Option 1: Include secondary stresses as a primary stress and conduct simple analyses with conservative safety factors.
 - Option 2: Include secondary stresses as a primary stress and conduct more complex leak-rate and fracture analysis with possibly lower safety factors.
 - Option 3: Conduct nonlinear time-history stress analysis, secondary stress contributions may be less important for fracture. Probably same applied safety factors on crack size as an Option 2 analysis.

Experimental assessments of secondary stresses were conducted on 16-inch-diameter pipes under dynamic and static loading in different test programs (IPIRG-1, IPIRG-2, BINP and DP3II). Based on these experiments, the following conclusions have been made:

- Original authors of the pipe system code recognized that global secondary stresses (not through-thickness stresses, i.e., weld residual stresses) can act as a primary stress under certain conditions. These conditions are difficult to quantify.
- For surface cracks in a pipe, having a failure stress below yield, the displacements from the local crack tip plasticity are much smaller than the pipe-system global displacements, so the secondary stresses are not relieved by yielding.
- For deeply surface-cracked pipes, the test programs illustrate that secondary stresses can behave like a primary stress.
- Through-wall-cracked pipes might behave differently, since the through-wall crack will allow for more rotation to relieve thermal expansion stresses than a surface crack. Validation of this is needed.

- Applied secondary stress safety factor for surface flawed pipes should depend on the predicted failure stress relative to the yield strength. Crack size could also be used rather than stress ratio if easier. Implication is that the safety factor for secondary stresses should be a function of the failure stress/yield strength-ratio of the pipe.
 - i) If failure stress/yield strength < 1.0 then the global secondary stresses are the same as primary stresses for fracture.
 - ii) If failure stress/yield strength > 1.0 , then the global secondary stresses become less important with some nonlinear function.

5.2 Dong et. al., Battelle, USA

Dong et. al. at Battelle have conducted a detailed study on welds in steel building structures under earthquake loading conditions [2005]. However, most of the important test data are still under embargo due to liability concerns from the funding agency. Based on their investigations on effects of the thermal and residual stresses, the following conclusions can be made:

- Residual stresses of a tri-axial nature, can have significant effects in structural integrity of cracked bodies. These stresses typically occur in complex joint types due to restraint effects. For simple joints and relatively small thickness, these effects are not significant.
- Thermal stresses, if they are of a so-called long range types (instead of forming equilibrium through thickness), can play an important role in both fracture driving force calculation and L_r calculation due to potential instability.

5.3 Mohr et. al., Edison Welding Institute, USA

Mohr et. al. at Edison Welding Institute studied treatment of residual stresses produced by welding in pipes and pressure vessels fabricated from ferritic steels [1997]. They studied the experimental data from the literature together with a finite element parametric survey to provide the basis for methods in treatment of the residual stresses in girth welds. These methods use either wall thickness and welding condition (shop or field) or the number of weld passes as input to determine an estimate of the welding residual stresses at the internal surface of the pipe. The estimate for axial residual stresses at the inside surface can then be correlated with a linearised bending residual stress that has been shown to accurately predict the effect of welding residual stresses on cracks connected to the internal surface.

They found that while welding residual stresses can reach or exceed yield in certain situations, this approximation is often excessively conservative. Such conservatism can result in the unwarranted retirement of structures and the use of more expensive materials and welding procedures than necessary. Their study gives the following recommendations in treatment of residual stresses in fracture mechanics analysis of internal surface flaws in pipes.

- The hoop residual stresses were found to be somewhere between $0.2-1.0 \cdot \sigma_y$. No strong dependence was noted for either pipe thickness or welding heat input, either cumulative or as a net heat input per pass.
- The axial residual stresses at the internal surface were found to be dependent on the wall thickness of the pipe for welds within a limited range of net heat input per pass of 10 to 20 kJ/in. Small thickness pipes had the highest stresses while larger thickness pipes had progressively lower stresses.
- The pipe thickness and maximum heat input per pass are the two parameters which can be used to normalize the residual stress distributions at the weld in obtaining a more general treatment of these stresses.

- Based on the upper bound of the available data on residual stresses in pipes, a method is defined for estimating the axial residual stresses at the internal surface of pipes. The magnitude of residual stress σ_{RS} is estimated based on the nominal wall thickness t (inch), the welding heat input C_w (kJ/in) and the number of weld passes n as given below.
- Correlation based on welding heat input gives (also shown in Fig. 5.1):

$$\sigma_{RS} = \sigma_Y \quad \text{For } (t \leq 12.7 \text{ mm})$$

$$\sigma_{RS} = \sigma_Y \left(1.222 - \frac{t}{57.15 / C_w} \right) \quad \text{For } (12.7 < t \leq 69.85 \text{ mm})$$

$$\sigma_{RS} = 0 \quad \text{For } (t > 69.85 \text{ mm})$$

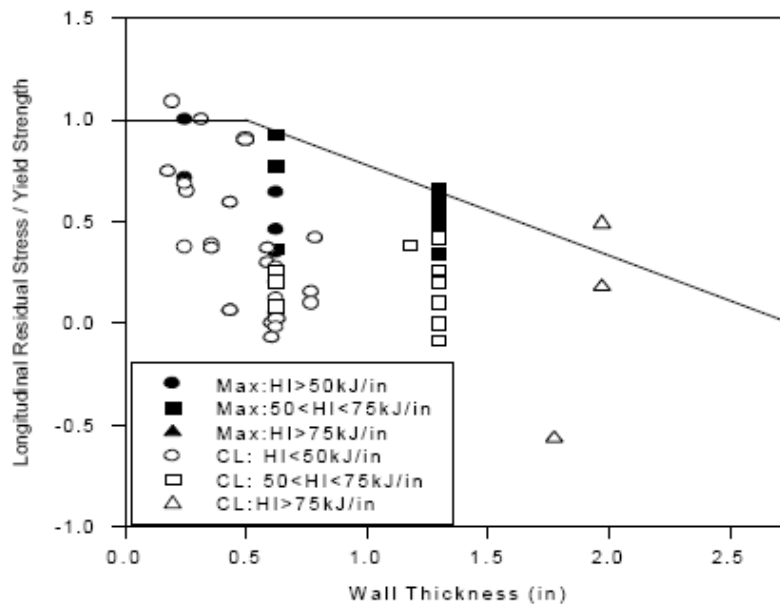


Fig. 5.1. The estimation method compared with measured data of axial residual stresses (based on welding heat input).

- Correlation based on number of weld passes gives (also shown in Fig. 5.2):

$$\sigma_{RS} = \sigma_Y \quad \text{For } n \leq 5$$

$$\sigma_{RS} = \sigma_Y \left(1.33 - \frac{n}{15} \right) \quad \text{For } 5 < n \leq 20$$

$$\sigma_{RS} = 0 \quad \text{For } n > 20$$

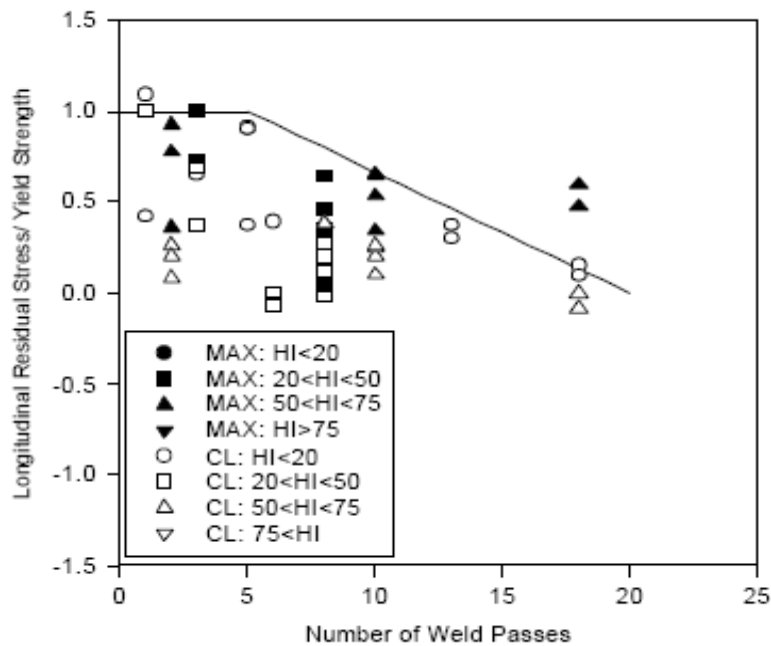


Fig. 5.2. The estimation method compared with measured data of axial residual stresses (based on number of weld passes).

5.4 Sharples et. al., AEA Technology, UK

Sharples et al at AEA Technology experimentally studied the effect of residual stresses on fracture behaviour of plates subjected to combined primary and secondary stresses [1995]. The test program was designed to cover failures from the fracture to the plastic collapse regimes, i.e. from low to high L_r values on the R6 failure assessment diagram. The test programme was conducted in several pair tests, each pair consisting of one specimen containing residual stresses and the other of identical plate and crack dimensions, but without residual stresses.

The test specimens were large plates containing through-thickness centre cracks. The test plates were of the aluminium 2024 material, with the room temperature 0.2% proof stress of 395 MPa and the ultimate tensile stress of 505 MPa. Electron beam welding was used to introduce tensile residual stresses in the central region of the plate balanced by compression in the outer region. Welding residual stresses of magnitudes varying between zero to 0.57 times yield stress of the material were introduced in different test plates. CT specimens of thickness 6.25mm and 25mm were used to determine fracture toughness properties of the material.

The general Option 1 Failure Assessment Diagram (FAD) of the R6-method was used in fracture analysis of these tests. It was considered that using Option 1 would be adequate, since this option has been shown to be a lower bound curve for most engineering materials. Fig. 5.3 shows the R6 predictions of two pairs of these tests. Here, tests 2P and 3P are loaded using only primary stresses (without residual stresses), and tests 2S and 3S are loaded using both primary (mechanical tension) and residual stresses.

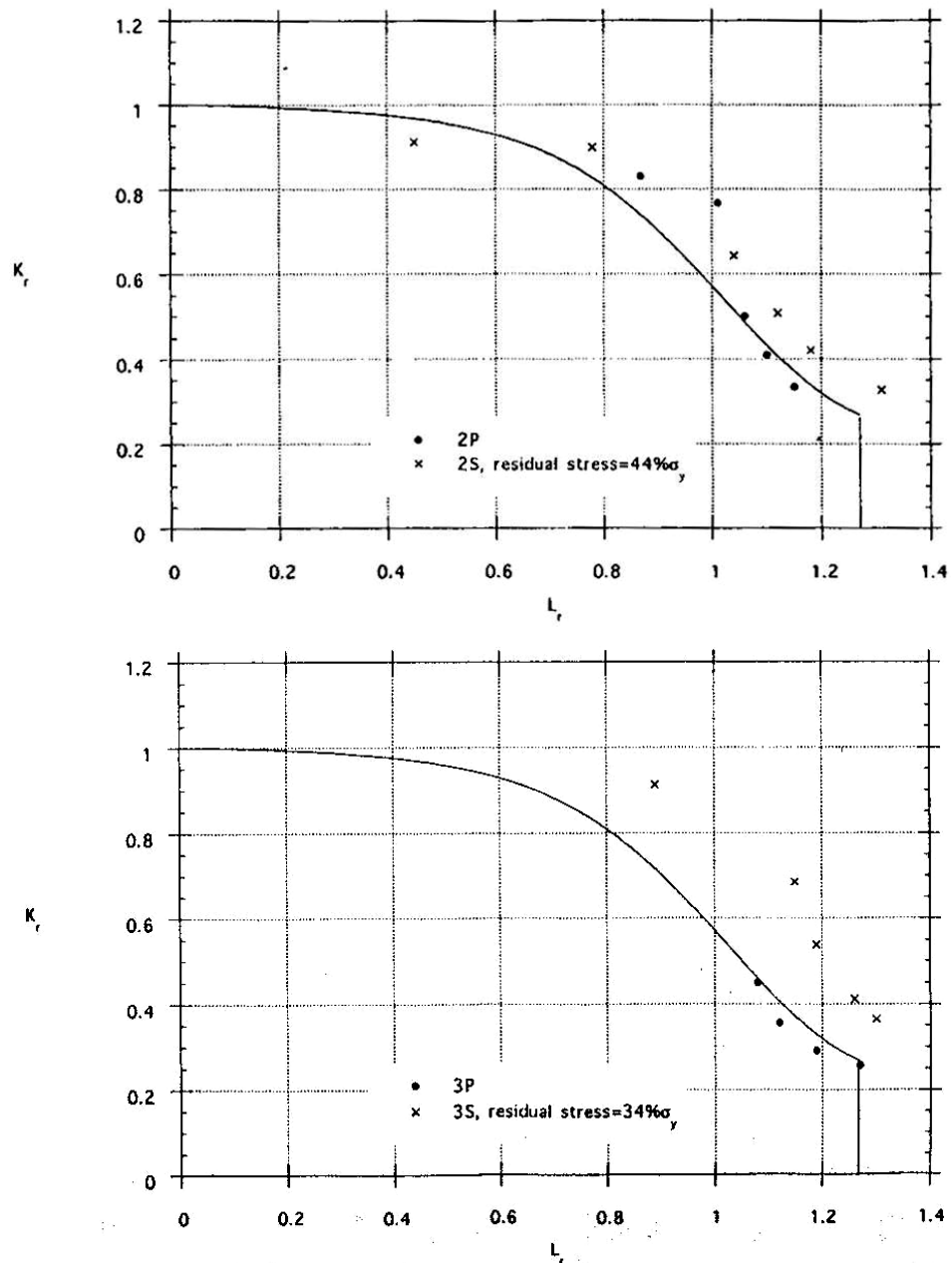


Fig. 5.3. R6 analysis of two pair tests without and with residual stresses (Sharples et. al., 1995).

Based on the study of ductile tearing in the specimens tested in this experimental programme, the following conclusions have been made:

- There is a large influence of residual stresses on load-bearing capacity of the specimens at low L_r values. The influence is greater for higher levels of residual stresses than for lower levels (see Fig. 5.4).
- The influence of residual stresses reduces as L_r increases until L_r values of approximately unity, and beyond that, where there is no effect at all (see Fig. 5.4).
- The Option 1 of the R6 method gives slightly conservative values of applied load for various amounts of crack extension for most of the tests of this study.

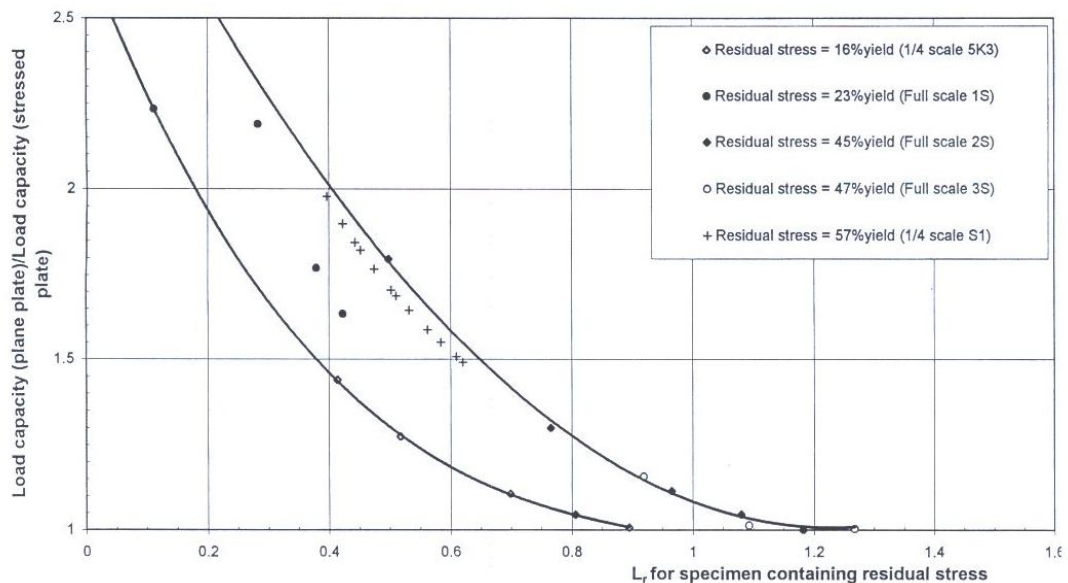


Fig. 5.4. Ratio of load-bearing capacity of aluminium alloy plates with and without residual stresses as a function of L_r . The lines are simple fits bounding the data (Sharples et. al., 1995).

It should be noted that since this study is conducted on an aluminium alloy, its conclusions for other materials (used in nuclear reactor pressure vessels and pipes) need to be validated.

5.5 Sharples and Gardner, AEA Technology, UK

Sharples and Gardner at AEA Technology studied the influence of residual stresses on fracture behaviour of Type 316 stainless steel plates and welds [1996]. The test programme consisted of 12 wide plates containing different crack configurations, through-thickness and surface cracks located in base material and welds. All tests were conducted at room temperature and under tension loading. Material properties used in these assessments were obtained from small specimens cut from the appropriate test plates. Fracture toughness and ductile resistance curve were obtained from compact tension (CT) specimens for the base and weld materials using a similar thickness as in the relevant large-scale tests.

All tests were assessed by Option 1 failure assessment diagram (FAD) of the R6-method. The R6 calculations for the weld tests were carried out both excluding and including residual stresses. For one weld test, a constant value equal to the yield strength of the weld was assumed as a residual stress. For two other weld tests, the residual stresses were evaluated by finite element calculations based on recorded measurements of post-weld shrinkage.

Based on the study of ductile tearing in the specimens tested in this experimental programme, the following conclusions have been made:

- Significant amounts (in general over 10 mm) of ductile tearing were observed in both the plain plates and weld plates containing through-thickness cracks. Thus, fracture assessments based solely on initiation fracture toughness are hence likely to be unduly conservative in determination of critical crack sizes.

- For through-thickness cracks in welds, the results indicated that residual stresses should be included in the R6 calculations for initiation to be conservatively predicted. A good estimate of the residual stresses was needed for a more adequate predication of the test results.
- The R6 calculations were shown to give conservative underprediction of instability for through-thickness cracks in both base and weld materials. For cracks in weld tests, the conservatism was still present when residual stresses were excluded from the calculations.
- The R6 predictions for the case with a semi-elliptical surface crack in a repair weld have indicated that the residual stresses should be excluded in order to ensure conservatism in a leak-before-break (LBB) assessment. However, the through-wall residual stress field should be included to ensure conservatism in a leak tightness calculation.
- There was some evidence to suggest that considerations of residual stresses may depend on the extent of plasticity present in the section of the component containing the crack. Having to include residual stresses or not may depend on whether the section containing the crack is in contained yielding or not.

5.6 The IPIRG project, Battelle, USA

During the IPIRG project, the U.S. Degraded Piping Program, an effort was undertaken to assess the significance of weld residual stresses on the fracture behaviour of low toughness stainless steel flux welds, Wilkowski et. al. (1987). Experiments were conducted on identical welds with similar circumferential flaws, but in one case the weld was in the as-welded condition and in the other case the weld was solution annealed. Tests on 406 mm (16-inch) diameter pipe were conducted with internal circumferential surface flaws in the centre of the welds. Experiments on 152 mm (6-inch) diameter pipe were conducted with circumferential through-wall cracks in the centre of the welds. The solution annealing raised the *J-R* curve of the weld metal when standard 1T-CT specimens were used.

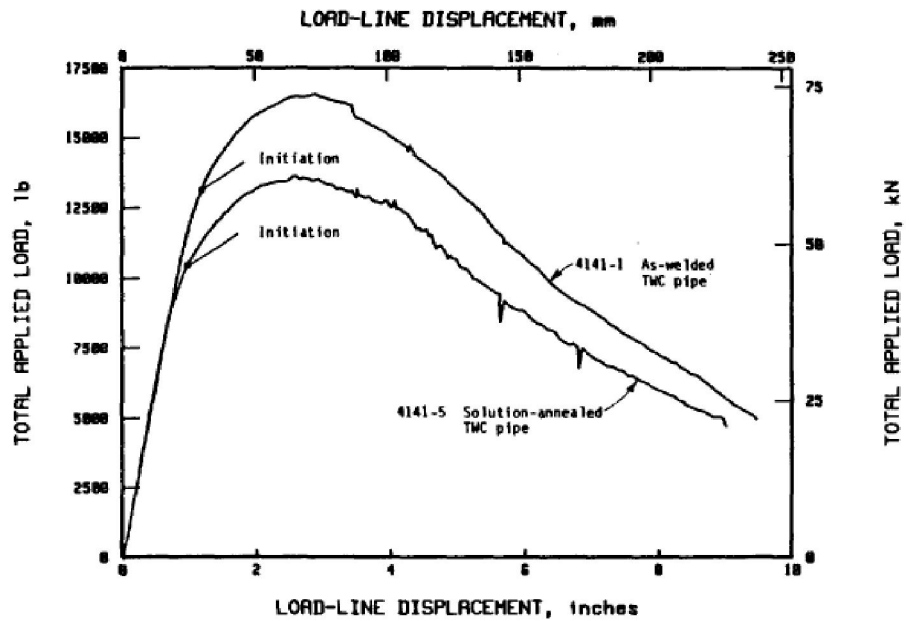
The strength of the base metal was not affected by the solution annealing, but the weld metal yield strength was significantly decreased. Since it is typically recommended that the base metal stress-strain curve and the weld metal fracture properties be used in fracture analyses, it was anticipated that the solution-annealed weld would have a higher load-carrying capacity. The elimination of the weld residual stresses should have further increased the solution-annealed welded pipe load-carrying capacity. All of the pipe experiments were conducted under constant internal pressure and loaded in four-point bending until failure. The pipes were pressurized with water at 550 °F (288 °C).

Fig. 5.5 shows the results of the 152 mm (6-inch) and 406 mm (16-inch) diameter pipe experiments. The surprising aspect was that the as-welded pipes had higher load-carrying capacities by 15 to 20 percent. Hence, the effect of the lower weld metal strength for the solution-annealed weld was much more important than the weld residual stresses or the effect of increasing the weld metal toughness by the solution annealing. Consequently, for pipe fracture applications where ductile tearing will occur, even in the elastic-plastic fracture mechanics range, the weld residual stresses can be ignored. This may not necessarily be true for Class 2 or 3 piping that operate at lower temperatures where LEFM fracture maybe possible.

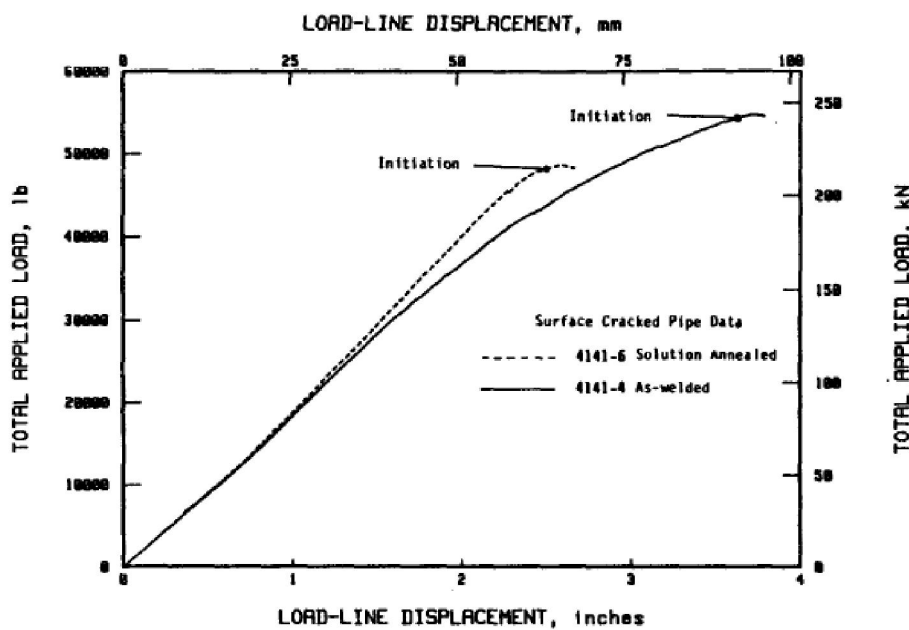
It should be noted that this observation of the effects of residual stresses is from an individual effort, and should not be generalized. It should be noted hat this outcome has not been included in the general conclusions of the IPIRG project, Wilkowski et. al. (1997).

Regarding the significance of large secondary stresses on pipe fracture, the data from the IPIRG-1 program showed that seismic anchor motion and thermal expansion stresses contribute as much to fracture as do the primary stresses for the case where the surface crack is large. In this case, the failure

stresses are below the yield strength of the pipe system. This is consistent with the “Local Overstrain” warnings in the ASME piping design stress rules. Hence, a screening criterion can be created to show when the secondary stresses should be treated as a primary stress. In the post-yield regime, the criterion should be sensitive to the pipe-system geometry, and strain-hardening of the uncracked pipe material. No simple modifiable criteria exists yet for determining how much the effect of the secondary stresses maybe diminished if the failure stresses in the pipe system would be above yield, Wilkowski et al. (1997).



(a) 152-mm (6-inch) through-wall-crack experiments



(b) 406-mm (16-inch) surface-crack experiments

Fig. 5.5. Comparison of total applied load as a function of load-line displacement for Type 304 stainless steel SAW pipe experiments with as-welded and solution-annealed stainless steel submerged arc welds.

5.7 Lei et. al., Imperial College, UK

Lei et. al. at the Department of Mechanical Engineering of Imperial College have presented a modified J -integral to produce a path-independent integral when residual stresses are present [2000]. The residual stress problem is treated as an initial strain problem. Note that this is not an experimental study. However, its outcomes are judged to be very interesting for treatment of secondary stresses in fracture analyses of components subjected to both primary and secondary stresses.

When initial strains (due to residual stresses) are present, the total strain is written as the sum of the mechanical strain, ε_{ij}^m , and the initial strain, ε_{ij}^0 , in the following form:

$$\varepsilon_{ij} = \varepsilon_{ij}^m + \varepsilon_{ij}^0 \quad (5-1)$$

The initial strain remains constant during subsequent deformation and the mechanical strain is related to the stress through the mechanical constitutive law. Thus, the modified J -integral can be obtained from the following equation:

$$J = \int_{\Gamma} (W \delta_{ij} - \sigma_{ij} \frac{\delta u_j}{\delta x_i}) n_i ds + \int_A \sigma_{ij} \frac{\delta \varepsilon_{ij}^0}{\delta x_i} dA \quad (5-2)$$

Where W is defined as the mechanical strain energy density having the following form:

$$W = \int_0^{\varepsilon_{ij}^m} \sigma_{ij} d\varepsilon_{ij}^m \quad (5-3)$$

Implementation of this integral in finite element procedures is given in Lei et. al. [2000]. The results of this integral compared with the common J -integral in calculation of J for an edge-cracked plate is given in Fig. 5.6. The plate contains welding residual stresses, and is subjected to four-point bending.

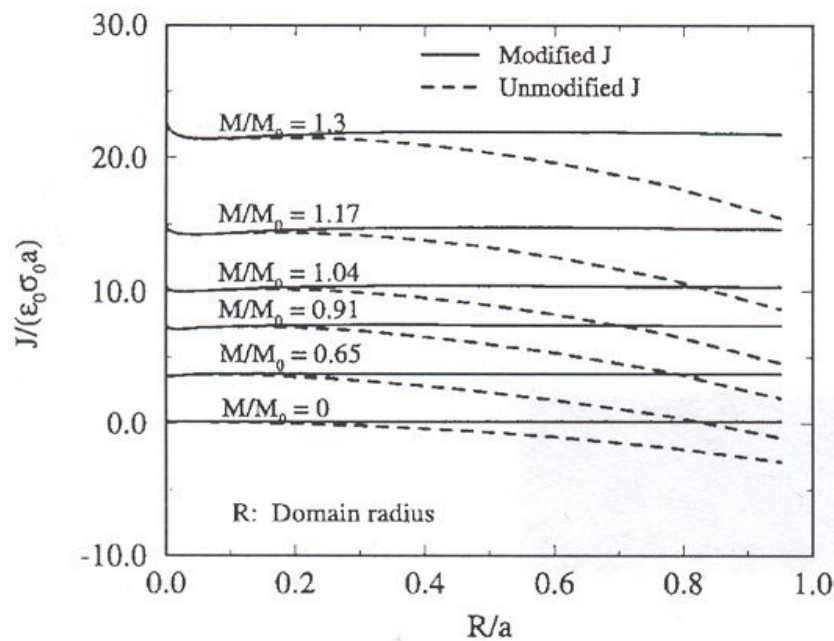


Fig. 5.6. Normalized J versus domain radius ahead of the crack obtained by modified and unmodified J in a plate subjected to 4P-bending, M_0 is the limit load (from Lei et. al. [2000]).

As can be seen in Fig. 5.6, one gets a path independent J -integral for all load levels from a primary stress of zero up 1.3 times the limit load (with weld residual stresses present at all load levels).

5.8 Discussion

Although consideration of the secondary stresses in fracture assessment of cracked components has been addressed as an important issue, there are very limited experimental results published in the open literature. There is no systematic study that could be found in the literature. The published experiments are individual tests on different materials (aluminium, stainless steel, welds), and give mostly quantitative conclusions. A common conclusion from these experiments is that for high level of primary loads ($L_r > 1.0$), the significance of the through-thickness secondary stresses (i.e. weld residual stresses or stresses from a thermal transient) are negligible. This issue needs to be verified for L_r -values close to unity.

6 A STRATEGY FOR FRACTURE ASSESSMENT OF DEFECTS IN DUCTILE MATERIALS

The significance of secondary stresses (mainly weld residual stresses, but also stresses from thermal transients) for cracks in pipes of ductile materials has been investigated. Both thin-walled and thick-walled pipes were studied. This was done by calculating the relative contribution from the weld residual stresses to CTOD and the J -integral. Both circumferential and axial cracks were analysed. However, the general conclusions from this study are also valid for others components made of ductile materials. Also presented in this report are some published experimental investigations conducted on cracked components of ductile materials subjected to both primary and secondary stresses. Based on the outcome the presented investigations, an analysis strategy for fracture assessment of defects in ductile materials of nuclear components are proposed below.

6.1 Motivation for a new strategy for fracture assessment of defects in ductile materials

The treatment of secondary stresses as expressed in the SACC handbook by Andersson et al [1996] or the ProSACC handbook by Dillström et. al. [2004] is believed to be too conservative for ductile materials. This is because of the general approach does not account for the improved fracture resistance caused by ductile tearing and furthermore there is experimental evidence that the contribution of residual stresses to fracture diminishes as the degree of yielding increases to a high level. The investigations presented in this report verify this.

One drawback (and the major reason for conservatism in the handbooks above) with the deterministic safety evaluation system used today, is that it overestimates the contribution from secondary stresses (i.e. welding residual stresses or stresses from a thermal transient) for ductile materials. A new strategy for fracture assessment should therefore give a quantitative recommendation on how to treat secondary stresses for both low and high L_r -values in a R6 fracture assessment. We propose that the new strategy define new safety factors against fracture described by K_I and differentiate between $SF_K^{Primary}$ (relating to primary stresses) and $SF_K^{Secondary}$ (relating to secondary stresses).

Before presenting a quantitative recommendation for the new deterministic safety evaluation system, we first analyse the three cases presented in this report.

6.2 Case study 1, a thin-walled pipe containing a circumferential surface crack

The first case to be analysed, in order to define the new deterministic safety evaluation system, is the case with a thin-walled pipe containing a circumferential surface crack (see section 2 in this report, more details are given in Delfin et al. [1997]).

The pipe has an inner radius, $r_i = 38$ mm and a wall-thickness, $t = 11$ mm (see Fig. 2.1). The weld is oriented circumferentially. The crack is a completely circumferential crack with a depth of 3.26 mm.

Using a pipe material with a yield strength, $\sigma_y = 230$ MPa and an assumed tensile strength, $\sigma_u = 230$ MPa (assuming an elastic perfectly plastic material model), gives a handbook limit load of 162 MPa (see section 2.2.1). This data will be used in the analysis below. Another possible choice would be to use the finite element analysis presented in section 2 that gives a limit load of 228 MPa, which is equivalent to using a handbook solution with a yield strength, $\sigma_y = 230$ MPa and an assumed tensile strength, $\sigma_u = 324$ MPa. However, for the purpose of this investigation, these two data sets would lead to similar results.

The baseline load case consists of a primary membrane load (acting in the axial direction of the pipe) and a secondary load (welding residual stresses, see Fig. 2.2). The primary load is increased up to a load equivalent to $L_r \approx 2.0$ ($\sigma_{mem}^{primary} \approx 162 \cdot 2 = 324$ MPa).

The goal of this analysis is to do a handbook analysis (using the ProSACC handbook, Dillström et. al. [2004]) which resembles the FE-analysis presented in section 2, i.e. gives the same decreasing contribution to J from the secondary stresses as L_r increases.

In section 2 the relative difference of J with and without secondary stresses are given in Fig. 2.6 (also summarised in Table 6.1 below).

Table 6.1. The relative difference of J with and without residual stresses (for the case with a thin-walled pipe containing a circumferential surface crack).

L_r	$(J_{combined} - J_{axial}) / J_{axial}$	$\sigma_{mem}^{primary}$ [MPa]
0.8	7.0	129.6
0.9	2.5	145.8
1.0	0.73	162.0
1.1	0.366	178.2
1.2	0.244	194.4
1.4	0.126	226.8
1.6	0.069	259.2
2.0	0.025	324.0

In Fig. 6.1 a handbook analysis (using the ProSACC handbook, Dillström et. al. [2004]) of this case is compared to the analysis given by Delfin et al. [1997]. As can be seen, the handbook analysis overestimates the contribution from secondary stresses (the results are presented using both linear and log scales). In the handbook analysis, J is estimated using equation (6.1)

$$J = \frac{(1-\nu^2)K_I^2}{E} \frac{1}{[f_{R6}(L_r) - \rho]^2} \quad (6-1)$$

where f_{R6} is the R6 option 1 curve and ρ is a parameter that takes into account plastic effects because of interaction between secondary and primary stresses.

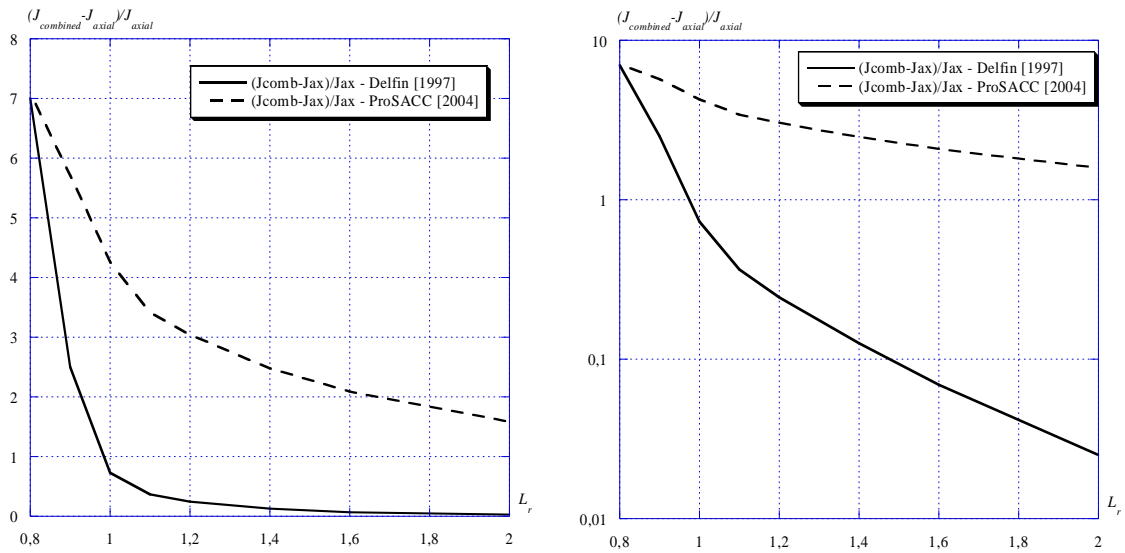


Fig. 6.1. The relative difference of J with and without residual stresses, comparison between a handbook solution and the analysis given by Delfin et al. [1997].

By scaling the secondary stresses it is possible to get a result using the handbook solution that is equal to the results presented by Delfin et al. [1997]. The resulting scale factor, S_{Case1} , is given in Fig. 6.2 (the results are presented using both linear and log scales).

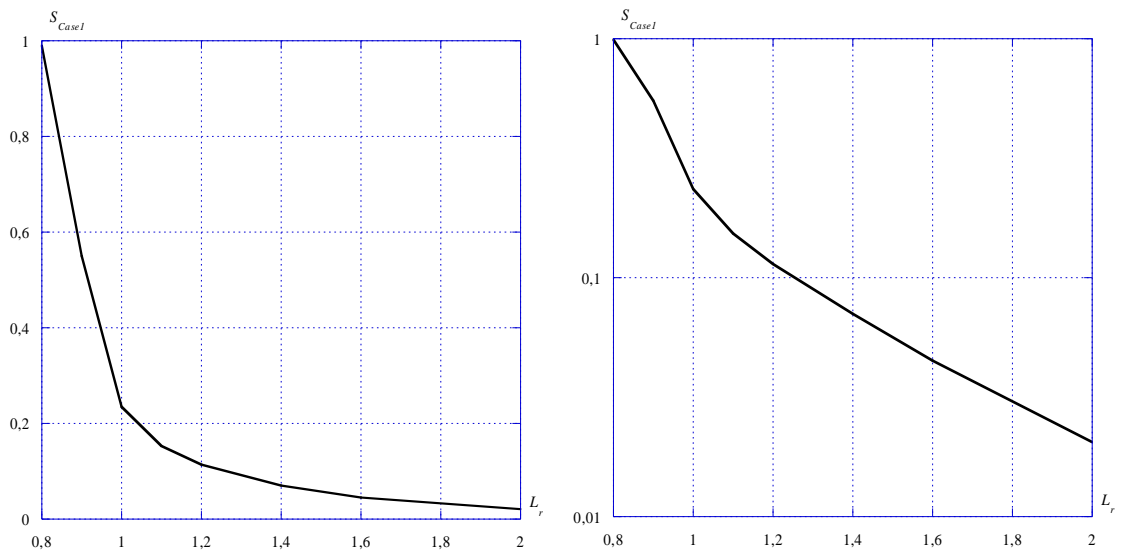


Fig. 6.2. Scale factor. S_{Case1} , used in the handbook solution to get a result that is equal to the results presented by Delfin et al. [1997].

6.3 Case study 2, a thick-walled pipe containing a circumferential surface crack

The second case to be analysed, in order to define the new deterministic safety evaluation system, is the case with a thick-walled pipe containing a circumferential surface crack (see section 3 in this report, more details are given in Anderson and Dillström [2004]).

The pipe has an inner radius, $r_i = 300$ mm and a wall-thickness, $t = 40$ mm (see Fig. 3.2). The weld is oriented circumferentially. The crack is a completely circumferential crack with a depth of 5 mm.

Using a pipe material with a yield strength, $\sigma_y = 230$ MPa and an assumed tensile strength, $\sigma_u = 230$ MPa (assuming an elastic perfectly plastic material model), gives a handbook limit load of 201.2 MPa. This data will be used in the analysis below.

The baseline load case consists of a primary membrane load (acting in the axial direction of the pipe) and a secondary load (welding residual stresses, see Fig. 3.4). The primary load is increased up to a load equivalent to $L_r \approx 2.0$ ($\sigma_{mem}^{primary} \approx 201.2 \cdot 2 = 402.4$ MPa).

The goal of this analysis is to do a handbook analysis (using the ProSACC handbook, Dillström et. al. [2004]) which resembles the FE-analysis presented in section 3, i.e. gives the same decreasing contribution to J from the secondary stresses as L_r increases.

In section 3 the relative difference of J with and without secondary stresses are given in Fig. 3.13-3.14 (also summarised in Table 6.2 below). Data for $L_r = 0.8-0.9$ should not be used in the comparison, since the difference between J -based data and CTOD-based data is too large for these L_r -values.

Table 6.2. The relative difference of J with and without residual stresses (for the case with a thick-walled pipe containing a circumferential surface crack).

L_r	$(J_{combined} - J_{axial}) / J_{axial}$	$\sigma_{mem}^{primary}$ [MPa]
1.0	1.32	201.2
1.1	0.36	221.3
1.2	0.15	241.4
1.4	0.054	281.7
1.6	0.016	321.9
2.0	~0.001	402.4

In Fig. 6.3 a handbook analysis (using the ProSACC handbook, Dillström et. al. [2004]) of this case is compared to the analysis given by Anderson and Dillström [2004]. As can be seen, the handbook analysis overestimates the contribution from secondary stresses (the results are presented using both linear and log scales). In the handbook analysis, J is estimated using equation (6.1).

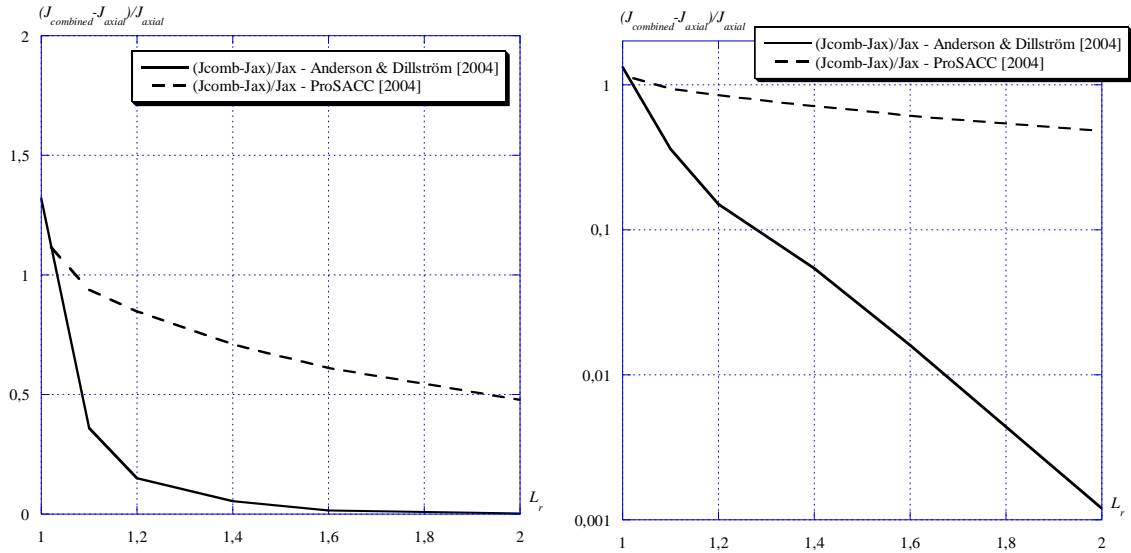


Fig. 6.3. The relative difference of J with and without residual stresses, comparison between a handbook solution and the analysis given by Anderson and Dillström [2004].

By scaling the secondary stresses it is possible to get a result using the handbook solution that is equal to the results presented by Anderson and Dillström [2004]. The resulting scale factor, S_{Case2} , is given in Fig. 6.4 (the results are presented using both linear and log scales).

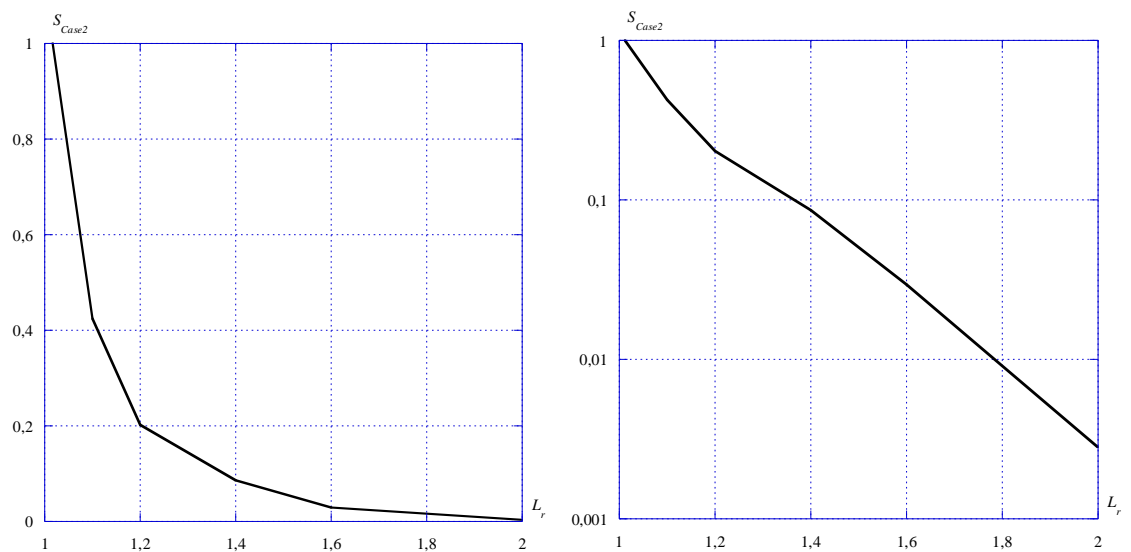


Fig. 6.4. Scale factor. S_{Case2} , used in the handbook solution to get a result that is equal to the results presented by Anderson and Dillström [2004].

6.4 Case study 3, a thick-walled pipe containing an axial surface crack

The third case to be analysed, in order to define the new deterministic safety evaluation system, is the case with a thick-walled pipe containing an axial surface crack (see section 4 in this report, more details are given in Anderson and Dillström [2004]).

The pipe has an inner radius, $r_i = 348.5$ mm and a wall-thickness, $t = 84$ mm (see Fig. 4.1). The weld is oriented circumferentially. Different crack depths was used (between $0.06 \cdot t \leq a \leq 0.14 \cdot t$, i.e. between 5.04 and 11.76 mm). All the cracks were assumed to be semicircular axial surface cracks.

Using a pipe material with a yield strength, $\sigma_y = 380$ MPa and an assumed tensile strength, $\sigma_u = 380$ MPa (assuming an elastic perfectly plastic material model), gives a handbook limit load (“pressure”) of 91,3 MPa (for the different crack depths that was used in this study). This data will be used in the analysis below.

The baseline load case consists of a primary load (a pressure acting at the inner surface of the pipe) and a secondary load (welding residual stresses, see Fig. 4.2). The primary load is increased up to a load equivalent to $L_r \approx 2.0$ ($p_i^{primary} \approx 91.3 \cdot 2 = 182.6$ MPa).

The goal of this analysis is to do a handbook analysis (using the ProSACC handbook, Dillström et. al. [2004]) which resembles the FE-analysis presented in section 4, i.e. gives the same decreasing contribution to J from the secondary stresses as L_r increases.

In section 4 the relative difference of J with and without secondary stresses are given in Fig. 4.10-4.11 (also summarised in Table 6.3 below, $a = 11.76$ mm).

Table 6.3. The relative difference of J with and without residual stresses (for the case with a thick-walled pipe containing an axial surface crack surface crack, $a = 11.76$ mm).

L_r	$(J_{combined} - J_{primary}) / J_{primary}$	$p_i^{primary}$ [MPa]
0.8	1.745	73.0
0.9	1.175	82.2
1.0	0.527	91.3
1.1	0.133	100.4
1.2	0.0396	109.6
1.4	0.0132	127.8
1.6	0.00763	146.1
2.0	0.00380	182.6

In Fig. 6.5 a handbook analysis (using the ProSACC handbook, Dillström et. al. [2004]) of this case is compared to the analysis given by Anderson and Dillström [2004]. As can be seen, the handbook analysis overestimates the contribution from secondary stresses (the results are presented using both linear and log scales). In the handbook analysis, J is estimated using equation (6.1).

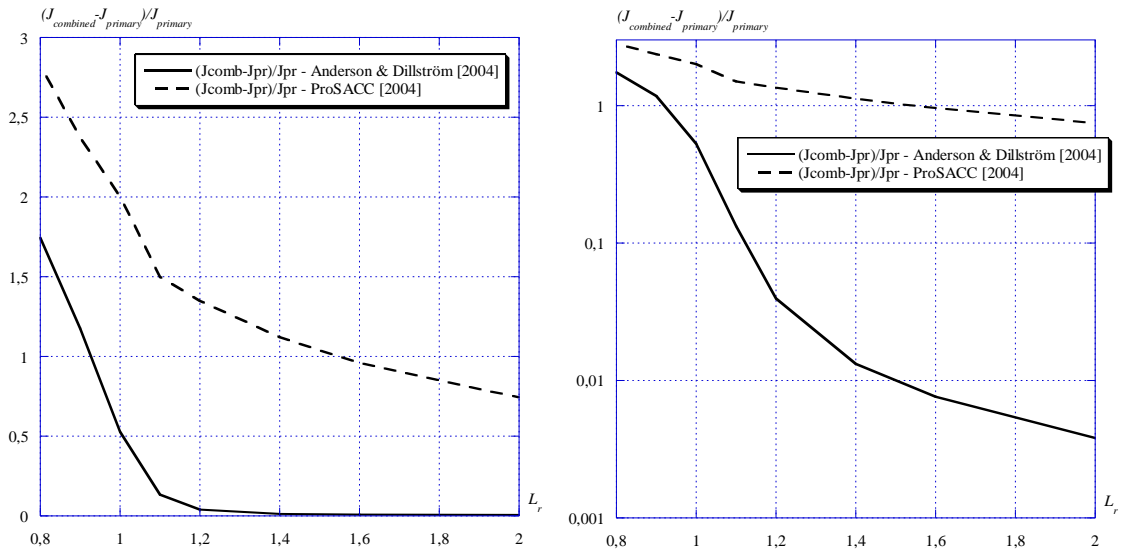


Fig. 6.5. The relative difference of J with and without residual stresses, comparison between a handbook solution and the analysis given by Anderson and Dillström [2004].

By scaling the secondary stresses it is possible to get a result using the handbook solution that is equal to the results presented by Anderson and Dillström [2004]. The resulting scale factor, S_{Case3} , is given in Fig. 6.6 (the results are presented using both linear and log scales).

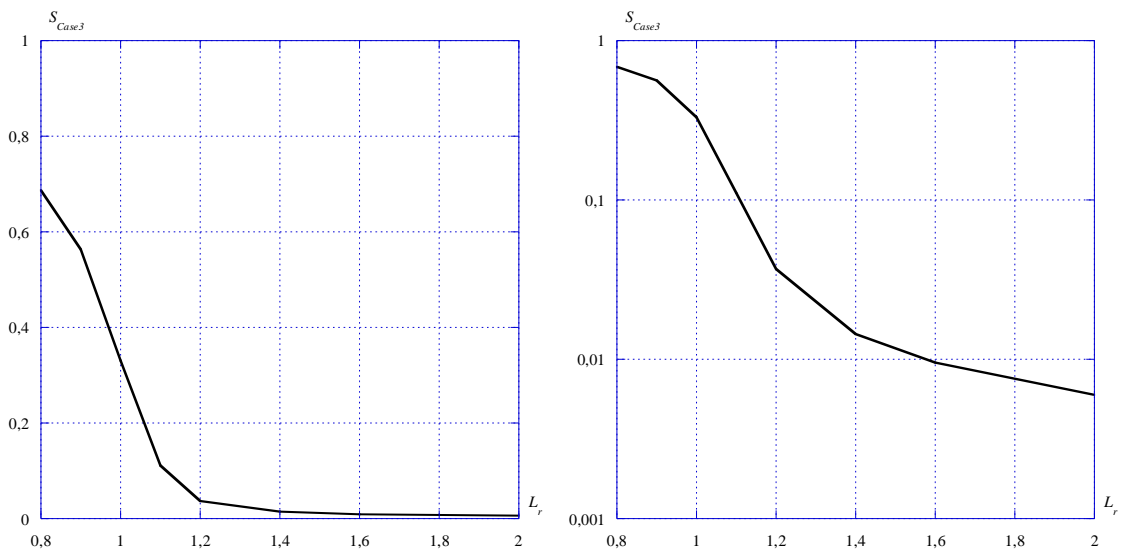


Fig. 6.6. Scale factor. S_{Case3} , used in the handbook solution to get a result that is equal to the results presented by Anderson and Dillström [2004].

6.5 Case study 4, components with through-wall cracks

In the three case studies presented above, only surface cracks are considered. To check the conditions for through-wall cracks the experimental study by Sharples et. al. [1995] was chosen.

The plate used in this study had a wall-thickness, $t = 25$ mm. Different crack lengths were used (between 25 and 157 mm). All the cracks were through-wall cracks.

Using an aluminium plate material with a yield strength, $\sigma_y = 397$ MPa and an assumed tensile strength, $\sigma_u = 397$ MPa (assuming an elastic perfectly plastic material model), gives a handbook limit load of 397 MPa (for the different crack lengths that was used in this study). This data will be used in the analysis below.

The baseline load case consists of a primary membrane load and a secondary membrane load (welding residual stresses). The primary load is increased up to a load equivalent to $L_r \approx 1.2$ ($\sigma_{mem}^{primary} \approx 397 \cdot 1.2 = 476.4$ MPa).

The goal of this analysis is to do a handbook analysis (using the ProSACC handbook, Dillström et. al. [2004]) which resembles the experimental data presented in Sharples et. al. [1995], i.e. gives the same decreasing contribution to J from the secondary stresses as L_r increases.

In Sharples et. al. [1995] the relative difference of the load capacity with and without secondary stresses is given. This data is re-evaluated as a relative difference of J (and summarised in Table 6.4 below, $l = 157$ mm).

Table 6.4. The relative difference of J with and without residual stresses (for the case with a through-wall crack in a plate, $l = 157$ mm).

L_r	$(J_{combined} - J_{primary}) / J_{primary}$	$\sigma_{mem}^{primary}$ [MPa]
0.6	0.582	238.2
0.8	0.275	317.6
1.0	0.082	397.0
1.2	0.009	476.4

In Fig. 6.7 a handbook analysis (using the ProSACC handbook, Dillström et. al. [2004]) of this case is compared to the experimental data presented in Sharples et. al. [1995]. As can be seen, the handbook analysis overestimates the contribution from secondary stresses (the results are presented using both linear and log scales). In the handbook analysis, J is estimated using equation (6.1).

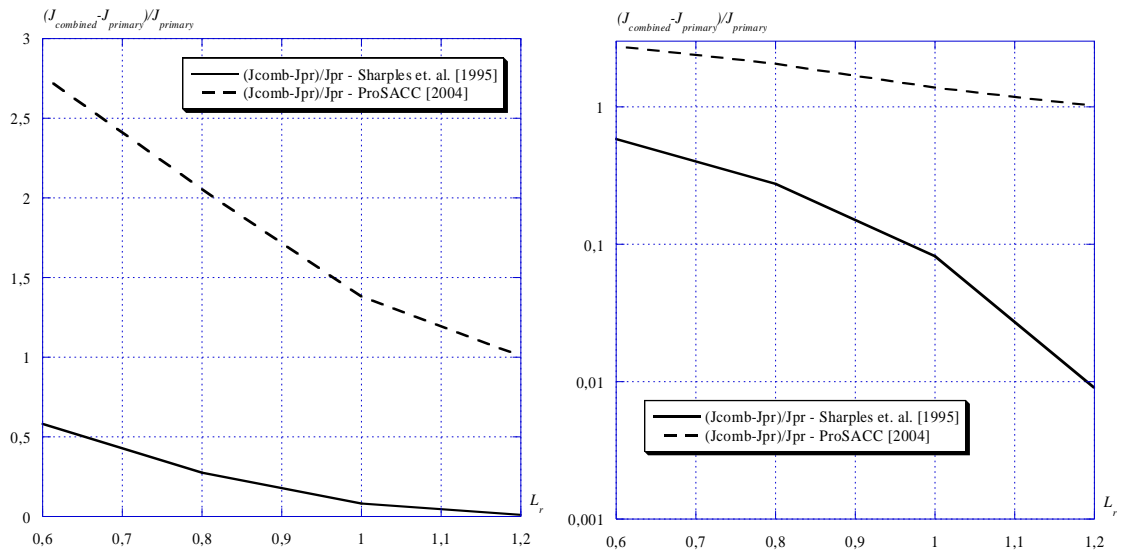


Fig. 6.7. The relative difference of J with and without residual stresses, comparison between a handbook solution and the experimental data presented in Sharples et. al. [1995].

By scaling the secondary stresses it is possible to get a result using the handbook solution that is equal to the experimental data presented in Sharples et. al. [1995]. The resulting scale factor, S_{Case4} , is given in Fig. 6.8 (the results are presented using both linear and log scales).

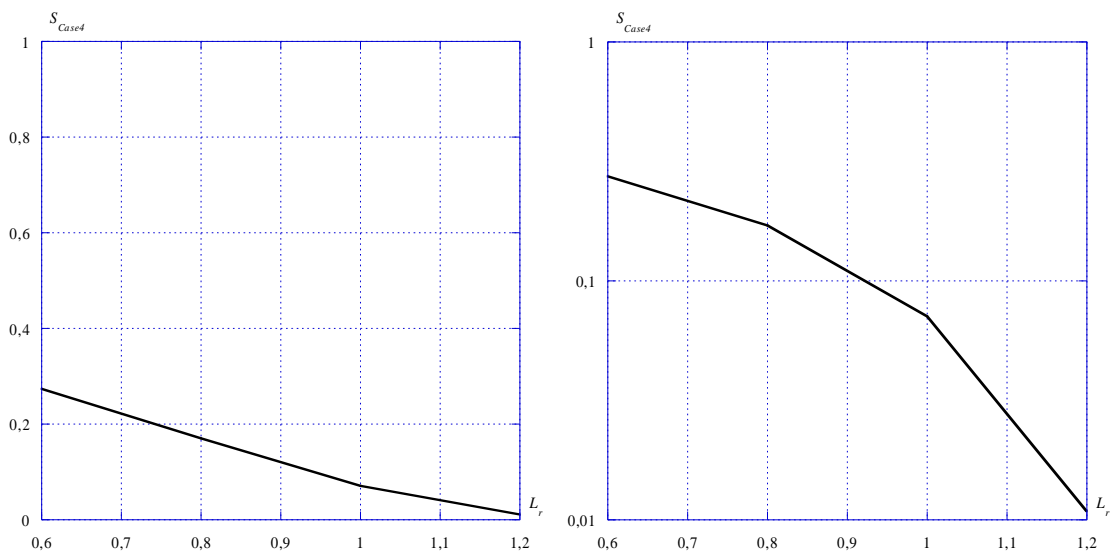


Fig. 6.8. Scale factor. S_{Case4} , used in the handbook solution to get a result that is equal to the experimental data presented in Sharples et. al. [1995].

6.6 Recommendations for a new procedure for fracture assessment of defects in ductile materials

The main purpose of this work is to investigate the significance of the secondary stresses for defects (cracks) in ductile materials within nuclear applications. The treatment of secondary stresses as expressed in the SACC/ProSACC handbooks is believed to be too conservative for ductile materials. This is because of the general approach does not account for the improved fracture resistance caused by ductile tearing and furthermore, and in this case most important, there is experimental evidence that the contribution of residual stresses to fracture diminishes as the degree of yielding increases to a high level. Available procedures for flaw assessments, such as the ASME XI code and the R6 procedure (as expressed within the SACC/ProSACC handbooks) treat this issue differently. For instance, the ASME XI code does not consider weld-induced residual stresses in some materials e.g. stainless steel welds.

One drawback (and the major reason for conservatism in the SACC/ProSACC handbooks) with the deterministic safety evaluation system used today, is that it overestimates the contribution from secondary stresses (i.e. welding residual stresses or stresses from a thermal transient) for ductile materials. A new strategy for fracture assessment should therefore give a quantitative recommendation on how to treat secondary stresses for both low and high L_r -values in a R6 fracture assessment. We propose that the new strategy define new safety factors against fracture described by K_I and differentiate between $SF_K^{Primary}$ (relating to primary stresses) and $SF_K^{Secondary}$ (relating to secondary stresses).

The analyses and experimental data presented in this report support the assumption on differentiation between primary and secondary stresses in the deterministic safety evaluation system. The relative contribution of secondary stresses to fracture diminishes as the degree of yielding increases, which means that the new procedure is only valid for ductile materials. Also, the experimental data indicates that the procedure is only valid for local through-thickness secondary stresses (i.e. weld residual stresses or stresses from a thermal transient) but not for global secondary stresses (global bending stresses, i.e. thermal expansion stresses).

6.6.1 A new deterministic safety evaluation system

To get results from the safety evaluation that is consistent with the presented analyses and experimental data we propose the following:

- That the safety factor relating to primary stresses ($SF_K^{Primary}$ and SF_L) should not be changed in the new deterministic safety evaluation system.
- That the safety factor relating to global secondary stresses ($SF_{K,global}^{Secondary}$) should not be changed in the new deterministic safety evaluation system.
- That the safety factor relating to local through-thickness secondary stresses ($SF_{K,local}^{Secondary}$) should be changed in the new deterministic safety evaluation system. This change should be consistent with the presented analyses and experimental data.

To define a new safety factor relating to local through-thickness secondary stresses ($SF_{K,local}^{Secondary}$) we propose a scaling of the safety factor against fracture described by K_I (SF_K) used in the current revision of the ProSACC handbook. This scaling should be consistent with the presented analyses and experimental data, which is summarised in Fig. 6.9.

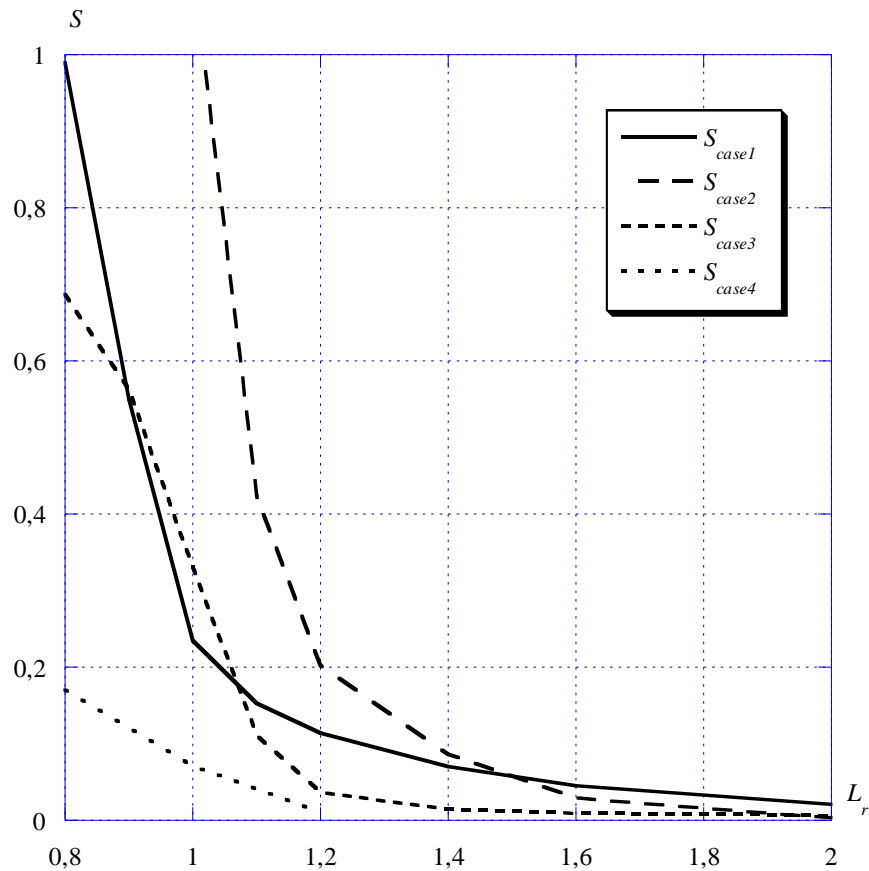


Fig. 6.9. Scale factors used in the ProSACC handbook analysis to get a result that is equal to the presented FE analyses and experimental data.

To define a new deterministic safety evaluation system the following are considered (which is summarised in Fig. 6.10a and Fig. 6.10b):

- The new procedure should be simple to use.
 - We suggest that only one parameter be used when deciding on the new safety factor relating to local through-thickness secondary stresses ($SF_{K,local}^{Secondary}$). This parameter should be L_r , which is consistent with the presented FE analyses and experimental data.
 - When applying the procedure one first make a standard handbook analysis to get an evaluation point within the R6-diagram. Secondly, one increases the primary load until one intersects the R6-curve. The L_r -value at the intersection point should be used when deciding on the new safety factor $SF_{K,local}^{Secondary}$. This is also consistent with the presented FE analyses and experimental data.
- The new procedure should only be valid for sufficiently ductile materials (i.e. austenitic stainless steel, nickel base alloys etc). Therefore, a check for ductility should be included in the procedure.
 - We suggest that this check should be related to the fracture toughness of the material. When increasing the primary load one finally intersects the R6-curve (as suggested above). If this happens at a low L_r -value, it has the practical interpretation that the material is not ductile enough. When increasing the fracture toughness, one pushes the intersection point to higher L_r -values. We suggest that the intersection point should be located at $L_r \geq 0.8$ (as indicated by Fig. 6.9), otherwise no reduction of $SF_{K,local}^{Secondary}$ should be accepted.

- We also suggest that the user of the procedure should be aware of the possibility of a non-ductile behaviour after initiation. This means that the user should verify that the material has sufficient amount of ductile tearing.
- The most commonly used safety factor (against fracture described by K_I) in the present deterministic safety evaluation system is $SF_K = \sqrt{10} = 3.16$ (for a normal/upset load event). If one wants to get a more realistic estimate of the contribution from secondary stresses $SF_{K,local}^{Secondary} = 1$ could be used. This is equivalent to use a scaling of $1/3.16 = 0.316$. Using the most conservative estimate in Fig. 6.9 (i.e. case 2), this scale factor is equivalent to $L_r \leq 1.15$. This defines the intersection point that reduces $SF_{K,local}^{Secondary}$ down to 1.0.
- In the case of an emergency/faulted load event the safety factor is $SF_K = \sqrt{2} = 1.41$. $SF_{K,local}^{Secondary} = 1$ is then equivalent to use a scaling of $1/1.41 = 0.707$. Using the most conservative estimate in Fig. 6.9 (i.e. case 2), this scale factor is equivalent to $L_r \leq 1.05$. This defines the intersection point that reduces $SF_{K,local}^{Secondary}$ down to 1.0 (for an emergency/faulted load event).
- As can be seen in Fig. 6.9, for even higher L_r -values the contribution from secondary stresses becomes negligible. If one wants to include this into the new deterministic safety evaluation system, we suggest a cut off value (i.e. using a scale factor $S = 0$) at $L_r = 2.0$. Another more conservative possibility, is to stop at a scale factor that is equivalent to $SF_{K,local}^{Secondary} = 1$.

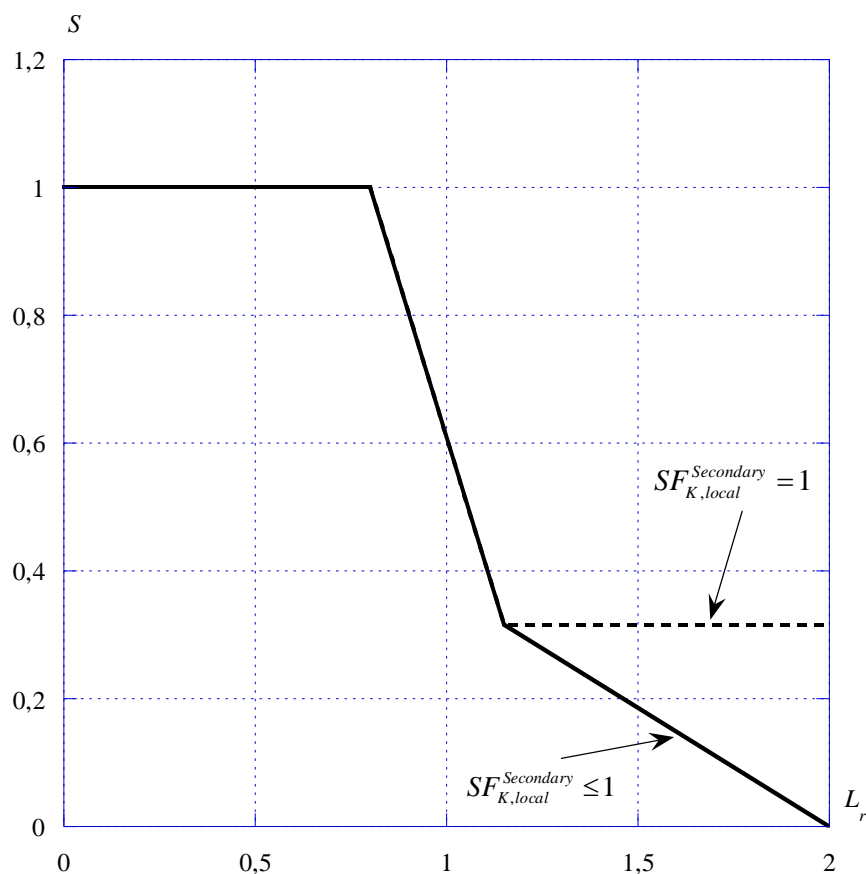


Fig. 6.10a. Scale factors (S) used in the proposed deterministic safety evaluation system (as a function of the L_r -value at the intersection with the R6-curve).

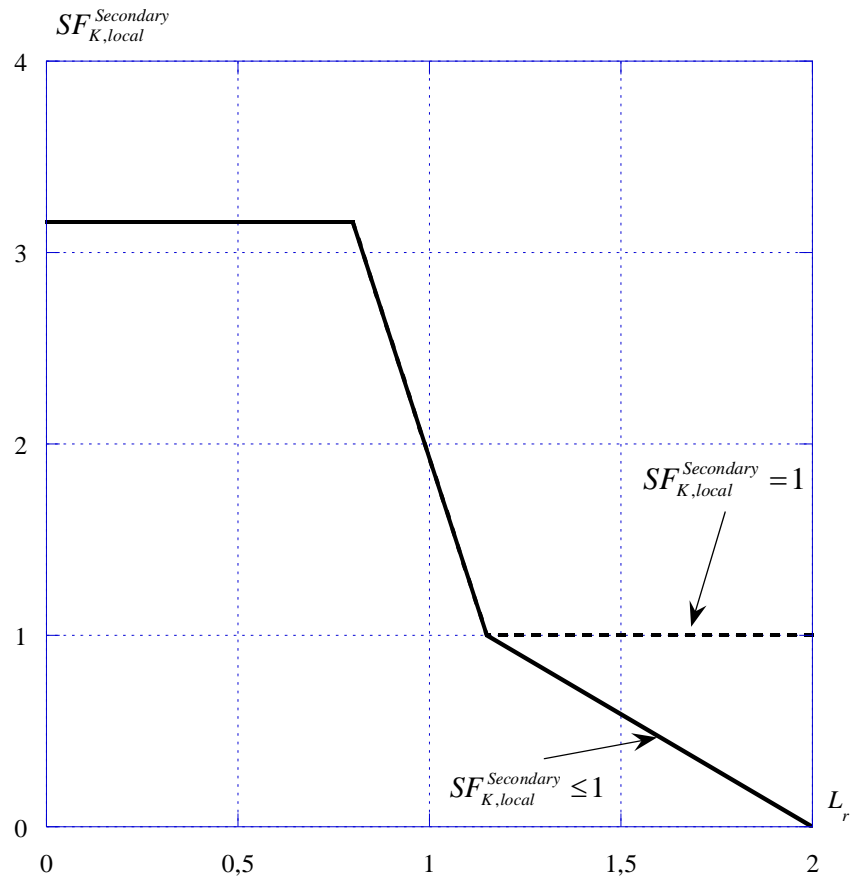


Fig. 6.10b. Secondary safety factors ($SF_{K,local}^{Secondary}$) used in the proposed deterministic safety evaluation system (as a function of the L_r -value at the intersection with the R6-curve).

- When doing a damage tolerance analysis, different crack sizes are considered in order to define an acceptable crack size. In this case the procedure will use different safety factors ($SF_{K,local}^{Secondary}$) for the different crack sizes that are needed in the analysis (see Fig. 6.11). This means that the actual secondary safety factor used to define an acceptable defect size is part of the analysis and not known in advance. An example is presented in section 6.6.2 below (the different crack sizes needed are given in Table 6.5).

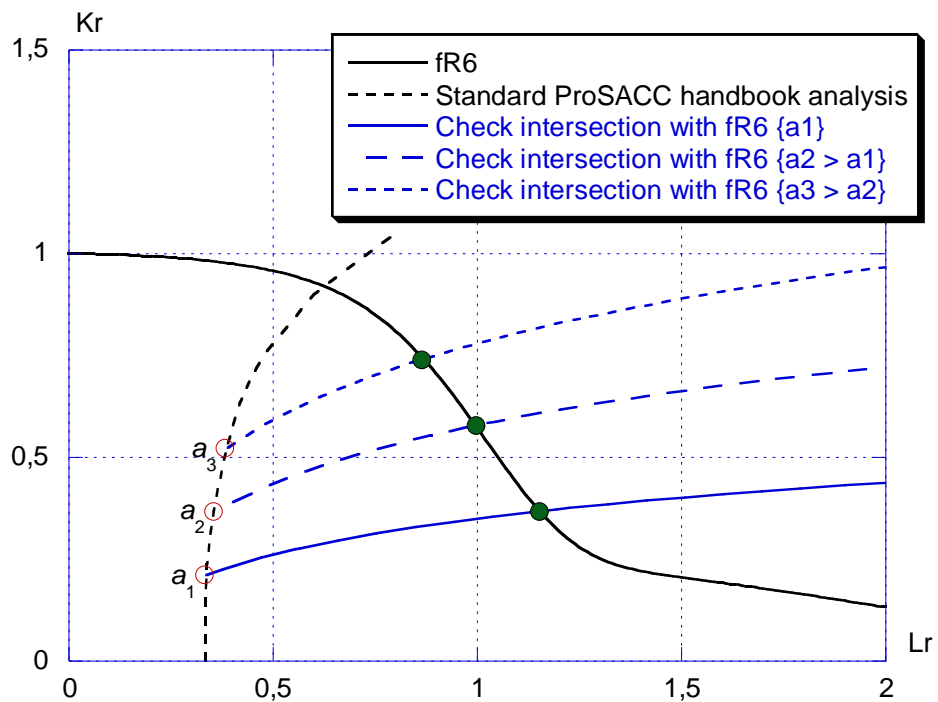


Fig. 6.11. When doing a damage tolerance analysis, different crack sizes are considered in order to define an acceptable crack size. Increase the primary load only until you hit the R6 failure assessment curve (here shown using three different crack sizes a_1 , a_2 and a_3).

6.6.2 Application of the new deterministic safety evaluation system

As an example we choose to analyse the case of axial cracks in the reactor vessel nozzle to pipe weld region (Dillström [2002]). The geometry (see Fig. 6.12) has a remaining thickness of 44.5 mm and the material is Alloy 182 with a fracture toughness of $K_{Ic} = 285 \text{ MPa}\sqrt{\text{m}}$.

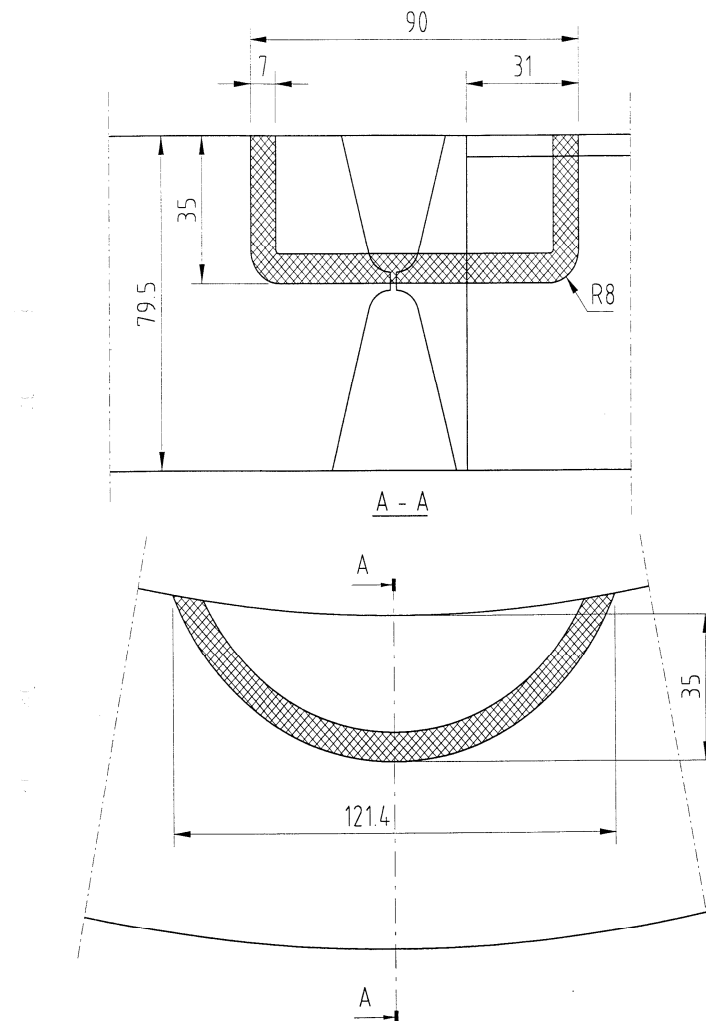


Fig. 6.12. Analysed geometry, for the case of axial cracks in the reactor vessel nozzle to pipe weld region.

The loading consists of internal pressure (primary stress) and stress from thermal transients (secondary stress) together with weld residual stresses (secondary stress). This is summarised in Fig. 6.13.

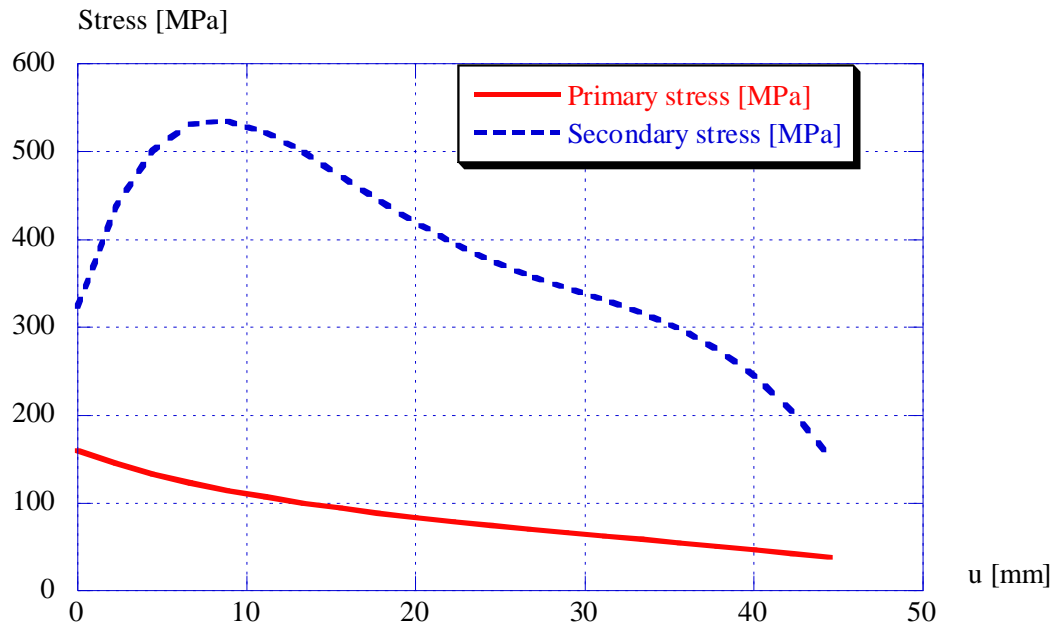


Fig. 6.13. Stress distribution used in the analysis.

When analysing this case using the current revision of the ProSACC handbook and the deterministic safety evaluation system that is used today (i.e. $SF_K^{Primary} = SF_K^{Secondary} = 3.16$) we get an acceptable defect depth of 8.2 mm and an acceptable operation time of 2460 hours. In this analysis we start with an initial defect depth $a = 2$ mm ($l = 24$ mm) and considers the possibility of stress corrosion crack growth.

Now we start a new analysis using the new proposed deterministic safety evaluation system (where $SF_K^{Primary} \neq SF_K^{Secondary}$).

- i) Calculate the assessment point in the R6 FAD.
- ii) Increase the primary load only until you hit the R6 failure assessment curve.
- iii) Check the L_r -value when you hit the R6 curve (L_r^{Hit-R6}).
- iv) Use this L_r -value to get a new secondary safety factor $SF_K^{Secondary}$ (use the scale factor from Fig. 6.10a).
- v) Check if the defect is acceptable or not.
- vi) Repeat step i) to v) for each assessment point needed in the analysis to get an acceptable defect size. Please note that the secondary safety factor increases with an increasing defect size. This clearly shows that the actual secondary safety factor used to define an acceptable defect size is part of the analysis and not known in advance.

The result of the damage tolerance analysis is summarised in Table 6.5.

Table 6.5. Summary of the results from the damage tolerance analysis.

a [mm]	l [mm]	t^{oper} [h]	K_r	L_r	L_r^{Hit-R6}	$SF_K^{Secondary}$	Accept?
2	24	0	0.189	0.233	1.240	0.89	Yes
10	37	3230	0.392	0.233	1.056	1.58	Yes
20	57	7160	0.481	0.234	0.968	2.12	Yes
20.7	58.3	7440	0.484	0.234	0.963	2.16	Yes
21	59	7580	0.486	0.234	0.958	2.19	No
30	77	11090	0.520	0.239	0.811	3.09	No

With the new proposed deterministic safety evaluation system we get an acceptable defect depth of 20.7 mm and an acceptable operation time of 7440 hours. This is large improvement compared to old system that gave an acceptable defect depth of 8.2 mm and an acceptable operation time of 2460 hours.

Obviously, the results presented above are dependent on the assumed fracture toughness (i.e. assumed ductility). In the analysis, we used the initiation fracture toughness value ($K_{Ic} = 285 \text{ MPa}\sqrt{\text{m}}$), but for a truly ductile material a toughness value that includes a small amount of stable crack growth could also be used. For Alloy 182 and $\Delta a = 1\text{-}2 \text{ mm}$ one gets $K_{cr, \Delta a=1\text{mm}} = 335 \text{ MPa}\sqrt{\text{m}}$ and $K_{cr, \Delta a=2\text{mm}} = 411 \text{ MPa}\sqrt{\text{m}}$ (Dillström [2002]). In table 6.6 and Fig. 6.14 we present the results from a sensitivity study with varying assumed fracture toughness (for the case with $a = 20.7 \text{ mm}$ and $l = 58.3 \text{ mm}$).

Table 6.6. Results from the sensitivity study with varying assumed fracture toughness (for the case with $a = 20.7 \text{ mm}$ and $l = 58.3 \text{ mm}$). S = Scale factor, " a_{acc} " = acceptable defect depth using $SF_K^{Secondary} = f(K_{cr})$.

K_{cr}	K_r	L_r	L_r^{Hit-R6}	S	$SF_K^{Secondary}$	" a_{acc} "
100	1.236	0.234	— *)	— *)	3.162	1.1
150	0.850	0.234	0.450	1	3.162	2.2
200	0.657	0.234	0.734	1	3.162	4.0
250	0.541	0.234	0.889	0.826	2.612	9.0
285	0.484	0.234	0.963	0.682	2.155	21.5
300	0.464	0.234	0.987	0.635	2.007	26.4
335	0.424	0.234	1.037	0.537	1.698	35.4
350	0.409	0.234	1.052	0.508	1.605	> 35.6
400	0.368	0.234	1.091	0.431	1.364	> 35.6
411	0.360	0.234	1.099	0.416	1.315	> 35.6
450	0.335	0.234	1.124	0.367	1.161	> 35.6
500	0.310	0.234	1.154	0.315	0.995	> 35.6

*) Note: The intersection could not be defined since $K_r > 1$.

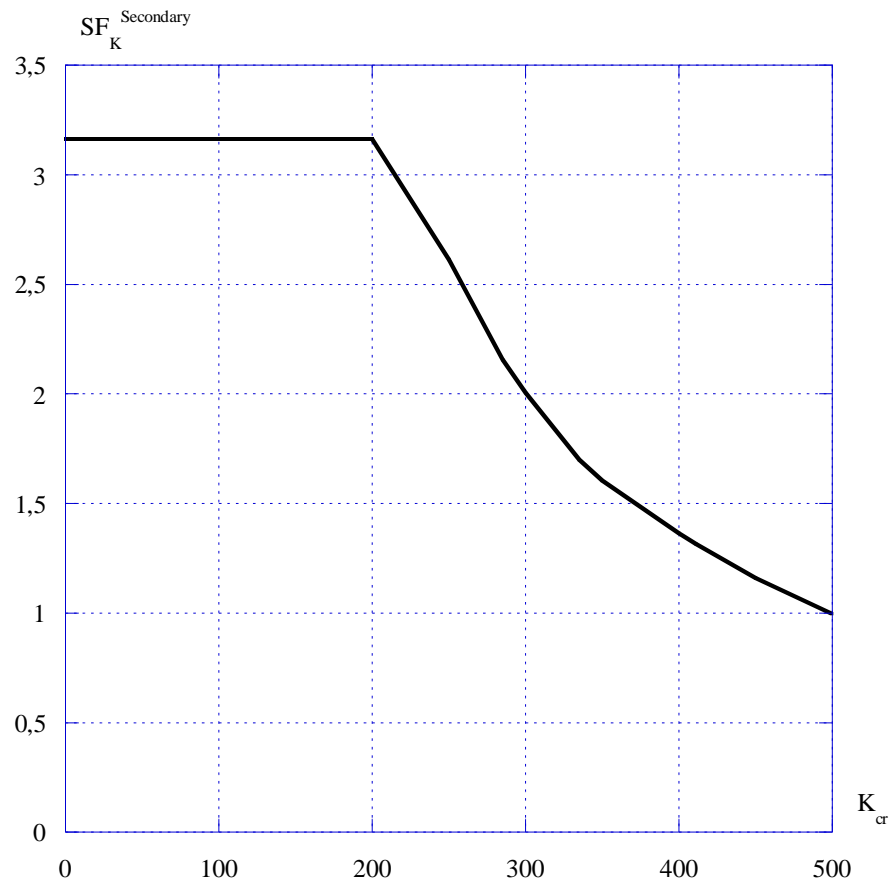


Figure 6.14. Results from the sensitivity study with varying assumed fracture toughness (for the case with $a = 20.7$ mm and $l = 58.3$ mm). This figure shows $SF_K^{Secondary} = f(K_{cr})$.

7 IMPLEMENTATION OF THE NEW PROCEDURE IN THE FRACTURE ASSESSMENT SOFTWARE PROSACC

In the present version of the ProSACC software and handbook (Dillström et. al. [2004]), the acceptance criteria is defined as,

$$K_r = \frac{K_I^P + K_I^S}{K_{cr}} + \rho / SF_K \leq f_{R6}(L_r) / SF_K \quad (7-1)$$

where SF_K in Eqn. (7-1) is the safety factor against fracture described by K_I .

In order to be able to use the different safety factors for primary stresses and secondary stresses (and to differentiate between global secondary stresses and local through-thickness secondary stresses), Eqn (7-1) is modified as,

$$K_r = \frac{K_I^P + K_B^S + (K_I^S - K_B^S) * SF_{K,local}^{Secondary} / SF_K}{K_{cr}} + \rho / SF_K \leq f_{R6}(L_r) / SF_K \quad (7-2)$$

where in Eqn. (7-2) $SF_{K,local}^{Secondary}$ is the safety factor for the local through-thickness secondary stress and K_B^S is the stress intensity factor due to global secondary bending stress.

7.1 Estimation of safety factors in the new deterministic safety evaluation system

For a given crack size (a and l) and a given loading, ProSACC can calculate the stress intensity factors (K_I^P and K_I^S) and limit load parameter L_r . Then the primary load is increased until the R6 failure assessment curve is reached such that,

$$\frac{c \cdot K_I^P + K_I^S}{K_{cr}} + \rho = f_{R6}(c \cdot L_r) \quad (7-3)$$

Eqn. (7-3) is then used to obtain the load parameter c and the limit load parameter at failure (L_r^*),

$$L_r^* = c \cdot L_r \quad (7-4)$$

7.1.1 *Safety factors for a normal/upset load event, $SF_K = 3.162$*

The new safety factor for secondary stress is then defined as ($SF_{K,local}^{Secondary} \geq 0.0$, in the case of a normal/upset load event),

$$\begin{cases} SF_{K,local}^{Secondary} = SF_K & \text{if } L_r^* \leq 0.80 \\ SF_{K,local}^{Secondary} = SF_K - (SF_K - 1) \cdot (L_r^* - 0.80) / (1.15 - 0.80) & \text{if } 0.80 < L_r^* < 1.15 \\ SF_{K,local}^{Secondary} = 1 - (L_r^* - 1.15) / (2.00 - 1.15) & \text{if } 1.15 < L_r^* < 2.00 \\ SF_{K,local}^{Secondary} = 0.0 & \text{if } L_r^* \geq 2.00 \end{cases} \quad (7-5)$$

If one want to stop at a scale factor that is equivalent to $SF_{K,local}^{Secondary} = 1$ (in the case of a normal/upset load event), then the new safety factor is defined as,

$$\begin{cases} SF_{K,local}^{Secondary} = SF_K & \text{if } L_r^* \leq 0.80 \\ SF_{K,local}^{Secondary} = SF_K - (SF_K - 1) \cdot (L_r^* - 0.80) / (1.15 - 0.80) & \text{if } 0.80 < L_r^* < 1.15 \\ SF_{K,local}^{Secondary} = 1.0 & \text{if } L_r^* \geq 1.15 \end{cases} \quad (7-6)$$

7.1.2 *Safety factors for an emergency/faulted load event, $SF_K = 1.414$*

The new safety factor for secondary stress is then defined as ($SF_{K,local}^{Secondary} \geq 0.0$, in the case of an emergency/faulted load event),

$$\begin{cases} SF_{K,local}^{Secondary} = SF_K & \text{if } L_r^* \leq 0.80 \\ SF_{K,local}^{Secondary} = SF_K - (SF_K - 1) \cdot (L_r^* - 0.80) / (1.05 - 0.80) & \text{if } 0.80 < L_r^* < 1.05 \\ SF_{K,local}^{Secondary} = 1 - (L_r^* - 1.05) / (2.00 - 1.05) & \text{if } 1.05 < L_r^* < 2.00 \\ SF_{K,local}^{Secondary} = 0.0 & \text{if } L_r^* \geq 2.00 \end{cases} \quad (7-7)$$

If one want to stop at a scale factor that is equivalent to $SF_{K,local}^{Secondary} = 1$ (in the case of an emergency/faulted load event), then the new safety factor is defined as,

$$\begin{cases} SF_{K,local}^{Secondary} = SF_K & \text{if } L_r^* \leq 0.80 \\ SF_{K,local}^{Secondary} = SF_K - (SF_K - 1) \cdot (L_r^* - 0.80) / (1.05 - 0.80) & \text{if } 0.80 < L_r^* < 1.05 \\ SF_{K,local}^{Secondary} = 1.0 & \text{if } L_r^* \geq 1.05 \end{cases} \quad (7-8)$$

7.2 Choice of options within the ProSACC software

The user should have the possibility to choose between the following options:

- According to ASME (as in the old deterministic safety evaluation system)
- Manually set SF_K and SF_L
- Manually set $SF_K^{Primary}$, $SF_{K,local}^{Secondary}$ and SF_L
- Let ProSACC calculate $SF_{K,local}^{Secondary}$ (condition $SF_{K,local}^{Secondary} \geq 0.0$)
- Let ProSACC calculate $SF_{K,local}^{Secondary}$ (condition $SF_{K,local}^{Secondary} \geq 1.0$)

The different options should be set using the Acceptance Tab within the ProSACC software. An example is given in Fig. 7.1.

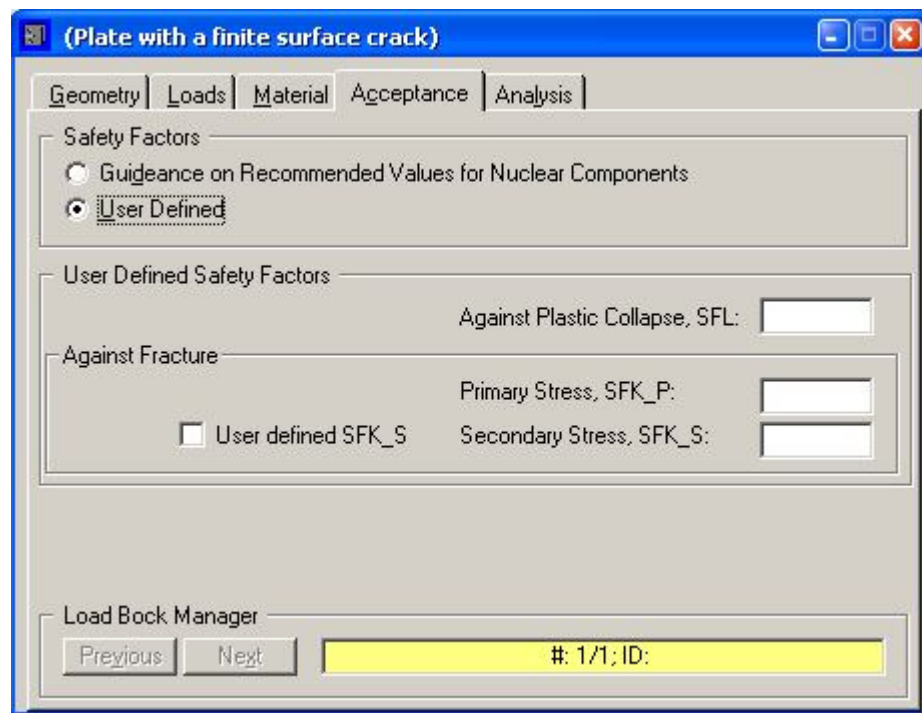


Fig. 7.1. An example on how to input the case where one manually set $SF_K^{Primary}$, $SF_{K,local}^{Secondary}$ and SF_L .

8 CONCLUSIONS AND RECOMMENDATIONS

An investigation on the significance of secondary stresses for defects (cracks) in ductile materials and how the residual stresses in a component contributes to the CTOD and the J -integral has been performed. The main conclusions from this investigation are:

Conclusions related to the new strategy for fracture assessment of defects in ductile materials

- Using a two-dimensional analysis of a thin-walled pipe with a complete circumferential crack, it is shown that the relative contribution to J or CTOD from the residual stress decreases rapidly between $L_r = 0.8$ and $L_r = 1.3$. For $L_r = 1.3$ the contribution of the residual stresses is 20% of the axial load contribution. For $L_r = 1.6$ the contribution of the residual stresses is about 7%. For higher L_r -values the contribution becomes negligible.
- Using a two-dimensional analysis of a thick walled pipe with a complete circumferential crack, it is shown that the relative contribution to J or CTOD from the residual stress decreases rapidly with increasing L_r . For $L_r = 1.3$ the contribution of the residual stresses is 10% of the axial load contribution. For $L_r = 1.6$ the contribution of the residual stresses is about 2%. For higher L_r -values the contribution becomes negligible.
- Using a three-dimensional analysis of a thick walled pipe with an axial surface crack, it is shown (crack depths between 6% up to 14% of the wall thickness is included) that the relative contribution to J or CTOD from the residual stress decreases rapidly with increasing L_r . For $L_r \geq 1.1$ the contribution of the residual stresses is less than 10% of the axial load contribution. For $L_r \geq 1.5$ the contribution of the residual stresses is almost 0%.
- For the studied case, the relative contribution from the weld residual stresses to CTOD or J , decreases rapidly for high values of L_r . For very high L_r -values the contribution becomes negligible. This is believed to be valid qualitatively also for other material models, crack geometries and residual stress distributions. The exact limit of L_r at which the relative contribution from welding residual stresses (or thermal stresses) to CTOD or J is sufficiently small to be neglected is likely to depend on the particular material model, crack geometry and the shape and level of the residual (or thermal) stress distribution.
- Using the results presented in this report, a new deterministic safety evaluation system is defined, that more realistically handles the contribution to J or CTOD from secondary stresses. In the new procedure we define new safety factors against fracture described by K_1 and differentiate between $SF_K^{Primary}$ (relating to primary stresses) and $SF_K^{Secondary}$ (relating to secondary stresses). The procedure is consistent with the presented analyses and experimental data.

Conclusions related to the different analyses presented in this report

- If CTOD can successfully be used in fracture analyses of welded components, the conventional J -integral seems also to be a useful parameter in numerical analyses, for analysing welded components. This is true at least if J is evaluated for contours very near the crack tip in a refined mesh.
- The contribution from residual stresses does decrease for high L_r , as shown in this study. A linear kinematic hardening model was used. However, in a real material the hardening is non-linear and E/E_T decreases with L_r . It was found, by varying the slope of the hardening curve, that an additionally decreasing effect on the contribution from residual stresses to CTOD or J due to the decreasing hardening, should be taken into account for high L_r -values.
- The choice of hardening model is important. It is believed that kinematic hardening is a better choice than isotropic hardening in low cycle simulations i.e. in a few-pass welding process, as in the present study.

- For the case of weld residual stresses in combination with high thermal stresses, it is found that the plasticity induced by the thermal stresses is not sufficient to suppress the influence of weld residual stresses on CTOD or J , even for very high thermal loads.
- The residual stresses can be relaxed by unloading from a primary tensile load. Unloading from a load level corresponding to $L_r = 0.83$ will result in almost a complete relaxation of the weld residual stresses for the studied case.

Conclusions related to the published experimental data presented in this report

- There are limited experimental results published in the open literature. There is no systematic study of these this matter found in the literature. The published experiments give mostly qualitative conclusions. A common conclusion from these experiments is that for high level of primary loads ($L_R > 1.0$), the significant of the secondary stresses are negligible. This issue needs to be verified for L_R close to unity.

9 ACKNOWLEDGEMENT

This research project is sponsored by the Swedish Nuclear Power Inspectorate (SKI) under contracts 14.42.011210/02094 (2002-03-13) and 14.42.011210/22094 (2003-12-15). This support is greatly appreciated.

10 REFERENCES

- ABAQUS, (1995), Users manual, version 5.5, Hibbit, Karlsson and Sorenson, USA.
- ABAQUS, (2003), Users manual, version 6.3, Hibbit, Karlsson and Sorenson, USA.
- ANDERSSON, P., BERGMAN, M., BRICKSTAD, B., DAHLBERG, L., NILSSON, F. and SATTARI-FAR, I., (1996), "A procedure for safety assessment of components with cracks-Handbook", SAQ/FoU-Report 96/08, SAQ Kontroll AB, Stockholm, Sweden.
- ANDERSSON, M. and DILLSTRÖM, P., (2004), "Effect of secondary stresses on the J -integral and CTOD when analysing thick walled components", DNV RSE R&D Report No. 2004/04, Det Norske Veritas, Sweden.
- ARGYRIS, J. H., SZIMMAT, J., and WILLIAM, K. (1983), Finite element analysis of the arc welding process, Numerical methods in thermal problems - Proceedings of the third international conference, Seattle WA, USA, Pineridge press, Swansea UK, 249-258.
- BERGMAN, M. (1991), "A fracture mechanical analysis of secondary stresses-part 1", SAQ/FoU-Rapport 94/03 (in Swedish), SAQ Kontroll AB, Stockholm, Sweden.
- BRICKSTAD, B. and L. JOSEFSSON, (1996), "A parametric study of residual stresses in multipass butt-welded stainless steel pipes", SAQ-FoU-Report 96/01, SAQ Kontroll AB, Sweden.
- DELFIN, P., SATTARI-FAR, I., and B. BRICKSTAD, (1997), "Effect of thermal and weld-induced residual stresses on the J -integral and CTOD in elastic-plastic fracture analyses", SAQ/FoU-Report 97/02, SAQ Kontroll AB, Sweden.
- DELFIN, P., BRICKSTAD, B. and L. JOSEFSSON, (1998), "Residual stresses in multi-pass butt-welded bimetallic piping, part I", SAQ/FoU-Report 98/12, SAQ Kontroll AB, Sweden.
- DILLSTRÖM, P., et. al. (2004), "A combined deterministic and probabilistic procedure for safety assessment of components with cracks — handbook", DNV Research Report 2004/01, Rev. 4-1, Det Norske Veritas AB.
- DILLSTRÖM, P. and I. SATTARI-FAR, (2003), "Limit load solutions for surface cracks in plates and cylinders", DNV RSE R&D Report no. 2002/01, Rev. 2, Det Norske Veritas, Sweden.
- DILLSTRÖM, P., and W. ZANG., (2004), "User manual ProSACC Version 1.0", DNV Research Report 2004/02, Det Norske Veritas AB, Stockholm, Sweden.
- DILLSTRÖM, P., (2002-09-06), "Ringhals 4 – Skadetålighetsanalys av defekter i svetsen mellan utloppsstuts och safe-end", DNV Teknisk Rapport 10941100-1, Rev. 0, Det Norske Veritas AB, Stockholm, Sweden.
- DONG, P., (2005), Private communications.
- DRUGAN, W. J., RICE, J. R. and SHAM, T-L. (1982), "Asymptotic analysis of growing plane strain tensile cracks in elastic-ideally plastic solids", Journal of Mechanics and Physics of Solids, Vol. 30, 447-473, Erratum in Vol. 31.

GREEN, D., SHARPLES, J. K. and STEWART, G. (1993), "Experimental evidence in support of proposals for the treatment of residual stress in fracture assessment of pressure vessels", Pressure Vessel Integrity, ASME, PVP-Vol. 250, 1-9.

GREEN, D. and KNOWLES, J., (1994), "The treatment of residual stress in fracture assessment of pressure vessels", Journal of Pressure Vessel Technology, Vol. 116, 345-352.

HOU, Y. C., KIM, M., PAN, J. and BRUST, F.W., (1996), "Effects of residual stresses on fracture of welded pipes", Residual Stresses in Design, Fabrication, Assessment and Repair, ASME, PVP-Vol. 327, 67-75.

KANNINEN, M. F., BRUST, F. W., AHMAD, J. and ABOU-SAYED, I. S., (1982), "The numerical simulation of crack growth in weld-induced residual stress fields", Residual Stress and Stress Relaxation, Plenum Publishing Corporation, 227-248.

KUMAR, V., SCHUMACHER, B.I. and GERMAN, M.D., (1991), "An engineering approach for examining crack growth and stability in flawed structures", Computers and structures, Vol. 40, 487-501.

LEI, Y., O'DOWD, N.P. AND WEBSTER, G.A., (2000), "Fracture mechanics of a crack in a residual stress field", Int. Jour of Fracture, Vol. 106, pp. 195-216.

MILNE, I., R. A. AINSWORTH, A. R. DOWLING and A. T. STEWART, (1988), "Assessment of the integrity of structures containing defects", Int. Jour. of Pressure Vessel and Piping, Vol. 32, pp. 3-104.

MOHR, M.C., MICHALERIS, P. and KIRK, M.T., (1997), "An improved treatment of residual stresses in flaw assessment of pipes and pressure vessels fabricated from ferritic steels", ASME PVP Conference, Vol. 359.

RICE, J. R. (1968), "A path independent integral and the approximate analysis of strain concentration by notches and cracks", Journal of Applied Mechanics, Vol. 35, 379-386.

SHARPLES, J. K., HARRISON, M., MAY, K. A., CHIVERS, T. C. and SMITH, E., (1993), "The effect of residual stresses on fracture behaviour", Pressure Vessel Integrity, ASME, PVP-Vol. 250, 105-113.

SHARPLES, J.K., SANDERSON, D.J., BOWDLER, B.R., WIGHTMAN, A.P. AND AINSWORTH, R.A., (1995) "Experimental programme to assess the effect of residual stresses on fracture behaviour", ASME-PVP, Vol. 304, pp. 539-551.

SHARPLES, J.K. and GARDNER, L., (1996), "Ductile tearing tests of 316 stainless steel wide plates containing weldments", Int. Jour of Pres. Ves. & Piping, Vol. 65, pp. 353-363.

SHIH, C. F. (1981), "Relationship between the J -Integral and the crack opening displacement for stationary and extending cracks", Journal of Mechanics and Physics of Solids, Vol. 29, 305-326.

WILKOWSKI, G. M., ET AL. (1987), "Analysis of Experiments on Stainless Steel Flux Welds", NUREG/CR-4878, U.S. Nuclear Regulatory Commission (NRC), USA.

WILKOWSKI, G. M., OLSON, R.J., SCOTT, P.M. (1997), "State-of-the-Art Report on Piping Fracture Mechanics", NUREG/CR-6540, U.S. Nuclear Regulatory Commission (NRC), USA.

WILKOWSKI, G.M. and RUDLAND, D., (2001), "Effects of secondary stresses on pipe fracture", LBB Workshop, SMiRT-16, USA.

APPENDIX A. THE J -INTEGRAL AND CTOD AS FRACTURE PARAMETERS

The J -integral introduced by Rice [1968] was derived using a non-linear elastic material model to account for plasticity (deformation theory plasticity). As long as the loading is monotonically increasing and no unloading occurs, i.e. the loading is proportional; Rice's J -integral is applicable also for incremental plasticity models. The J -integral as a function of integration contour for a stationary crack are shown (from Delfin et. al. [1997]) for an axial load Fig. A1 and for a thermal load as defined by Equation (2-5) in Fig. A2. The first integration contour is the crack-tip itself, the second contour is the closest ring of elements around the crack-tip and the third contour is the ring of element closest to the second contour and so on. It can be seen that the J -integral values are fairly path independent for the stationary crack.

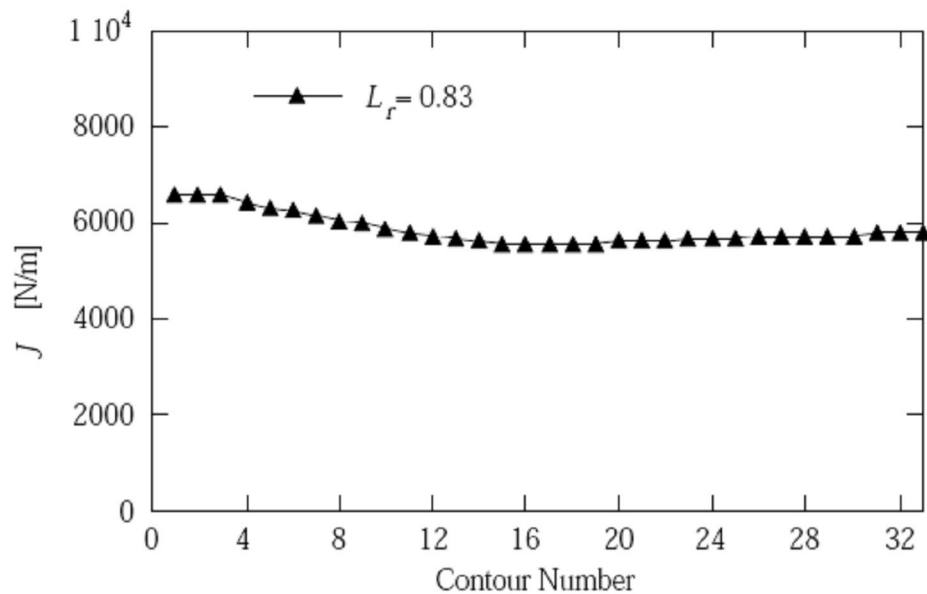


Fig. A1. The J -integral values for 33 different contours of integration for the pipe subjected to an axial tension only (from Delfin et. al. [1997]).

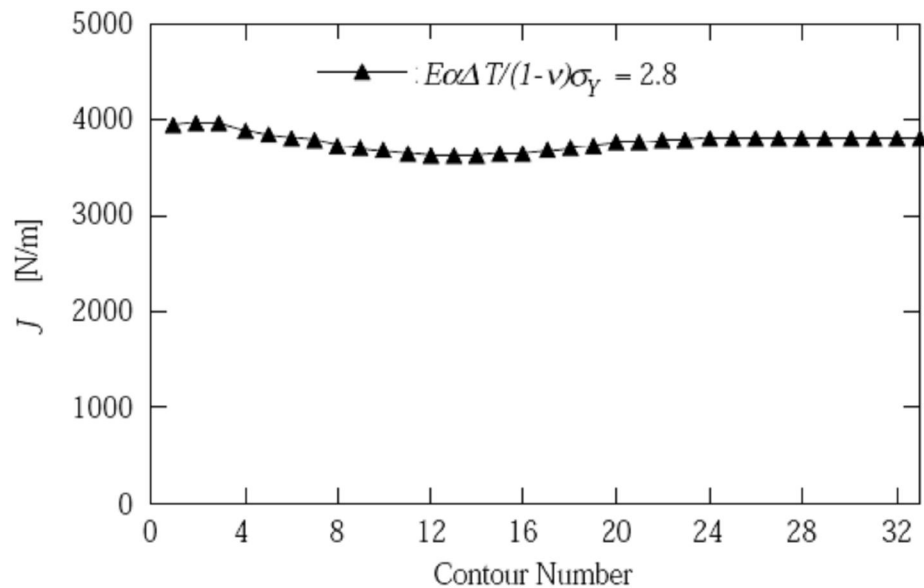


Fig. A2. The J -integral values for 33 different contours of integration for the pipe subjected to a thermal loading only (from Delfin et. al. [1997]).

The welding process causes a highly non-proportional load situation. Thus the J -integral is not applicable for a crack experiencing loading during a welding process. Instead Delfin et. al. [1997] considered a crack which had grown subcritically (IGSCC or fatigue) influenced by the residual stresses after the completion of the welding process.

- The growth of a crack is a non-proportional load situation and the J -integral becomes path dependent. Furthermore the crack opening profile of a quasistatically growing crack is very different from a stationary crack, c.f. Drugan, Rice and Sham [1982], which makes it practically impossible to measure CTOD.
- After the crack has stopped an axial tensile load is applied. During the loading a plastic redistribution of stresses may occur in the regions with weld-induced strains, this redistribution is likely to result in a non-proportional load situation, giving a meaningless J -integral.
- However, the path dependency, whether it originates from the crack growth or the redistribution of stresses, may become a minor disturbance when sufficient monotonic load (thermal or mechanical) is applied to the stationary crack. This seems to be the case when a kinematic hardening model is used. For the isotropic hardening model, however, the redistribution of stresses has a substantial effect also at later stages in the loading history. The crack-tip even experiences unloading at a certain stage.
- It can be observed in Fig. A3 and Fig. A4, that even for quite high load levels, the J -integral becomes strongly path dependent from about contour number 20 (see Fig. A3a and Fig. A4a). On the other hand J seems fairly path independent for contours within contour number 20 (see Fig. A3a and Fig. A4a). It is only for very large load levels that J becomes practically path independent for all contours (see Fig. A3b and Fig. A4b).
- CTOD was evaluated as described in Appendix B and J was evaluated for the tenth contour in Delfin et. al. [1997]. A relation, Equation (2-4), between J and CTOD was established. The correlation between J and CTOD remained approximately constant as the axial load was increased.

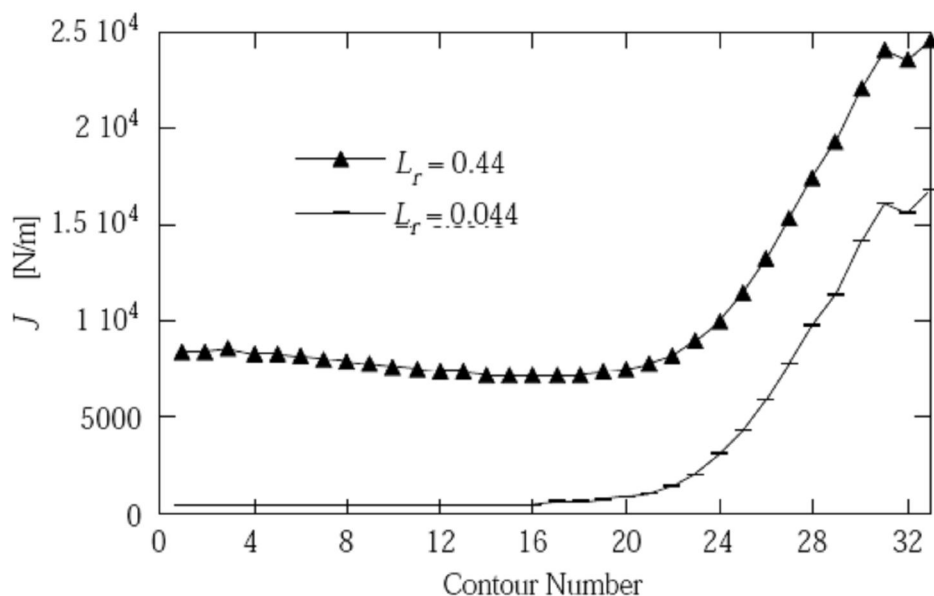


Fig. A3a. The J -integral values for 33 different contours of integration for the welded pipe subjected to different levels of axial tension, $L_r = 0.044-0.44$ (from Delfin et. al. [1997]).

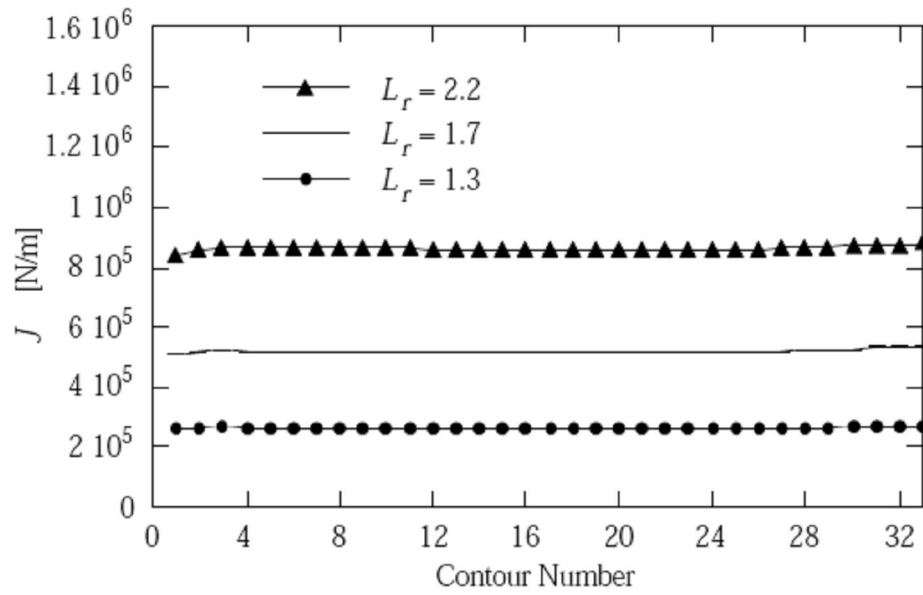


Fig. A3b. The J -integral values for 33 different contours of integration for the welded pipe subjected to different levels of axial tension, $L_r = 1.3$ -2.2 (from Delfin et. al. [1997]).

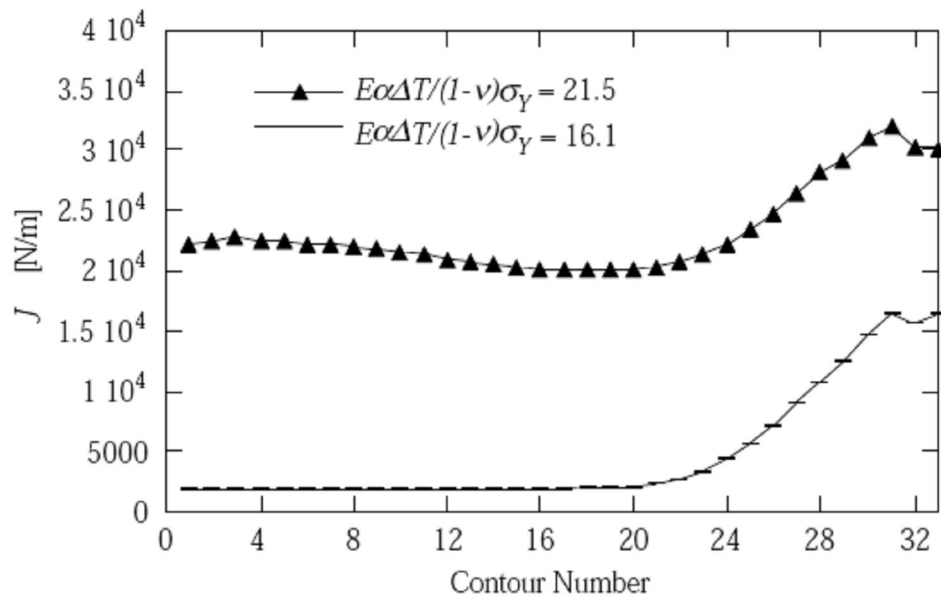


Fig. A4a. The J -integral values for 33 different contours of integration for the welded pipe subjected to low levels of thermal loading (from Delfin et. al. [1997]).

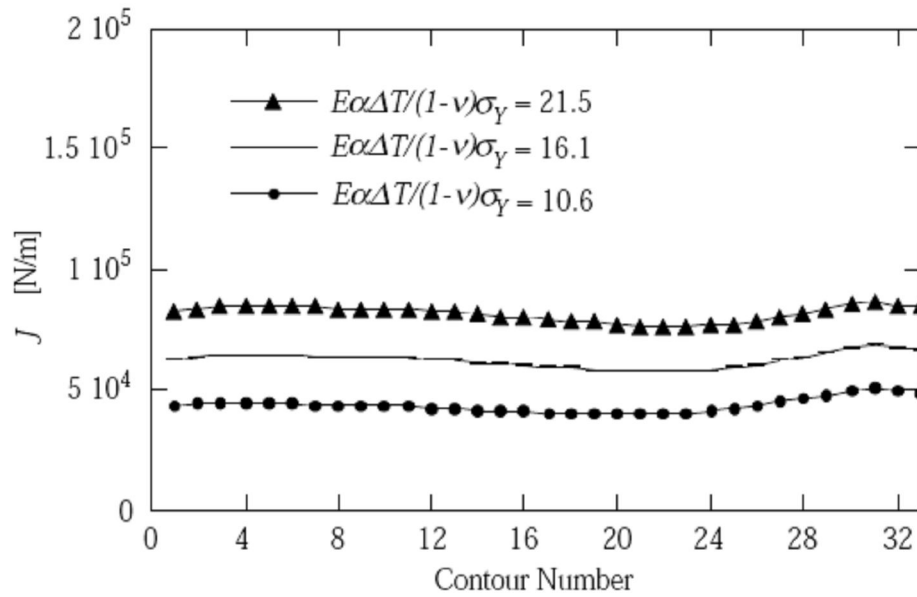


Fig. A4b. The J -integral values for 33 different contours of integration for the welded pipe subjected to higher levels of thermal loading (from Delfin et. al. [1997]).

An explanation of the path dependence of J for contours a certain distance away from the crack-tip may be connected to the way the J -integral is calculated in ABAQUS [1995], where initial strains and strain-induced residual stresses are not considered. However, ABAQUS takes into account thermally induced stresses when calculating the J -integral. The problem in this case is that the crack is not present during the welding process, in other words ABAQUS cannot take into account thermally induced strains that was produced before the crack was introduced. This can be one part of the explanation why the J -integral is path independent within contour 20, which is less than 1 mm from the crack-tip. Within that distance, the singular stress field dominates over the residual stresses. Thus the contribution of the residual stresses to the J -integral becomes small and the J -integral calculated in ABAQUS becomes path independent.

In the work by Lei et. al. [2000] a modified J -integral was presented to produce a path-independent integral when residual stresses are present (see section 5.7 in this report). The results from this work indicates that it is possible to define such a path independent J -integral for all load levels from a primary stress of zero up 1.3 times the limit load (with weld residual stresses present at all load levels).

APPENDIX B. CALCULATION OF CTOD

During the primary axial tension loading, the CTOD and the J -integral are calculated. The definition of CTOD is shown in Fig. B1. CTOD is defined as twice the axial displacement which coincides with a 45° angle from the crack tip (from Anderson and Dillström [2004]).

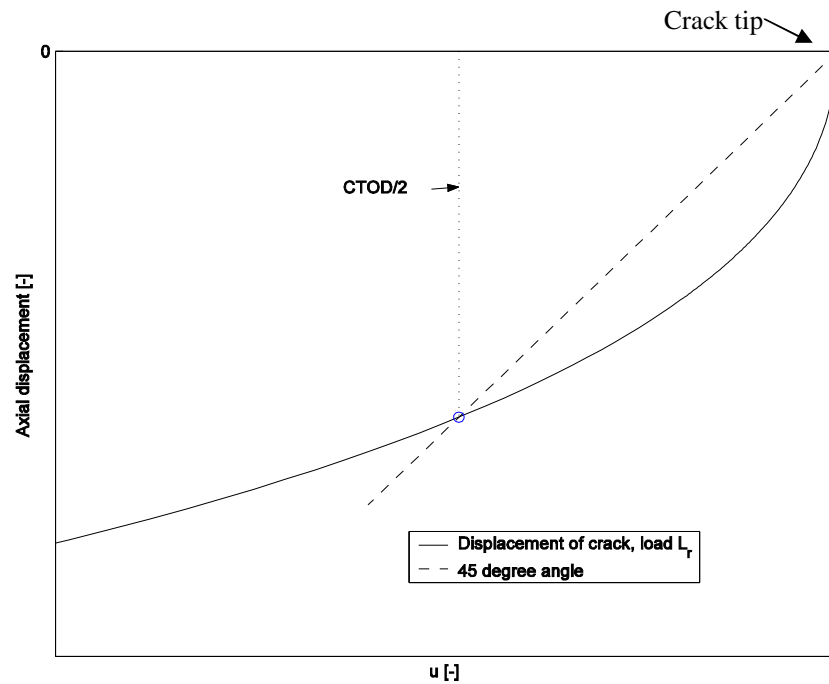


Fig. B1. Definition of CTOD.

Fig. B2 and Fig. B3 shows the axial displacements close to the crack tip for the 2D model. The loading consists of both weld residual stresses and primary loading.

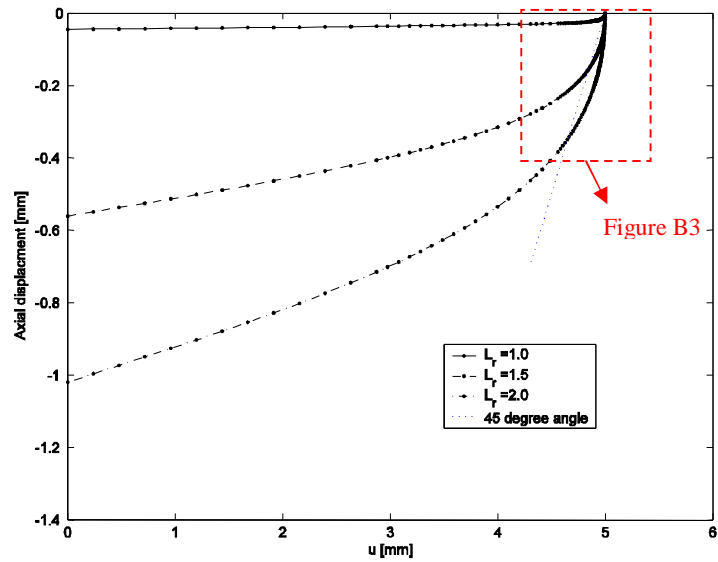


Fig. B2. Axial displacements for different L_r -values for the 2D model including weld residual stresses. The dots represent the node locations. $u = 0$ mm corresponds to the weld root.

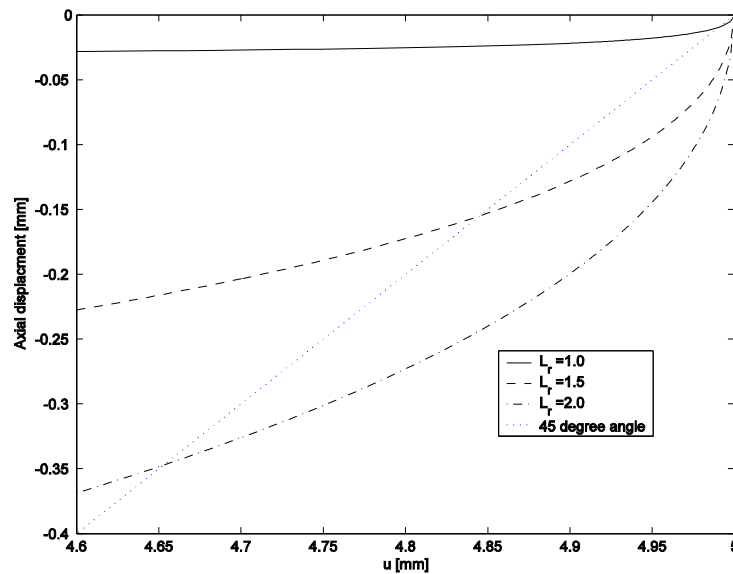


Fig. B3. Axial displacements for different L_r -values for the 2D model including weld residual stresses (details of Fig. B2). $u = 0$ mm corresponds to the weld root.

APPENDIX C. LIMIT LOAD OF 2D MODEL

The FE model described in section 3 ($R_i = 300$ mm, $t = 40$ mm, circumferential surface crack, $a = 5$ mm) is also used for the limit load analysis (from Anderson and Dillström [2004]). The definition of the limit load that is used in this report is the same as in Dillström and Sattari-Far [2003]. The limit load is defined as the load when yielding occurs through the whole thickness. Fig. C1 and Fig. C2 shows the von Mises stress at two adjacent load levels, the axial nominal stress is $\sigma_{axial} = 211.1$ MPa and $\sigma_{axial} = 215.6$ MPa. As can be seen in Fig. C2, the cross section is fully yielded but in Fig. C1, it is not. The limit load is defined as the average of the two load levels: $\sigma_{axial} = 213.4$ MPa ($0.928 \cdot \sigma_y$). The yield stress is $\sigma_y = 230$ MPa.

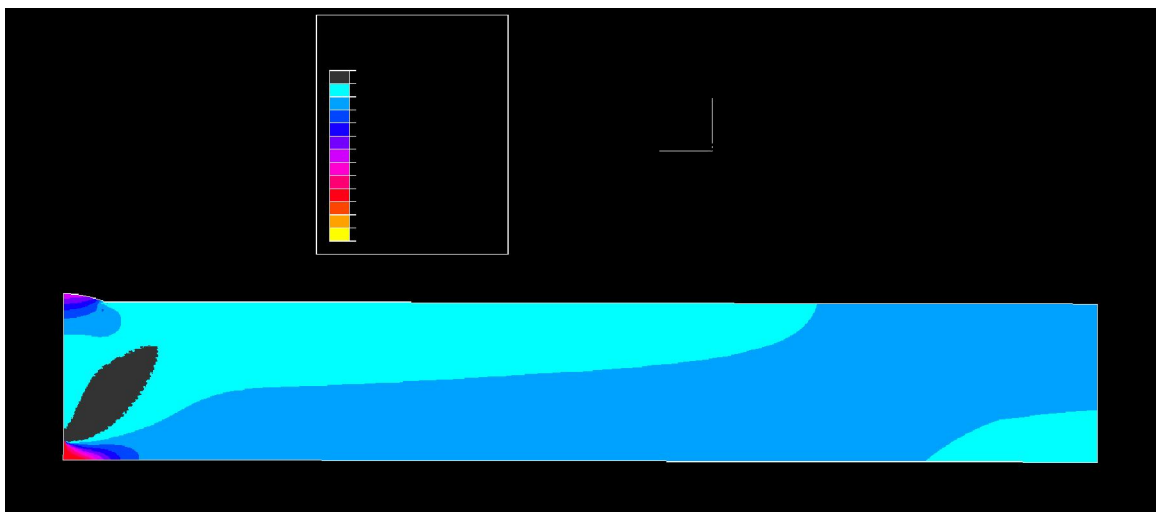


Fig. C1. Von Mises stress [Pa] at an applied axial stress level of 211.1 MPa.

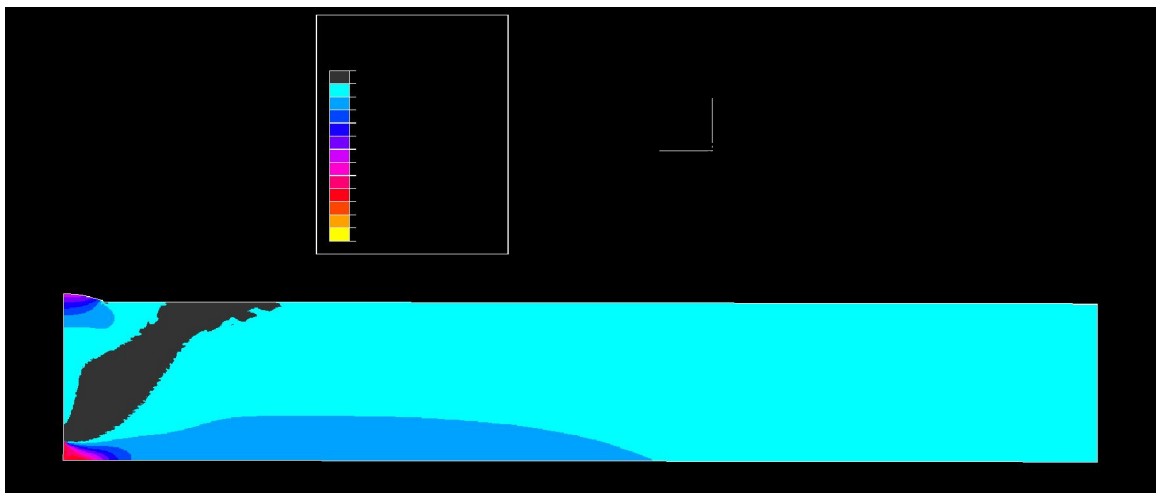


Fig. C2. Von Mises stress [Pa] at an applied axial stress level of 215.6 MPa.

APPENDIX D. LIMIT LOAD OF 3D MODEL

The FE model described in section 4 ($R_i = 348.5$ mm, $t = 84$ mm, axial surface crack, $a = 0.08 \cdot t$) is also used for the limit load analysis (from Anderson and Dillström [2004]). The definition of the limit load that is used in this report is the same as in Dillström and Sattari-Far [2003]. The limit load is defined as the load when yielding occurs through the whole thickness. Fig. D1 and Fig. D2 shows the von Mises stress at two adjacent load levels, the “pressure” $p = 84$ MPa and $p = 88$ MPa. This corresponds to the nominal hoop stresses ($R = 390.5$ mm, $t = 84$ mm, $\sigma_y = 380$ MPa) $1.028 \cdot \sigma_y$ and $1.077 \cdot \sigma_y$. As can be seen in Fig. D2, the cross section is fully yielded but in Fig. D1, it is not. The limit load is defined as the average of the two load levels: $p = 86$ MPa ($1.052 \cdot \sigma_y$).

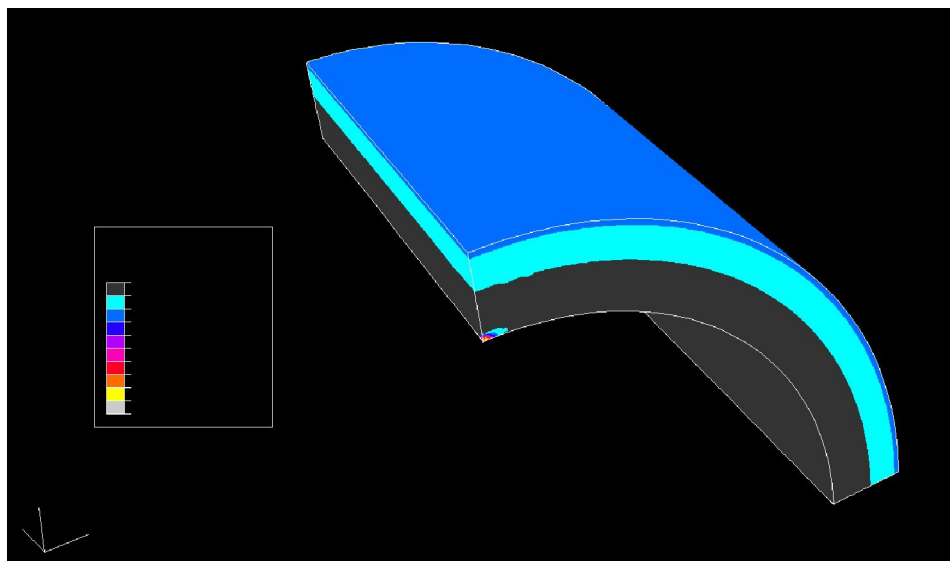


Fig. D1. Von Mises stress [Pa] at the pressure 84 MPa, nominal hoop stress $1.028 \cdot \sigma_y$.

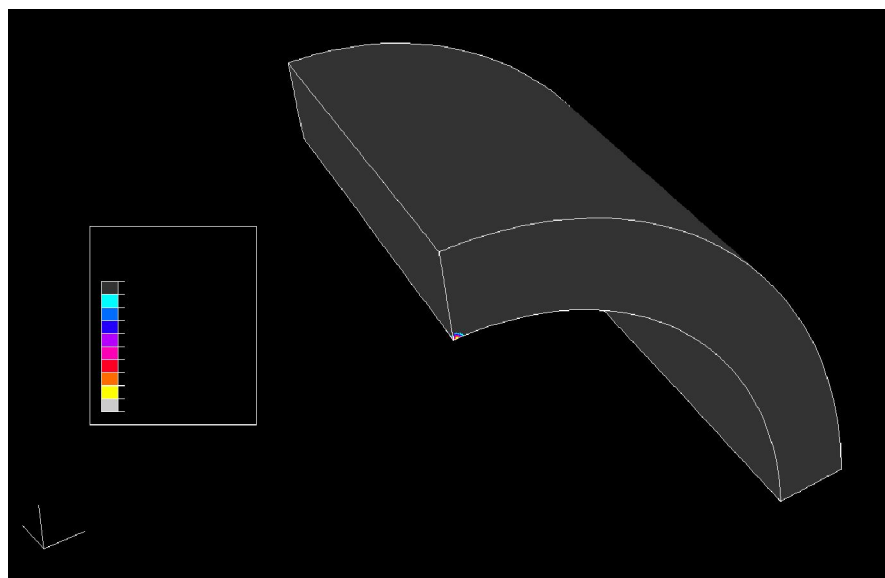


Fig. D2. Von Mises stress [Pa] at the pressure 88 MPa, nominal hoop stress $1.077 \cdot \sigma_y$.



Strålsäkerhetsmyndigheten
Swedish Radiation Safety Authority

SE-171 16 Stockholm
Solna strandväg 96

Tel: +46 8 799 40 00
Fax: +46 8 799 40 10

E-mail: registrator@ssm.se
Web: stralsakerhetsmyndigheten.se